NTNU

Norwegian University of
Science and Technology

# Using Microfluidics to Study the EOR Potential of Nanocellulose

Siri Hjelt Salvesen

Petroleum Geoscience and Engineering
Submission date: June 2018
Supervisor: Ole Torsæter, IGP

Norwegian University of Science and Technology
Department of Geoscience and Petroleum

# Preface

This master thesis was written at the Norwegian University of Science and Technology, Department of Geoscience and Petroleum during the spring of 2018. I would like to thank my supervisor Ole Torsæter for guidance and support throughout the process.

All planning and execution of the laboratory work was performed together with Ph.D student Reidun Cecilie Grønfur Aadland, with guidance from Ole Torsæter. I would like to thank Reidun for all help and valuable discussions trhoughout the semester.

# Summary

As many of the existing oil reservoirs show declining production, there is a need for research on enhanced oil recovery (EOR) techniques that can accelerate further production. The use of nanoparticles to enhance oil recovery is a promising trend that is believed to introduce a green alternative EOR technique. An apparatus and method that can be used to study the flow of these nanofluids through a porous medium is microfluidics. Microfluidics is a method that enables visualization of fluid flow at the micrometer scale.

This master thesis aims to study the possibilities of using nanocellulose to enhance oil recovery. A microfluidics apparatus was used as a tool to study the oil saturation during secondary and tertiary flooding of two types of nanocellulose: CNC and TEMPO-CNF. 1 % CNC and 0.1 % TEMPO-CNF in a low salinity water solution (0.1 wt% NaCl) were used for all experiments. CNC was additionally heated to 120 $^{\circ}C$ and injected tertiary in the microfluidics apparatus. Some important properties of the fluids were measured to support the results obtained from the microfluidics flooding. An optimization study of the experimental setup was performed continuously during this master thesis, and some of the experiments were performed on both the old and the improved setup.

No significant decrease in oil saturation was observed during microfluidics flooding with the two nanofluids, except for secondary flooding with TEMPO-CNF. However, some of the measurements of the nanofluid properties showed promising results. Microfludicis is a relatively new method, and the possibilities of using microfluidics to study the oil saturation is not yet fully established. The validity of the microfluidics experiments is unclear as there were a lot of uncertainties related to the apparatus. Microfluidics might work better as a tool to visualize the flow rather than focusing primarily on flooding and oil saturation.

# Sammendrag

Mange av dagens eksisterende oljereservoar viser nedgang i produksjonen, og det er derfor et behov for forskning på metoder som kan akselerere videre produksjon. Bruken av nanopartikler for å øke oljeutvinningen er en lovende metode, og den antas å kunne introdusere et grønt alternativ til eksisterende metoder for økt oljeutvinning. Microfluidics er en metode som kan bli brukt til å studere strømningen av disse nanofluidene gjennom et porøst medium. Denne metoden muliggjør visualisering og fløming av fluider på et mikronivå.

Mulighetene for å bruke nanocellulose til å øke oljeutvinningen ble studert i denne masteroppgaven. Et microfluidics-apparat ble brukt til å studere oljemetningen i løpet av sekundær og tertiær fløming av to typer nanocellulose: CNC og TEMPO-CNF. 1 % CNC og 0.1 % CNF i vann med en saltkonsentrasjon på 0.1 % ble brukt i alle forsøk. CNC ble i tillegg varmet opp til 120 $^{\circ}C$ og fløtmet tertiært gjennom microfluidics-apparatet. Noen av nanofluidenes egenskaper ble målt for å underbygge resultatene fra fløtmingen med microfluidics. En optimalisering av det eksperimentelle oppsettet ble gjennomført kontinuerlig i løpet av denne masteroppgaven, og noen av eksperimentene ble gjennomført både på det gamle og det nye oppsettet.

Ingen betydelig reduksjon i oljemetningen ble observert under microfluidics fløming med de to nanofluidene, foruten for den sekundære fløtmingen med TEMPO-CNF. Noen av nanofluidenes egenskaper viste derimot lovende resultater. Microfluidics er en relativt ny metode, og mulighetene for å bruke microfluidics til å studere oljemetning er ikke fullstendig etablert. Gyldigheten til microfluidics eksperimentene er uklar da det var flere usikkerheter knyttet til apparatet. Microfluidics fungerer kanskje bedre som et verktøy for selve visualisering av strømningen istedenfor å i hovedsak fokusere på fløming og oljemetning.

# Table of Contents

# List of Tables

# List of Figures

# Nomenclature

**Acronyms**

| | |
|---|---|
| CNC | Cellulose nanocrystals |
| CNF | Cellulose nanofibrils |
| EOR | Enhanced oil recovery |
| HLP | hydrophobic and lipophilic |
| HPAM | Hydrolyzed polyacrylamid |
| IFT | Interfacial tension |
| LHP | Lipophobic and hydrophilic |
| LSW | Low salinity water |
| PV | Pore volume |

**Greek Symbols**

| | | |
|---|---|---|
| $\Delta\rho$ | Density difference between two phases | $\frac{kg}{m^3}$ |
| $\Delta P$ | Pressure difference between two phases | Pa |
| $\gamma$ | Shear rate | $\frac{1}{s}$ |
| $\lambda$ | Mobility | $\frac{m^3 s}{kg}$ |
| $\mu$ | Dynamic viscosity | Pa s |
| $\nu$ | Kinematic viscosity | $\frac{m^2}{s}$ |
| $\rho$ | Density | $\frac{kg}{m^3}$ |
| $\sigma$ | Interfacial tension | $\frac{N}{m}$ |

| | | |
|---|---|---|
| $\tau$ | Shear stress | Pa |

**Roman Symbols**

| | | |
|---|---|---|
| $A$ | Cross-sectional area | $m^2$ |
| $d_e$ | Equatorial diameter | m |
| $d_s$ | Diameter distance $d_e$ from bottom of drop | m |
| $dc$ | Liquid velocity | $\frac{m}{s}$ |
| $dy$ | Distance between layers of fluid | m |
| $g$ | Gravity of the Earth | $\frac{m}{s^2}$ |
| $H$ | Shape determining variable | |
| $k$ | Absolute permeability | $m^2$ |
| $k_i$ | Effective permeability | $m^2$ |
| $k_{ri}$ | Relative permeability | |
| $L$ | Length | m |
| $M_r$ | Mobility ratio | |
| $N_C$ | Capillary number | |
| $P_1$ | Pressure of convex side of spherical cap | Pa |
| $P_2$ | Pressure of concave side of spherical cap | Pa |
| $P_c$ | Capillary pressure | Pa |
| $q$ | Flow rate | $\frac{m^3}{s}$ |
| $r_1$ | Inner radii of curvature | m |
| $r_2$ | Outer radii of curvature | m |
| $S$ | Shape dependant quantity | |
| $v$ | Pore flow velocity | $\frac{m}{s}$ |

**Subscripts**

| | |
|---|---|
| o | Oil |
| w | Water |

Chapter 1

# Introduction

The oil and gas industry is facing some challenges when it comes to meeting the growing energy demand (Kapusta et al., 2011). At the same time, many of the existing reservoirs are at the end of their production life, and there is a need for methods that can enhance the oil recovery (Hendraningrat et al., 2013a). The existing EOR methods has shown good results in the past, but there is a need for new technology that can meet the changes that the oil industry is facing. As the recent oil crisis has made the oil industry focus on more cost effective solutions, it would be favorable to take advantage of a larger volume of the reservoir before shutting the production down. This should be done using cheap, effective and environmental friendly methods.

Nanotechnology has had a great impact in many industries during the past years, and could have a similar impact in the oil and gas industry (Kapusta et al., 2011). Water is usually injected in the reservoir to maintain pressure and sweep more oil out. It is believed that nanoparticles can enhance the properties of this water, and more oil can potentially be recovered. Cellulose is a naturally occurring material that can be added to water as nanoparticles, and could have the potential of being a green EOR method. As many of the current EOR techniques could potentially harm the environment, there is a need for a green alternative (Wei et al., 2016).

Microfluidics is a relatively new technology that can be used to study the flooding of fluids. It is a method and apparatus that allows for visualization and flooding of fluids at the micrometer scale. There are several advantages related to this method and apparatus. Microfluidics allows for visualization during the flooding, making the experiments less ”black box” than core flooding experiments. It requires small sampling volumes, which will reduce the costs of the fluids used in the experiments. In addition, the experiment time is shorter than for conventional core flooding.

The objective of this master thesis is to study the possibility of using nanocellulose to enhance oil recovery, by using microfluidics as a tool to study the fluid injections. This goal is achieved by doing tertiary and secondary flooding in the microfluidics apparatus with two types of nanocellulose: CNC and TEMPO-CNF. The oil saturation is calculated by a MATLAB code and studied during the process. The water used to mix the final nanofluid solutions and initially saturate the microchip is a low salinity water solution with 0.1 wt% NaCl, while crude oil C is the oil used. The interfacial tension and contact angle between the nanofluids and oil is measured to see if there are any changes in these properties when adding the nanoparticles. The viscosity of each fluid is also measured so that both the capillary and viscous effects by the nanofluids can be discussed. A part of the objective of this thesis is also to improve the experimental setup of the microfluidics apparatus. The design of the apparatus is changed throughout the experimental work to minimize factors that can affect the results.

This master thesis will first give a short literature study on the topic of microfluidics and nanocellulose in chapter 2. This chapter is included to give an overview of the previous work done on the topic. Chapter 3 includes some theory on microfluidics, nanotechnology and reservoir properties that plays an important role in the field of enhanced oil recovery. This master thesis builds on some of the same theory as the specialization project written on the topic of EOR and nanocellulose (Salvesen, 2017), and major parts of chapter 3 is taken and modified from this specialization project. Chapter 4 goes through the experimental work, which is the main part of this thesis. Chapter 5 presents all results obtained during the experimental work. The results are discussed in chapter 6 and final conclusions are made in chapter 7.

Chapter 2

# Literature Review

## 2.1 Microfluidics

There is a great amount of literature on the topic of microfluidics, both in the field of enhanced oil recovery and other fields concerning flow in porous media. Many of the publications refers to the setup of these micromodels, while the experimental part of this thesis will use an already set up model and only make some changes on the design. However, the principals and processes in this literature is still relevant.

Khezrnejad et al. (2015) studied whether the oil recovery by injection of nanofluids is due to changes in the mobility ratio or effects of enhanced surface chemistry. The change in mobility ratio would be due to increased water viscosity, and effects on surface chemistry would be due to reduction in interfacial tension. The micromodel used had a pore volume of 1.15 $cm^3$, making it larger than the one used in this master thesis. The micromodel also had a more uniform network as shown in figure 2.1. The authors used silica and alumina nanoparticles, and compared them with polymer injection. The results showed that surface chemistry plays an important role when using nanofluids compared to polymers as the IFT is reduced between oil and water.

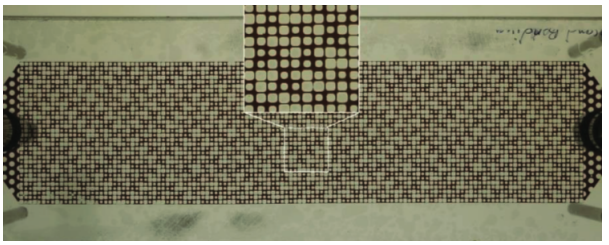

**Figure 2.1:** Micromodel used in experimental study by Khezrnejad et al. (2015).

Another study investigated the nanoparticles' role in mobilizing the trapped oil droplets in a porous media by direct observation in microfluidic structures (Xu et al., 2015). Silica nanoparticles with varying concentrations and rates were used also in this study. The results showed that an increase in nanoparticle concentration could decrease the required flow rate needed to push out a certain oil droplet for a fixed geometry. In addition, the authors concluded with the fact that the nanofluid had a similar effect as surfactants, by reducing the trapped oil size through reduction in IFT.

Avraam and Payatakes (1995) measured pressure drops during the steady-state two-phase flow of oil and deionized water, and used Darcy's law to obtain relative permeability. The pressure drop was measured separately for each fluid phase, which was made possible by special pressure taps. This study investigated the flow regimes of the two-phase flow in a micromodel and tried to relate the flow phenomena observed with macroscopic quantities as relative permeability. Measuring pressure requires additional special equipment and work, but has the advantage of a more detailed presentation of the process. The experimental setup and how the pressure measurements are included is shown in figure 2.2:

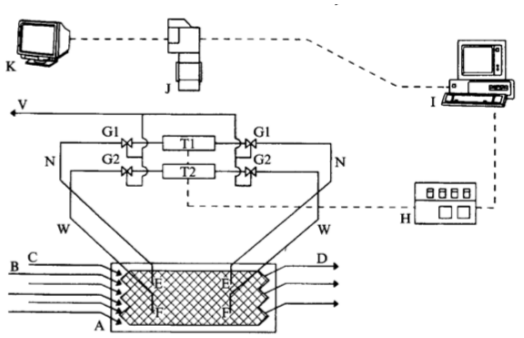


**Figure 2.2:** Micromodel used in experimental study by Avraam and Payatakes (1995). A shows the micromodel, while B and C are the inlet ports for the oil and water, respectively. D are the outlet ports for the fluids. E and F are pressure taps, while N and W are tubes connecting the pressure taps with the pressure transducers T1 and T2. H is the digital pressure indicator.

## 2.2 Nanocellulose

Many of the studies in the literature use silica nanoparticles in their experimental work. It seems like nanocellulose is not as widely used, and that the effects of these particles on EOR mechanism are not as well established as for silica. However, there are some literature where the EOR potential of nanocellulose is studied, which gives some indications on how nanocellulose can enhance the oil recovery.

Wei et al. (2016) studied the physical properties of modified nanocellulose (NC) and used a micromodel to study the oil recovery mechanisms. The nanocellulose used contained a small portion of surface active groups as well. Two types of this modified nanocellulsoe were investigated, both with the same chemical structure but different content of surface active groups. The micromodel used was less complex than the one used in the Avraam and Payatakes (1995) study, and pressure was not measured. The experimental setup is shown in figure 2.3, and is somewhat similar to the setup in this master thesis. Two main conclusions were drawn from the study concerning the use of nanocellulose for EOR purposes:

- The crude oil/nanofluid IFT could be reduced to the order of $10^{-1}$ mN/m for this particular nanofluid
- The nanofluids had a much slower viscosity loss at higher temperature compared to the polymer HPAM.

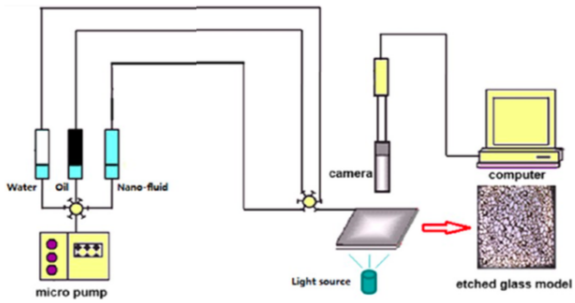


**Figure 2.3:** Micromodel used in experimental study by Wei et al. (2016).

Cellulose nanocrystals (CNC) have been studied through core flooding by Molnes et al. (2016). The core was a high-permeable (210 mD) sandstone, and CNC with different concentrations in low salinity water was injected. The following main conclusions were made:

- CNC showed good injectivity in the high-permeable core for all concentrations used.
- CNC showed good colloidal stability in low salinity water.
- CNC behaved as a Newtonian fluid, and the viscosity was independent of shear rate. A slight decrease in viscosity was observed when increasing the salt concentration.

Kusanagi et al. (2015) studied the EOR potential of TEMPO-CNF through core flooding experiments with Berea sandstone. The nanocellulose was injected tertiary with a concentration of 0.1 %, which is similar to the concentration used in thesis. Purified water was used to dilute TEMPO-CNF, while API brine was used to saturate the core.

The following results and conclusions were made:

- Additional oil was recovered by use of CNF.
- The suspensions of CNF with a higher concentration than 0.1 % showed a clear shear thinning effect, so that viscosity was decreased with increasing shear rate. CNF has high tensile strength, and the suspension could regain its original high viscosity after experiencing shear stress. Figure 2.4 shows the shear viscosity of CNF for different concentrations.
- Poor injectivity into the sandstone core was observed. The structural factors of this type of cellulose were believed to be the explanation, and could result in filtration in the porous media.
- The dispersion stability of CNF was sensitive to the electrolyte concentration in the porous media. The core was previously saturated with water containing sodium, calcium and magnesium ions, which would result in CNF aggregating. The salinity tolerance of CNF should be improved for CNF to have EOR potential in the oil industry.

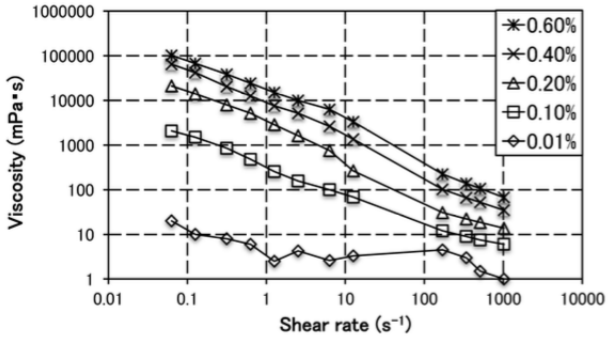


**Figure 2.4:** Shear viscosity of CNF suspension at different concentrations (Kusanagi et al., 2015)

This literature study shows that there has been several different experiments performed using microfluidics devices. Some experiments use complex models and can analyze flow regimes and calculate several properties, while others are less complex. The literature review also implies that nanocellulose could have potential as a green EOR method.

Chapter 3

# Theory

The theory in section 3.1-3.5, 3.7 and 3.8 is written as a part of the specialization project (Salvesen, 2017). Some changes have been made in some of the sections before including this theory. Theory has been added to the subsections 3.2.4, 3.3.1 and 3.5.2.

## 3.1 Enhanced oil recovery

A producing reservoir goes through different stages during its lifetime, and the recovery of the hydrocarbons can be divided into three phases: primary, secondary and tertiary recovery. Primary recovery is driven by the natural mechanisms of the reservoir, and no additional fluids are injected. Examples of these natural mechanisms are rock and fluid expansion, solution gas, water influx, gas cap and gravity drainage (Sheng, 2010). Secondary recovery is defined as recovery by injection of additional fluids as water or gas. The main purpose of injecting additional fluids is to maintain pressure and volumetric sweep efficiency. Tertiary recovery includes injection of special fluids as chemicals, miscible gasses and thermal energy (Sheng, 2010).

The term enhanced oil recovery covers techniques that go beyond the utilizing of only primary recovery, and is a possible solution to declining oil production (Sheng, 2010). The definition of enhanced oil recovery as stated by Schlumberger oilfield glossary (Schlumberger, 2018a) is: ”A stage of hydrocarbon production that involves sophisticated techniques to recover more oil”. Schlumberger also states that the global average recovery factor for a typical oilfield is approximately 40 %, which means that large amounts of discovered oil is left behind (Schlumberger, 2018b). There is a need to improve this recovery factor and accelerate further production, which is the main driver behind EOR projects. Enhanced oil recovery includes a range of different techniques, and can be divided into three main categories: thermal recovery, gas injection and chemical injection (DOE, 2017). All these techniques have shown success in varying degree and have their advantages and disadvantages.

## 3.2 Some current enhanced oil recovery techniques

### 3.2.1 Chemical injection

#### Polymer injection

Polymers are long-chained molecules that are added to water to increase the water viscosity, which is done to improve sweep efficiency (Npd, 2018a). A commonly used polymer is hydrolyzed polyacrylamide (HPAM) (Sheng, 2010). The use of polymers to enhance oil recovery on the Norwegian continental shelf has only been studied by injectivity tests, and is not an operating EOR technique as of today. This is mainly due to the fact that Norwegian authorities require that no environmentally harmful water is discharged to the sea. Norway is a part of the OSPAR agreement to protect and conserve the North-East Atlantic and its resources (Selle et al., 2013). Polymer injection is a more common practice in other parts of the world, where China is one example (Sheng, 2010).

#### Surfactant injection

Surfactants can be added to water to change the wettability of the system, and to reduce the interfacial tension between water and oil (Npd, 2018a). This may lead to mobilizing of the residual oil, as will be discussed later in this thesis. Surfactants are usually organic compounds that have a hydrocarbon chain which is hydrophobic, and a polar hydrophilic group. Surfactants are often classified based on the ionic nature of the polar hydrophilic group, as anionic, cationic, nonionic and zwitterionic. Anionic surfactants are the most widely used surfactants because of their relatively low adsorption on sandstone rocks, as the surface charge of sandstone is negative (Sheng, 2010).

As for polymer injection, no fields on the Norwegian continental shelf has been flooded by surfactants. Due to adsorption of surfactants on the rock surface, a large concentration is usually needed. Surfactants are expensive and some of them are toxic as well. Polymers are often injected together with surfactants to reduce the adsorption and costs, and to improve the surfactant performance (Skår, 2014).

#### Alkaline injection

Alkaline flooding is performed by adding alkali to the water. Sodium hydroxide and sodium carbonate are the most commonly used alkalis. These alkalis react with the organic acids in the oil and produce surfactants. Alkali can reduce the surfactant adsorption so that a smaller surfactant concentration is needed (Sheng, 2010).

### 3.2.2 Gas injection

Gas injection has been performed on the Norwegian continental shelf to improve oil recovery since 1975. Gas was originally re-injected into the reservoir simply because pipes that could transport the gas away did not exist (Npd, 2018c).

Natural gas, $CO_2$, nitrogen and air can be injected into the reservoir. Injection of nitrogen and air has huge reservoir and safety issues. Injection of natural gas has contributed to higher recovery on the Norwegian continental shelf, and has been used with alternating injection of water and gas (Npd, 2018d). Injection of $CO_2$ has been used for pressure support for many onshore reservoirs. As Norway only has offshore reservoirs, there are issues related to infrastructure and logistics. The gas has to be transported over a long distance for the injection of $CO_2$ from onshore industries. $CO_2$ injection has only been used for reservoirs with naturally occurring $CO_2$ on the Norwegian continental shelf, but the main issue has been the lack of access to gas (Npd, 2018b). $CO_2$ injection has been used primarily in the United States, as many of these reservoirs has naturally occurring $CO_2$ (Npd, 2018d).

### 3.2.3 Thermal recovery

Thermal recovery includes the adding of heat to lower the viscosity of oil, which can be achieved by injecting steam. As the reservoirs on the Norwegian continental shelf already has relatively high temperatures, this method is not used. However, the technique accounts for over 40 $\%$ of the enhanced oil recovery production in the United States (DOE, 2017).

### 3.2.4 Low salinity water injection

Low salinity water (LSW) injection is a technique that does not fall under chemical, thermal or gas injection. It is a type of water injection, but conventional seawater is not used. A salt concentration between 0.02 $\%$ and 0.8 $\%$ is generally said to be low salinity. Studies have shown that injection of low salinity water instead of conventional high salinity seawater improves the oil recovery (Arab and Pourafshary, 2013). LSW flooding changes the rock wettability towards more water-wet. Low salinity water typically has a lower ion concentration than the rock surface, and tends to exchange cations with the rock surface. This makes the rock surface more negative and decreases the electrostatic attractive forces between the rock surface and the crude oil. When the attractive forces between the surface and oil is lowered, more oil can be released (Arab and Pourafshary, 2013).

There are some challenges related to low salinity water injection as well. There exists a critical salt concentration in water sensitive sandstone. If the concentration falls below this critical limit, tiny particles start to migrate through the medium and can be trapped at pore sites (Arab and Pourafshary, 2013). This is known as formation damage and may result in less oil recovery. Hence, the water salinity should be low enough to improve the oil recovery but high enough to avoid formation damage. The adding of nanoparticles to low salinity water is in fact proposed as a solution to this issue. The nanoparticles could strengthen the attractive forces between the colloidal particles and the rock surface. This could make the colloidal particles attach on the rock surface and prevent them from migrating into the porous medium (Arab and Pourafshary, 2013).

## 3.3 Reservoir and fluid properties

### 3.3.1 Viscosity

The viscosity of a fluid is a parameter that describes the fluids resistance to flow, a fluid with low viscosity flows better than a fluid with high viscosity. The viscosity can be presented as dynamic or kinematic viscosity. Dynamic viscosity is given by Newton's law of friction presented in equation 3.1, which defines the shear stress. This shear stress is between fluids that is non-turbulent and Newtonian, and the dynamic viscosity represents the liquid's inner resistance to flow (Andreassen, 2015). All units are reported in SI for the equations presented in this thesis. However, there might be other more practical units for the experimental use of the equations.

$$\tau = \mu \frac{dc}{dy} \tag{3.1}$$

Where:
$\tau$= shear stress $[Pa]$.
$\mu$= dynamic viscosity $[Pa\ s]$.
$dc$= liquid velocity $[\frac{m}{s}]$.
$dy$= distance between layers $[m]$.

The SI unit of viscosity is $Pa\ s$, but viscosity is frequently expressed in centipoise ($cp$) in the oil industry, 1 $cp$=$10^{-3} Pa\ s$. The kinematic viscosity is defined as the ratio between dynamic viscosity and density (Andreassen, 2015):

$$\nu = \frac{\mu}{\rho} \tag{3.2}$$

Where:
$\nu$= kinematic viscosity $[\frac{m^2}{s}]$.
$\rho$= density $[\frac{kg}{m^3}]$.

As seen from equation 3.1, the viscosity is related to the shear stress. Shear is an important property that defines the fluid behavior. Fluids can be divided into two categories based on their behavior related to shear: Newtonian and non-Newtonian fluids (Al-Zahrani, 1997). Newtonian fluids are fluids that have a proportional relationship between the shear stress and shear rate, while non-Newtonian fluid exhibits a non-linear relationship. Some fluids are shear thinning fluids, which means that the viscosity decreases with increasing shear rate (Al-Zahrani, 1997). The following equation gives the shear rate in a porous media (Lake et al., 1989):

$$\gamma = \frac{4q}{A\sqrt{8k\phi}} \tag{3.3}$$

Where:
$\gamma$= shear rate [$\frac{1}{s}$].
$q$= volumetric flow rate [$\frac{m^3}{s}$].
$A$= cross-sectional area of the porous medium [$m^2$].
$k$= single phase permeability [$m^2$].
$\phi$= porosity.

### 3.3.2 Porosity

Porosity is a very important property of the reservoir as it is a measure of how much fluid the formation can hold. Equation 3.4 defines porosity (Torsæter and Abtahi, 2003):

$$\phi = \frac{pore\ volume}{bulk\ volume} = \frac{bulk\ volume - grain\ volume}{bulk\ volume} \tag{3.4}$$

Porosity can be presented in two different ways: total and effective porosity. Total porosity considers all the pores in a rock, while effective porosity only considers the pores that are interconnected. This means that the effective porosity is especially important in reservoir engineering, as this porosity is the amount of fluid that can be produced (Torsæter and Abtahi, 2003).

Porosity is dependent on grain size distribution, how much the rock is cemented and how the grains are arranged. If the reservoir rock has uniform grain size distribution, the grain size will not affect the porosity. However, most real reservoir rocks do not have a uniform distribution of grain size (Torsæter and Abtahi, 2003).

### 3.3.3 Surface and interfacial tension

Surface tension is a force that works to minimize the free surface of a liquid. Interfacial tension is a similar force, but exists when two liquids are in contact (Torsæter and Abtahi, 2003). This is the force that holds the surface of a phase together, and it works to decrease the area of interface (Rajagopalan and Hiemenz, 1997). The interfacial tension is a function of pressure, temperature and the composition of the phases (Petrowiki, 2017). The SI unit of surface and interfacial tension is Newton/meter, but dyne/cm is also often used, where 1 mN/m= 1 dyne/cm.

Figure 3.1 shows a spherical cap that is influenced by interfacial tension and two normal pressures. The interfacial tension ($\sigma$) will reduce the size of the sphere unless the pressure difference between $p_1$ and $p_2$ is large enough. This effect can be described by the Young-Laplace equation shown in equation 3.5, which is the mechanical equilibrium of an arbitrary surface (Torsæter and Abtahi, 2003). Figure 3.2 shows a pendant drop affected by a hydrostatic pressure p, and the radius $r_1$ and $r_2$ is shown. This photo is included to show $r_1$ and $r_2$, the pendant drop will be discussed in more detail later.

$$p_2 - p_1 = \sigma(\frac{1}{r_1} + \frac{1}{r_2}) \tag{3.5}$$

Where:
$p_1$= pressure on the convex side $[Pa]$.
$p_2$= pressure on the concave side $[Pa]$.
$r_1$ and $r_2$= inner and outer radii of curvature $[m]$.
$\sigma$= interfacial tension $[\frac{N}{m}]$.

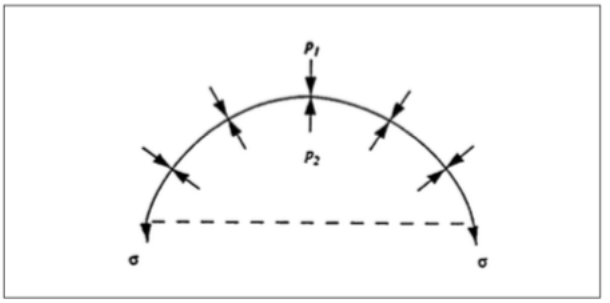


**Figure 3.1:** Capillary equilibrium of a spherical cap (Torsæter and Abtahi, 2003).

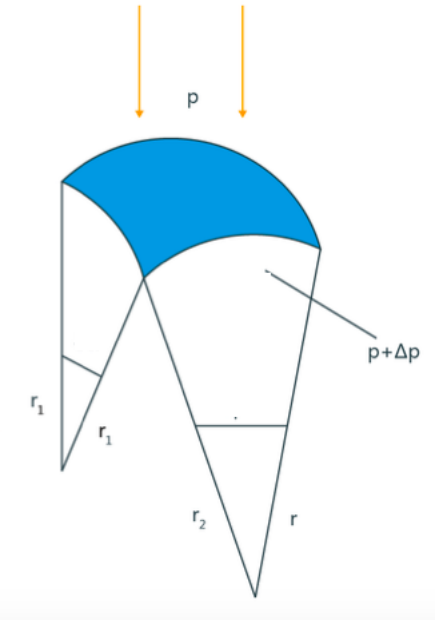


**Figure 3.2:** Sketch showing the inner and outer radii of curvature, modified from KRÜSS (2017b).

### 3.3.4 Wettability and contact angle

The wettability is the preference of a solid to contact the wetting phase rather than the other phase, so that one fluid spread on the surface (Schlumberger, 2018c). The different wettability systems can be defined based on the contact angle. The contact angle ($\theta$) is defined as the angle that is formed where the three phases meet, measured in the phase with the highest density (Rajagopalan and Hiemenz, 1997). Figure 3.3 shows the contact angle measured in the water phase. The wetting condition is said to be water-wet when the contact angle ranges from $0°$-$70°$, intermediate/neutral from $70°$-$110°$, and oil-wet from $110°$-$180°$. A contact angle of $0°$ describes a completely water-wetted system, $90°$ a neutral system, and $180°$ a completely oil-wetted system, measured in the water (Torsæter and Abtahi, 2003). The upper and lower limits of the scale is not definite, and there exists several similar definitions.

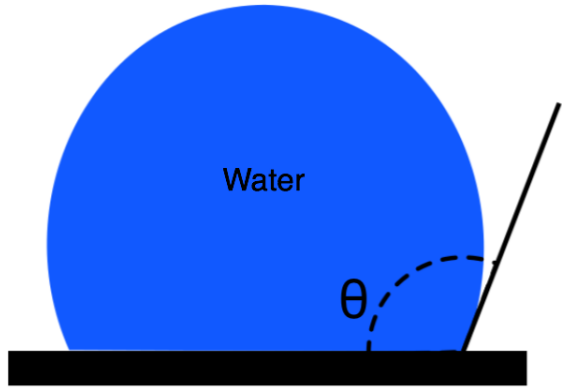


**Figure 3.3:** Sketch of a droplet of water, showing the contact angle ($\theta$) measured in the water.

### 3.3.5 Capillary pressure

Capillary pressure represents the pressure difference between two fluids in a thin tube, and is defined by the Young-Laplace equation presented in equation 3.5. This pressure difference is the difference between the non-wetting and wetting phase (Torsæter and Abtahi, 2003):

$$P_c = P_{non-wetting} - P_{wetting} \tag{3.6}$$

Where $P_c$ is the capillary pressure. The wetting phase is identified by its ability to diffuse across the capillary walls before the non-wetting phase (Torsæter and Abtahi, 2003). The SI unit of capillary pressure is the SI unit for pressure: Pascal.

### 3.3.6 Permeability and relative permeability

Permeability is another important property of a reservoir, and it can be presented as absolute, effective and relative permeability. Absolute permeability refers to 100 $\%$ saturation of one fluid. Absolute permeability defines the fluids capacity to flow through a porous media, and is defined by Darcy's law (Darcy, 1856):

$$q = -\frac{kA}{\mu}\frac{\Delta P}{L} \tag{3.7}$$

Where:
$\Delta P$= pressure drop [$Pa$].
$L$= length [$m$].

The SI unit of permeability is $m^2$ but the unit Darcy is often used, where 1 Darcy= $10^{-12}$ $m^2$. Effective permeability is the permeability of a porous material when there is more than one fluid present. Relative permeability is defined as the ratio of effective permeability to the absolute permeability as seen in equation 3.8 (Torsæter and Abtahi, 2003):

$$k_{ri} = \frac{k_i}{k} \tag{3.8}$$

Where:
$k_{ri}$= relative permeability of fluid i, unitless.
$k_i$ = effective permeability of fluid i [$m^2$].
$k$= absolute permeability [$m^2$].

The relative permeability is often presented as a function of saturation. The terms imbibition and drainage are introduced to describe the saturation history. Imbibition describes the case where the wetting phase increases in magnitude, drainage is when the wetting phase decreases in magnitude. Figure 3.4 shows the drainage and imbibition curves for relative permeability, where water is the wetting phase. $S_{wi}$ is the irreducible water saturation, while $S_{or}$ is the residual oil saturation. The endpoint saturations in figure 3.4 are directly related to the oil recovery in the way that they determine the movable saturation range. The smaller the saturation of one phase is, the less mobile it is (Torsæter and Abtahi, 2003).

#### Mobility

Mobility describes the ability to move, and mobility control is an important concept in enhanced oil recovery. Mobility control is based on the desire to maintain a favorable mobility ratio to improve sweep efficiency. The displacing fluid mobility should be equal to or less than the total mobility of displaced multiphase fluids. The mobility ($\lambda$) is defined as the ratio of effective permeability to the viscosity of the phase (Sheng, 2010):

$$\lambda = \frac{k_i}{\mu} \tag{3.9}$$

Mobility ratio is defined as the ratio of the displacing phase mobility to the displaced phase mobility:

$$M_r = \frac{\lambda_w}{\lambda_o} \tag{3.10}$$

Equation 3.10 shows the case where water is displacing oil. It is stated that $M_r \leq 1$ is favorable, while $M_r \geq 1$ is unfavorable (Sheng, 2010).

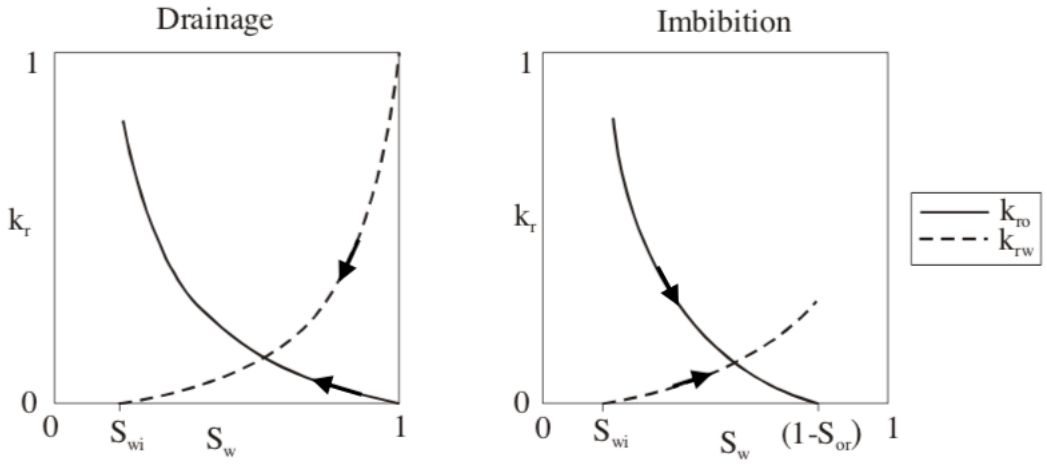


**Figure 3.4:** Drainage and imbibition curves for relative permeability, modified from Torsæter and Abtahi (2003).

## 3.4 Nanotechnology

A huge amount of research has been performed on nanotechnology since the 1980s, and it has developed into being a field that attracts great interest among scientists. Nanotechnology shows great potential in a variety of disciplines, and is believed to introduce many new applications in the future. The unique properties of the nanomaterials is the reason for the great interest in nanotechnology in modern research. The oil industry is among the many disciplines that has been involved in the development of this new technology, and the use of nanoparticles to enhance oil recovery is one of these areas (Negin et al., 2016).

### 3.4.1 What is nanotechnology?

Das et al. (2007) defines nanotechnology as follows: "The construction of functional material, devices and systems by controlling matter at the nanoscale level, and the exploitation of their novel properties and phenomena that emerge at that scale". Nanomaterials have unique mechanical, optical, electrical, magnetic and thermal properties, which make them behave different than other materials. A nanometer is defined as $10^{-9}$ m, and nanoparticles are usually described to have dimensions in the order of 100 nm or less (Negin et al.,

2016). Nanofluids are made by mixing nanoparticles in a heat transfer fluid such as water, oil or ethylene glycol. These fluids with nanoparticles have properties superior to the original fluids. The goal is to achieve the most desired properties at the smallest possible concentrations (Das et al., 2007).

### 3.4.2 Properties of nanoparticles

Solids are usually added to fluids to improve their properties and behavior. The size of the solid particles causes some problems when they are added to fluids. These are problems as clogging, erosion and settling of the large particles (Das et al., 2007). The small size of the nanoparticles can overcome these problems. Another unique property and advantage of nanoparticles are their high surface/volume ratio. The surface area of the nanoparticles is much higher than their interior. This means that the contact surface between the nanoparticles and other phases is large, allowing for better interaction (Youssif et al., 2017).

### 3.4.3 Structure of nanoparticles

A nanoparticle consists of a core and a thin shell. The shell is built up by a tail group, a hydrocarbon chain and an active head group (Hendraningrat et al., 2013a), as seen in figure 3.5. The active head group is located on the side of the hydrocarbon chain that is in contact with the core. All of these regions do not have to be present in every specific case of a nanoparticle. The hydrocarbon chain protects the nanoparticle, which can be long or short. This chain is long for a polymer, or non-existing for an ion. The solubility of the nanoparticle is determined by the chemical structure of the shell. A nanoparticle can be lipophobic and hydrophilic (LHP) dissolved in a polar solvent, or lipophilic and hydrophobic (HLP) dissolved in a non-polar solvent. Water is a polar solvent, while toluene is a non-polar solvent (Hendraningrat et al., 2013a). The above terms are related to the affinity of the particle's surface to the continuous phase. The original terms are lyophilic and lyophobic which literally means "solvent loving" and "solvent fearing". Hydrophilic and hydrophobic refers to the case where the solvent is water, while lipophilic and lipophobic is related to the ability to dissolve in a lipid (non-polar organic components) (Rajagopalan and Hiemenz, 1997).

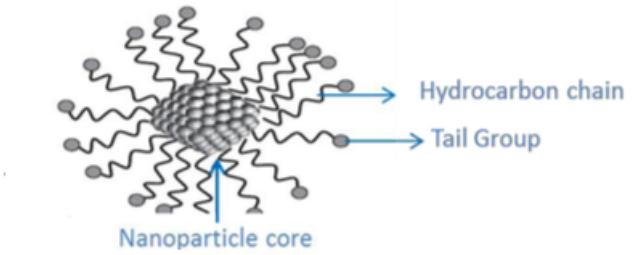


**Figure 3.5:** Illustration of the structure of a nanoparticle (Das et al., 2007).

### 3.4.4 Stability of nanofluids

The term stability of small particles in dispersion is often used for kinetic stability. A nanoparticle dispersion that is stable against coalescence or aggregation is called kinetically stable (Rajagopalan and Hiemenz, 1997). Coalescence is the process where at least two small particles form a single large particle, and the total surface area is reduced. Aggregation is the process where small particles clump together, but does not form a new particle. The competition between the repulsive and attractive forces determines whether the nanoparticle dispersion is stable or not. Whether or not a stable system is desirable depends on the context and application of the nanoparticle dispersion (Rajagopalan and Hiemenz, 1997). Stability is usually wanted in enhanced oil recovery because aggregates can block the pore sites.

## 3.5 Nanofluids in enhanced oil recovery

### 3.5.1 Nanocellulose

Cellulose is a naturally occurring material, and it is renewable, biodegradable and non-toxic (Dufresne, 2013). Purification of cellulose from plant fibers can be done to extract nanoparticles. The term nanocellulose covers materials derived from cellulose with at least one dimension in the nanometer range. Cellulose nanofibrils (CNF) and cellulose nanocrystals (CNC) are two types of nanocellulose that might have potential for EOR purposes. CNF are fibrils with length in the micrometer scale and width in the nanometer scale (Salas et al., 2014). Hence, they have a high length/width ratio. These nanofibrils contains both crystalline and amorphous cellulosic regions. Crystallinity usually makes the particles strong and brittle, while amorphous regions gives toughness in the way that they can bend without breaking. CNC has a lower length/width ratio than CNF, and is prepared from fibrils in a way that degrades the amorphous region, making CNC highly crystalline nanoparticles (Salas et al., 2014).

As nanocellulose is carbon-neutral, sustainable, recyclable and non-toxic, it has the potential to be a completely green nanofluid for use in enhanced oil recovery (Salas et al., 2014). Nanocellulose could therefore be a green alternative to the EOR techniques described in section 3.2.

### 3.5.2 Enhanced oil recovery mechanisms

The injection of nanofluids can enhance oil recovery in different ways. These mechanisms includes the important reservoir and fluid properties described previously.

#### Increased seawater viscosity

When water reaches the water break-through, the additional injected water follows the water paths without pushing more oil out, which can be due to the viscosity difference between oil and water (Aurland, 2015). Oil is more viscous than water, and the water will flow through the reservoir without pushing the oil out. The injection of nanofluids can alter

the viscosity of seawater, and more oil can be pushed out (Aurland, 2015). This can be related to the mobility described section 3.3.6. Mobility control can be achieved through injection of nanofluids to change displacing fluid viscosity (Sheng, 2010). By increasing the water viscosity, the water mobility will be reduced as seen from equation 3.9. As a result, the mobility ratio will be lowered. If the mobility of the oil phase is equal to or larger than the mobility of water, the mobility ratio will be equal to or lower than 1. As described earlier, this is favorable for enhanced oil recovery. However, the mobility is not only affected by viscosity but also permeability.

**Decreased interfacial tension**

Interfacial tension can cause a lot of oil to be left behind in the reservoir. Some oil is still trapped in well-swept zones after waterflooding due to a competition between the viscous and capillary forces. The viscous forces mobilize the oil, while the capillary forces trap the oil (SINTEF, 2011). The ratio between the viscous and capillary forces can be described by the capillary number. The capillary number is a dimensionless ratio between these two forces, shown in equation 3.11. As the capillary number increases, the residual oil saturation decreases. The capillary number has to be higher than a critical capillary number for the residual oil saturation to decrease. Hence, the interfacial tension must be lowered sufficiently to achieve this high capillary number (Sheng, 2010). The capillary number can be used to determine whether the flow is dominated by viscous or capillary forces. If the capillary number is less than $10^{-5}$, the flow is usually said to be capillary dominated. If the capillary number is large, the flow is viscous dominated. There exists a transition between those flow regimes as well, where both forces contribute (Chatzis et al., 1984).

$$N_C = \frac{v\mu}{\sigma cos\theta} \tag{3.11}$$

Where:
$N_C$= capillary number, unitless.
$v$= pore flow velocity [$\frac{m}{s}$].

As described in section 3.3.5, the capillary pressure is the pressure difference between the non-wetting phase and the wetting phase. If this pressure is high, it means that the pressure of the non-wetting phase is higher than the pressure of the wetting phase. If water is the wetting phase, this high pressure will hinder the water from flowing into the pores and recover more oil. By decreasing the interfacial tension, the capillary pressure will decrease.

It is desirable to examine whether the interfacial tension between the nanofluid and oil will be lower than for water and oil. When nanofluids are injected into a core, there are hydrophilic parts of the nanoparticles present in the aqueous phase, and hydrophobic parts in the oil phase. The adhesive forces between these two phases will then increase, and the IFT will decrease (Youssif et al., 2017).

### Wettability and Contact angle changes

Reservoirs are often initially water-wet, as the initial fluid often is believed to be water. When oil migrates into the reservoir, the wetting state might change to oil-wet or intermediate-wet (Hendraningrat et al., 2013b). If a reservoir is oil-wet and contains matrix blocks or tiny pore throats that blocks the flow, the water cannot imbibe spontaneously into the blocks and displace the oil. The water will then follow the flow path around this trapped oil, and not sweep out more oil. By changing the wettability from oil-wet, this problem can be solved (Onyekonwu et al., 2010). On the other hand, the wetting state can be reversed from water-wet towards oil-wet. As a result, the discontinuous non-wetting residual oil will be converted to a continuous wetting phase, which will provide a flow path for the trapped oil (Gong et al., 2016).

The goal is often to change the wettability towards a more water-wet system. Studies has reported that water-wet formations produce better than oil-wet formations, and intermediately-wet formations produce better than water-wet formations (Ogolo et al., 2012). However, different formations perform differently, so the most important thing is to change the rock's wettability to an ideal state. Different types of nanoparticles can change the wettability in different ways, so it is important to use the right nano-agent to get the desired wettability.

Wedge film

A special mechanism known as the wedge film is related to the wettability of the system. Nanoparticles can be used to create a wedge film that will separate the oil droplet from the rock surface, as seen in figure 3.6. The fluids ability to spread along the surface is related to the structural disjoining pressure, which is due to imbalance of the interfacial forces among the three phases present. The structural disjoining pressure is related to the difference between the pressure in the wedge film and the pressure in the bulk liquid. This pressure is driven by the Brownian motion and electrostatic repulsion between the particles. The repulsion is greater when the nanoparticles are smaller (Youssif et al., 2017). Brownian motion refers to particles and molecules in constant random thermal motion (KRÜSS, 2017d).

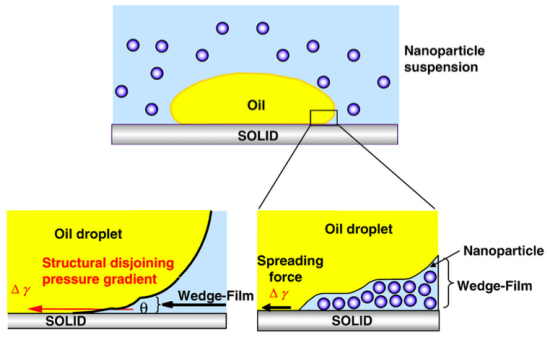


**Figure 3.6:** Illustration of the creation of the wedgefilm (Wasan et al., 2011).

## 3.6 Microfluidics

### 3.6.1 General theory and history

Microfluidics is a method where the flow of fluids is studied at the micrometer scale. Stone et al. (2004) defines microfluidics as "Devices and methods for controlling and manipulating fluid flows with length scales less than a millimeter". The field of microfluidics started to develop in the late 1980s, as the technology for building these systems was available. This was the beginning of the micro-electromechanical systems (MEMS), which were able to use electronic and mechanical elements together in a common system. This technology was also used to create the microfluidics devices (Atencia and Beebe, 2004). The motivation behind this new technology arose mostly from the field of biology, where it was a need to control fluids at the cellular length scale. It was also desirable to examine fluids with tools that is cheap and require small sampling volumes, which is desirable in many disciplines (Atencia and Beebe, 2004).

The flow of fluids in a porous media is important in several disciplines, so the use of microfluidics devices has potential for a wide range of fields. Examples of areas where the application of microfluidics systems is possible are biotechnology, chemical synthesis, analytical chemistry, geologic $CO_2$ sequestration, enhanced oil recovery and water infiltration into soil (Psaltis et al., 2006), (Zhao et al., 2016). When shrinking a system to a small size, other mechanisms are important compared to the macrometer scale. Diffusion, surface tension and viscosity are the dominating phenomena at the micrometer scale, while gravity and inertia becomes less dominant. This results in systems that behave differently from the macrometer world, which has to be remembered when studying fluids at the micrometer scale (Atencia and Beebe, 2004).

### 3.6.2 Microfluidics for enhanced oil recovery

Enhanced oil recovery is one of the fields were the application of microfulidics devices is of great interest. These devices gives the opportunity to study the flooding of fluids at the micrometer scale. It is desirable to study the fluid flow at this length scale, as the actual flow in reservoirs happens in tiny pores. Microfluidics uses a microchip to simulate the pore network instead of a core sample. This small chip can have random or uniform pore distribution, and there is an inlet and outlet enabling the fluids to flow through the microchip. As the volumes are small, the sampling time is often shorter than for conventional core flooding. This flow is often performed together with optical measurements, by placing the microchip under a microscope while flooding. The flow can then be analyzed visually, and the oil saturation can be calculated. The detailed description of the procedure will be addressed in chapter 4.

## 3.7 Theory behind experimental measurements

### 3.7.1 The pendant drop method

The pendant drop method calculates the interfacial tension based on the shape of the drop. Small drops of liquid tend to be spherical because surface forces depends on area (Torsæter and Abtahi, 2003). As a consequence of the interfacial tension between the inner and outer phase of the drop, an increased pressure is produced inside the drop (KRÜSS, 2017b). This pressure difference is given by the Young-Laplace equation presented in subsection 3.3.3.

The drop is deformed under the effect of gravity, and a hydrostatic pressure is formed inside the drop due to its weight, which affects $r_1$ and $r_2$. The hydrostatic pressure is dependent on the height, so the curvature of the drop changes in the vertical direction and gives the characteristic shape of the pendant drop (KRÜSS, 2017b). Surface tension and gravity forces are the two forces that in particular affects the shape of the drop. The surface tension tries to minimize the surface area and make the drop shape spherical, while gravity stretches the drop from the spherical shape (DataPhysics, 2018).

The method uses the experimentally measured shape dependent quantity in equation 3.12, which determines the degree of deviation from the shape of a sphere. Figure 3.7 shows the relationship between the dimensions in equation 3.12, where $d_e$ is the equatorial diameter and $d_s$ is the diameter measured distance $d_e$ from the bottom of the drop (Torsæter and Abtahi, 2003).

$$S = \frac{d_s}{d_e} \tag{3.12}$$

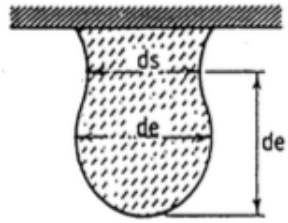


**Figure 3.7:** Relationship between the dimensions of a pendant drop (Torsæter and Abtahi, 2003).

If the density difference between the two fluids is known, interfacial tension can be calculated by the following equation (Torsæter and Abtahi, 2003):

$$\sigma = \frac{\Delta \rho g d_e^2}{H} \tag{3.13}$$

Where:
$\Delta\rho$= density difference of the two phases [$\frac{kg}{m^3}$].
$g$= gravity of the Earth [$\frac{m}{s^2}$].
$H$= shape determining variable, the relationship between $H$ and $S$ is determined empirically.

### 3.7.2 The sessile drop method

A commonly used method to measure the contact angle is by measuring the angle directly for a drop of liquid resting on a plane surface. The sessile drop is the standard arrangement when doing optical measurement of the contact angle with drop shape analysis (KRÜSS, 2017c). An enlarged image shows the dimensions of the sessile drop, and the contact angle can be determined in the three phase intersection.

### 3.7.3 Dynamic light scattering

Measuring the size is important in the process of characterizing the nanoparticles. Since the dimensions are very small, there are some special tools that can be used for this purpose. Dynamic light scattering is a method that can yield values for the size and size distribution of nanoparticles (Bhattacharjee, 2016).

The principle of dynamic light scattering is based on the particle's Brownian motion. Particles in this Brownian motion diffuse at a speed related to their size, and smaller particles diffuse faster than larger particles. To measure this diffusion speed, the pattern produced by illuminating the particles with a laser is observed and detected. The scattering intensity will fluctuate with time. These intensity changes are analyzed and generate a correlation function. Finally, this curve is analyzed to give the size and size distribution of the nanoparticles (KRÜSS, 2017d).

## 3.8 Error calculations

When doing experimental measurements, it can be useful to determine the error to get a sense of how reliable the measurements are. If multiple measurements are done, the error between those measurements can be calculated. A common method used to calculate this error is the standard error given by the following equation (Kenney and Keeping, 1951):

$$Error = \frac{\sigma}{\sqrt{N}} \tag{3.14}$$

Where $\sigma$ is the standard deviation given by equation 3.15, and $N$ is the number of measurements taken. The $\sigma$ in this equation should not be confused with interfacial tension which is also denoted by $\sigma$.

$$\sigma = \sqrt{\frac{1}{N-1}\sum(x_i - \bar{x})^2} \tag{3.15}$$

$x_i$ is the measured value i, where i goes from 1 to $N$. $\bar{x}$ is the average of all the N values measured.

Chapter 4

# Experiment

## 4.1 Materials

### 4.1.1 Fluids

#### Nanocellulose

Two types of nanocellulose were used in the experiments: cellulose nanocrystals (CNC) and TEMPO- cellulose nanofribrils (TEMPO-CNF). CNC was purchased from the University of Maine and delivered in a gel-form with a concentration of 12.18 %. TEMPO-CNF was provided by RISE PFI in a water solution with a total solid content of 0.66%.

#### Water and crude oil

A salt water solution with 0.1 wt% NaCl was used for the waterflooding and to saturate the microchip prior to flooding. 0.1 wt% NaCl was also used to mix the final solution of the nanofluids. The oil used was crude oil C provided by Equinor. Table 4.1 presents the density of the different fluids used in the experiments.

**Table 4.1:** Density of fluids used in the experiments.

| Fluid | Density [g/mL] |
|---|---|
| NaCl | 1,00 |
| CNC | 1,00 |
| TEMPO-CNF | 1,00 |
| crude oil C | 0,92 |

### 4.1.2 Microchip

The microchips used were EOR chips provided by Micronit. All microchips used in the experiments has a physical rock network, which means that the pores are randomly placed throughout the chip to resemble an actual pore network. An illustration of the microchip showing inlet, outlet and pore network is shown in figure 4.1. The microchip is made of borosilicate glass. Table 4.2 summarizes some other important properties of the microchip (Micronit, 2018).

**Table 4.2:** Microchip information.

| | |
|---|---|
| Permeability [Darcy] | 2,50 |
| Chip thickness [$\mu$m] | 1800 |
| Chip size [mm$^2$] | 45x15 |
| Porosity | 0,57 |
| Rock pore volume [$\mu$L] | 2,3 |
| Total internal volume [$\mu$L] | 5,7 |
| Flow area [mm$^2$] | 20x10 |

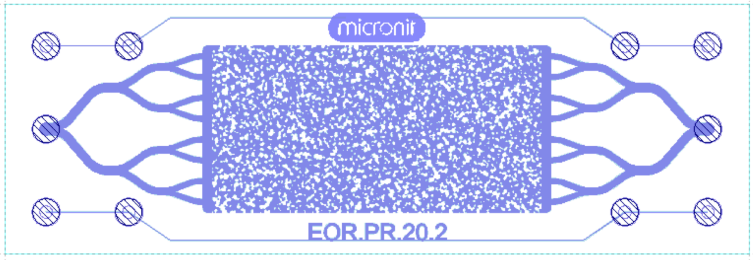


**Figure 4.1:** Illustration of the EOR physical rock microchip (Micronit, 2018).

## 4.2 Instruments

### 4.2.1 Microfluidics

A microfluidics apparatus was used for the flooding. Figure 4.2 shows a photo of the experimental setup. There are two syringe pumps, one for injection of oil and one for injection of water or nanofluids. The software OEMPump was used to manage the pump through the computer. The microscope is of the type Optika connected to a camera of the type Olympus UC90. The microchip is placed under the camera lens during injection, while the camera provides a live video of the process. The live video is seen through the software Stream Basic on the computer. A provided MATLAB code analyzes snapshots of the live video by comparing the yellow areas corresponding to the oil to the blank areas, and calculates oil saturation.

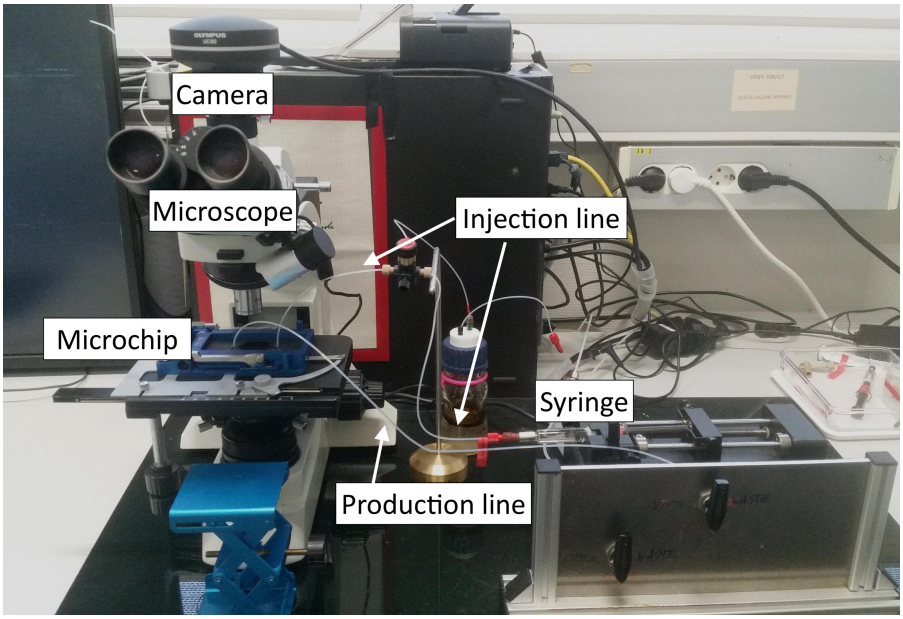


**Figure 4.2:** Photo of the experimental setup.

### 4.2.2 Drop Shape Analyzer DSA 100S

The apparatus used to measure the interfacial tension and contact angle in this thesis was the Drop Shape Analyzer DSA 100S, as can be seen in figure 4.3a. The interfacial tension measurements are based on the pendant drop method, while the contact angle measurements are based on the sessile drop, as described in chapter 3.

The Drop Shape Analyzer DSA 100S is a high-quality instrument that measures wetting processes, which can be used for multiple tasks related to wetting and adhesion (KRÜSS, 2017a). The apparatus gives the interfacial tension and contact angle values directly. The shape of the drop is controlled and analyzed by the corresponding software called ADVANCED software, to yield values for IFT or contact angle.

### 4.2.3 Zetasizer Nano ZS

The Zetasizer Nano ZS was the apparatus used to measure the size of the nanofluids, as can be seen in figure 4.3b. The apparatus uses dynamic light scattering, and the size is reported as the diameter of the particles (KRÜSS, 2017d).

### 4.2.4 Brookfield viscometer

A Brookfield viscometer DV-II+ Pro was used to measure the viscosity of the fluids. The viscometer rotates the spindle in the fluid sample over various of speeds and reports the torque and viscosity.

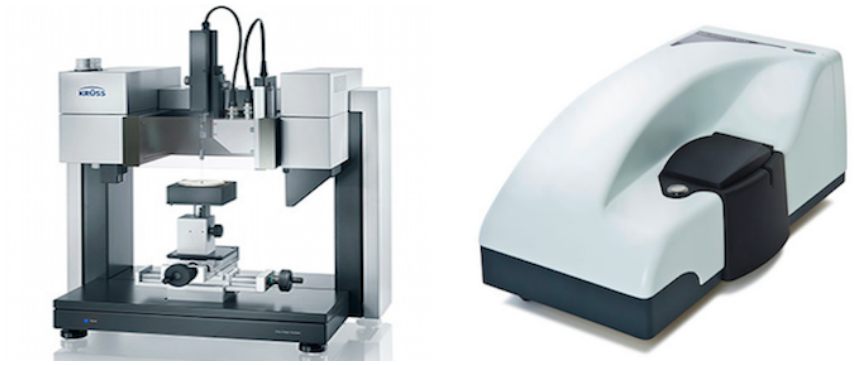

**(a)** **(b)**

**Figure 4.3:** (a) Drop Shape Analyzer DSA 100S (KRÜSS, 2017a). (b) Zetasizer nano ZS (KRÜSS, 2017d).

## 4.3 Preparations

### 4.3.1 Preparation of fluids

Solid NaCl was weighted and added to deionized water so that the solution contained 0.1 wt% NaCl. The solution was mixed in a magnet stirrer and filtrated through a 0.45 $\mu$m filter to make the final solution of water to be used in the experiments. The crude oil C was filtered twice using a 5 $\mu$m filter.

CNC was manufactured at the Forest Products Laboratory in Madison, USDA (U.S Dep. of Agriculture). The cellulose nanocrystals were produced using 64 % sulphuric acid to hydrolyze the amorphous regions. The final gel-like solution of CNC was delivered to the laboratory where the concentration was diluted to 1% CNC in 0.1 wt% NaCl. The solution was mixed using a ultra turrax for 1 minute to dissolve the gel as much as possible in the water.

The preparation of TEMPO-CNF was performed by RISE PFI. The term TEMPO means that the chemical TEMPO was used in the process of preparing CNF. The chemical formula for TEMPO is 2,2,6,6-tetramethylpiperidine-1-oxyl radical. The source cellulose material was never-bleached softwood pulp fibers. This source material was oxidized by TEMPO before being pretreated in a Mazuko-grinder prior to fibrillation. The fibrillation was done using a Rannie 15 type 12.56x homogenizer, fibrillated for 4 passes with a pressure drop of 1000 bar in each pass. The preparation of the final solution of 0.66% TEMPO-CNF was done using a sonikator. The sonikator used an amplitude of 20 % with 2 minutes as the effective time. However, all of these preparations were performed by RISE PFI. The final solution was delivered to the laboratory where the concentration was diluted to 0.1 wt% TEMPO-CNF in 0.1 wt% NaCl.

### 4.3.2 Testing of rates

Three test runs were performed prior to the actual experiments. Water was flooded through a microchip with different types of rates to see if the oil saturation would stabilize. As tertiary flooding was planned, a stabilization of the oil saturation prior to the nanofluid injection was wanted. These tests were performed to choose an appropriate rate for the waterflooding in the actual experiments, and the results were used to argue why the specific rates were chosen. It should be noted that these test runs were performed using the initial experimental setup, which was changed during the period of this master thesis.

Table 4.3 shows the rates and volumes used to saturate the microchip with oil and water prior to the waterflooding, while table 4.4 shows the rates and volumes of water used in each test.

**Table 4.3:** Rates and volumes for the initial saturation of the microchip with oil and water.

| Fluid | Water | Oil |
|---|---|---|
| Rate 1 [mL/min] | 0,01 | 0,006 |
| Volume 1 [mL] | 0,2 | 0,023 |
| Rate 2 [mL/min] | - | 0,06 |
| Volume 2 [mL] | - | 0,046 |
| Rate 3 [mL/min] | - | 1 |
| Volume 3 [mL] | - | 1 |

**Table 4.4:** Rates and volumes used in test runs.

| Test # | 1 | 2 | 3 |
|---|---|---|---|
| Rate 1 [mL/min] | 0,005 | 0,01 | 0,01 |
| Volume 1 [mL] | 0,99 | 1,38 | 1,38 |
| Volume 1 [#PV] | 400 | 600 | 600 |
| Rate 2 [mL/min] | 0,005 | 0,01 | 0,05 |
| Volume 2 [mL] | 0,99 | 1,38 | 2,3 |
| Volume 2 [#PV] | 400 | 600 | 1000 |
| Rate 3 [mL/min] | - | 0,01 | - |
| Volume 3 [mL] | - | 1,38 | - |
| Volume 3 [#PV] | - | 600 | - |

### 4.3.3 Cleaning and set up

Used microchips were used for the testing prior to the actual experiments. Toluene, methanol and distilled water were used to clean the chips in between the tests as these chips already contained some oil. This cleaning was not able to remove all the oil, but since the chips were only meant to be used for testing they were considered clean enough.

For the actual experiments, all the old inlet lines in the microfluidics systems were replaced with new lines. In addition, the valves and syringe pumps were detached and cleaned with toluene, methanol and distilled water. A new and clean microchip was used for each experiment to make sure that there were no fluids in the chip prior to the experiment. This means that all equipment used in the experiments were either completely new or properly cleaned, which should minimize the errors. The outlet lines in the microfluidics system were not changed or cleaned, but they only transport fluids out of the microchip and into the waste container.

The inlet lines were not replaced between every experiment, only once prior to all the experiments. The microfluidics apparatus was used for other research project prior to this master thesis, but was only used for this particular project during the whole period of experimental work. However, all equipment were cleaned between each experiment. Methanol was injected and flooded through a used microchip after each experiment, to clean all lines. The injection and syringe lines were then connected to a pressure tank to dry the lines. Each fluid has their own syringe, so the water syringe would never be filled with any other fluid than water. However, the nanofluid syringe would be used for both CNC and TEMPO-CNF, and was cleaned with distilled water between each experiment. The three-way valve used in the final experimental setup was cleaned with toluene and distilled water between each experiment as well.

## 4.4 Methods

**Improvement of the experimental setup**

The main goal of this master thesis was to study the possibilities of using nanocellulose to enhance oil recovery, by using microfluidics as a tool to study the oil saturation. However, a great part of this thesis was also to improve the experimental setup of the microfluidics, as described in the introduction. The microfluidics apparatus is a relative new addition to the laboratory at NTNU, and there was a need for more knowledge and improvement of the setup. These changes and recommendations for future work will be discussed in detail in chapter 6.

As seen from figure 4.4, changes were made in the original experimental setup during the experiments. In figure 4.4b, a two-way valve is added close to the microchip and a three-way valve removed. In the final experimental setup shown in figure 4.4c, the two-way valve is replaced by a four-way valve. However, the four-way valve is always blocked in one direction, making it a three-way valve. The system and setup was changed and improved during the whole process, making the results vary somewhat.

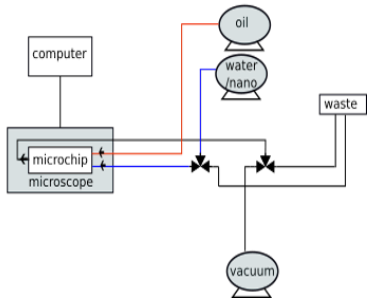


**(a)**

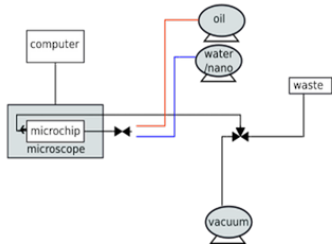


**(b)**

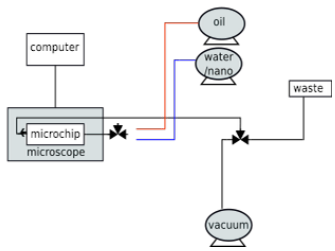


**(c)**

**Figure 4.4:** (a) Original experimental setup. (b) Experimental setup after adding the two-way valve. (c) Final experimental setup.

### 4.4.1 Viscosity measurements

The Brookfield viscometer was used to measure the viscosity of 0.1 % TEMPO-CNF, 1 % CNC and 1 % CNC heated to 120 $°C$. The viscosity of 0.1 wt% NaCl and crude oil C was previously measured, so the Brookfield viscometer was not used to measure these values during this master thesis. Equation 4.1 was used to calculate the shear rate for the values provided by the Brookfield viscometer. The shear rate of the microfluidics system was calculated using equation 3.3, and converted to RPM using equation 4.1. The viscosity was plotted against RPM for each experiment, and the line was extrapolated to find the RPM that fits the RPM calculated for the microfluidics system. This method should give a viscosity value that fits the conditions in the microfluidics system.

$$Shear\ rate = SRC\ RPM \tag{4.1}$$

SRC is a table value associated with the spindle used, while RPM is the rotation speed of the spindle. Table 4.5 shows the SRC values for the spindles, and which spindle that was used for each fluid

**Table 4.5:** SRC values for the different spindles used in the experiment, showing which spindle used for each fluid.

| Spindle | SRC | Fluid |
|---|---|---|
| S18 | 1,320 | TEMPO-CNF and CNC |
| S31 | 0,340 | CNC heated to 120 $°C$ |
| S00 | 1,223 | CNC |

### 4.4.2 Particle size measurements

A cell was filled with the diluted and prepared nanofluids and inserted into the Zetasizer nano ZS to measure the size. Three measurements were done for each run, making it possible to calculate the error. The apparatus reports whether or not the results are reliable, depending on how much the sample aggregates or if the particles vary too much in size. All measurements were performed in room temperature at 21-22 $°C$.

### 4.4.3 Contact angle and interfacial tension measurements

CNC, TEMPO-CNF or water was filled into the chamber in the Drop Shape Analyzer DS 100S, while a needle was filled with crude oil C. The chamber is made of glass and would resemble a quartz/sandstone surface. The needle used was a j-shaped needle with a diameter of 1.047 mm. The contact angle and interfacial tension between CNC and oil, TEMPO-CNF and oil and water and oil was measured.

Since the lighter crude oil was displaced in water or nanofluids, the captive bubble method had to be used to measure the contact angle. This means that the oil droplet was resting under a glass plate placed in the glass chamber. Figure 4.5a shows the oil droplet resting under the glass plate during an experiment, while figure 4.5b shows the setup without any

fluids. All contact angles and interfacial tension were measured over 12 hours, taking measurements every five minutes. The measurements for both interfacial tension and contact angle were performed in room temperature at 21-22 $°C$.

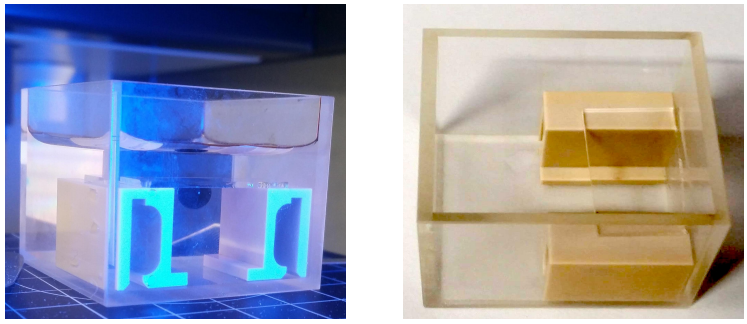

**(a)** **(b)**

**Figure 4.5:** (a) Oil droplet resting under the glass plate during an experiment. (b) Setup for contact angle measurements.

### 4.4.4 Flooding with microfluidics

Every experiment started with a procedure to fill the microchip and lines with vacuum prior to the flooding. The vacuum pump was connected to the outlet line, sucking vacuum from the inlet line through the microchip and all the way through the outlet line. When using the final experimental setup, the inlet line would be connected to the microchip and never removed during the experiment. The three-way valve would be closed towards the microchip during vacuum.

The same rates and volumes were used to initially saturate the chip with water and oil for all experiments, as shown in table 4.3. Water was injected with only one rate while the oil was injected with three increasing rates. This increasing oil rate was used to make sure that the chip was saturated as much as possible with oil prior to the flooding. Each fluid was bled through the syringe line and the three-way valve prior to the injection, which was done to avoid air or other fluids in the system. The three-way valve was opened towards the microchip after bleeding the valve, and the injection of the fluids would start. Table 4.6 shows an overview of all the microfluidics experiments done.

Whether or not the flooding was secondary or tertiary, the flooding of each fluid was always performed with two steps of rates and volumes. These values were chosen based on the tests done prior to the experiment, and are shown in table 4.7. When doing secondary flooding, the nanofluid was injected immediately after the initial saturation of the microchip with water and oil. The tertiary experiments were performed by first flooding water followed by nanofluid injection. The flooding with the low rate took 2.18 hours. Snapshots were taken with the time interval shown in table 4.8. All these photos were

analyzed to yield oil saturation at every time step. The flooding at the high rate took only 46 minutes, so snapshots were taken more often, as shown in table 4.9.

**Table 4.6:** Overview experiments.

| Experiment | Experimental setup |
|---|---|
| Secondary flooding with 1% CNC in 0.1 wt% NaCl | 4.4b |
| Tertiary flooding with 1% CNC in 0.1 wt% NaCl | 4.4a |
| Tertiary flooding with 1% CNC in 0.1 wt% NaCl | 4.4c |
| Tertiary flooding with 1% CNC in 0.1 wt% NaCl.<br>Solution previously heated to 120 $°C$ | 4.4c |
| Tertiary flooding with 0.1 wt% NaCl as both secondary and tertiary fluid | 4.4a |
| Secondary flooding with 0.1% TEMPO-CNF in 0.1 wt% NaCl | 4.4c |
| Tertiary flooding with 0.1% TEMPO-CNF in 0.1 wt% NaCl | 4.4c |
| Tertiary flooding with 1% CNC in 0.1 wt% NaCl.<br>Doing only low rate flooding for both fluids | 4.4c |

**Table 4.7:** Rates and volumes used for all fluids during flooding.

| | |
|---|---|
| Low rate [mL/min] | 0,01 |
| Volume [mL] | 1,38 |
| High rate [mL/min] | 0,05 |
| Volume [mL] | 2,3 |

**Table 4.8:** Time interval snapshots low rate.

| Time | Snapshot taken every |
|---|---|
| 0-2 min | 10 sec |
| 2-10 min | 30 sec |
| 10-30 min | 5 min |
| 30 min-end | 15 min |

**Table 4.9:** Time interval snapshots high rate.

| Time | Snapshot taken every |
|---|---|
| 0-2 min | 10 sec |
| 2-10 min | 30 sec |
| 10 min-end | 3 min |

Chapter 5

# Results

## 5.1 Viscosity

The viscosity of 0.1 wt% NaCl was previously measured to be 0.907 cp, while the viscosity for crude oil C was measured to be 55.9 cp. Table 5.1 shows the viscosity measurements for TEMPO-CNF and CNC heated to 120 $^{\circ}C$, while table 5.2 shows the measurements for CNC at room temperature. These measurements were performed with two different types of spindles, which will be further discussed in chapter 6.

**Table 5.1:** RPM, torque, viscosity and shear rate for TEMPO-CNF and CNC heated to 120 $^{\circ}C$.

| TEMPO-CNF | | | |
|---|---|---|---|
| RPM | Torque [%] | Viscosity [cp] | Shear rate [1/s] |
| 100 | 13,40 | 4,02 | 132,00 |
| 120 | 15,40 | 3,85 | 158,40 |
| 160 | 19,14 | 3,58 | 211,20 |
| 180 | 20,90 | 3,48 | 237,60 |
| 200 | 22,70 | 3,40 | 264,00 |
| CNC heated to 120 $^{\circ}C$ | | | |
| 100 | 22,80 | 68,90 | 34,00 |
| 120 | 23,85 | 59,70 | 40,80 |
| 160 | 25,90 | 46,70 | 54,40 |
| 180 | 25,20 | 42,00 | 61,20 |
| 200 | 25,20 | 37,80 | 68,00 |

**Table 5.2:** RPM, Torque, viscosity and shear rate for CNC at room temperature, using two different spindles.

| CNC using spindle S18 | | | |
|---|---|---|---|
| RPM | Torque [%] | Viscosity [cp] | Shear rate [1/s] |
| 100 | 5,10 | 1,50 | 132,00 |
| 120 | 6,10 | 1,52 | 158,40 |
| 160 | 8,40 | 1,57 | 211,20 |
| 180 | 9,50 | 1,58 | 237,60 |
| 200 | 10,50 | 1,57 | 264,00 |
| CNC using spindle S00 | | | |
| 100 | 29,70 | 1,78 | 122,30 |
| 120 | 35,70 | 1,78 | 146,76 |
| 160 | 57,50 | 2,16 | 195,68 |
| 180 | 68,70 | 2,29 | 220,14 |
| 200 | 83,00 | 2,49 | 244,60 |

Table 5.3 shows the calculated shear rate in the microfluidics system. Table 5.4 and 5.5 shows the RPM and viscosity for the different fluids in the microfluidics system, low rate and high rate flooding.

**Table 5.3:** Shear rate in microfluidics system for the low rate and high rate flooding.

| | Shear rate microfluidics [1/s] |
|---|---|
| Low rate flooding (q=0.01 mL/min] | 987,2 |
| High rate flooding (q=0.05 mL/min) | 4936,2 |

**Table 5.4:** RPM and viscosity in the microfluidics system for the low rate flooding.

| Fluid & Spindle | TEMPO-CNF, S18 | CNC 120 $°C$, S31 |
|---|---|---|
| RPM microfluidics | 747,88 | 2903,53 |
| Viscosity in microfluidics [cp] | 2,46 | 3,81 |

**Table 5.5:** RPM and viscosity in the microfluidics system for the high rate flooding.

| Fluid & Spindle | TEMPO-CNF, S18 | CNC 120 $°C$, S31 |
|---|---|---|
| RPM microfluidics | 3739,55 | 14518,24 |
| Viscosity in microfluidics [cp] | 1,66 | 0,95 |

## 5.2 Particle size

Table 5.6 shows the size and error calculations for the size measurements of TEMPO-CNF and CNC.

**Table 5.6:** Size and error calculations for CNC and TEMPO-CNF.

| Fluid | Average size [nm] | Variation between max and min [nm] | Standard deviation [nm] | Error [nm] |
|---|---|---|---|---|
| TEMPO-CNF | 237,68 | 12,60 | 4,97 | 2,22 |
| CNC | 139,47 | 3,90 | 2,03 | 1,17 |

## 5.3 Capillary number

The capillary number is calculated for each displacing fluid using equation 3.11. Table 5.7 shows the Darcy velocity for the low and high rate used in the experiments. The velocity is calculated as q/A. The viscosity used to calculate the capillary number is the average viscosity measured. The Interfacial tension and contact angle used was the average value of the measurements during the first 30 minutes of the experiment.

**Table 5.7:** Darcy velocity calculations.

| | |
|---|---|
| Flow area [$mm^2$] | 200 |
| Low rate velocity [m/s] | 8,33x$10^{-4}$ |
| High rate velocity [m/s] | 4,17x$10^{-3}$ |

**Table 5.8:** Capillary number for different displacing fluids at the low and high rate.

| Fluid | Capillary number low rate | Capillary number high rate |
|---|---|---|
| NaCl | 8,07x$10^{-5}$ | 5,82x$10^{-4}$ |
| CNC | 1,16x$10^{-4}$ | 9,14x$10^{-4}$ |
| CNF | 1,83x$10^{-4}$ | 4,03x$10^{-4}$ |

## 5.4 Contact angle

### 5.4.1 0.1 wt% NaCl and crude oil C

Figure 5.1 shows the contact angle over a period of 12 hours for a droplet of crude oil C in 0.1 wt% NaCl, while figure 5.2 shows a photo of the droplet at the end of the experiment.

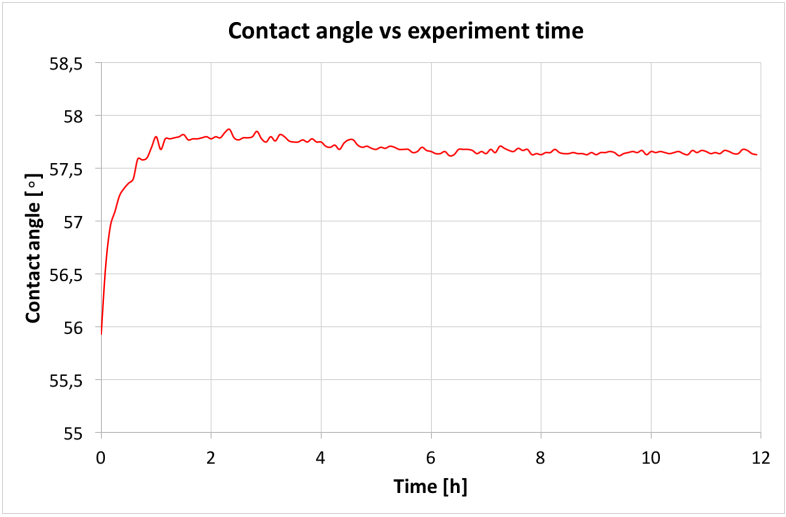


**Figure 5.1:** Contact angle vs experiment time for crude oil C and 0.1 wt% NaCl.

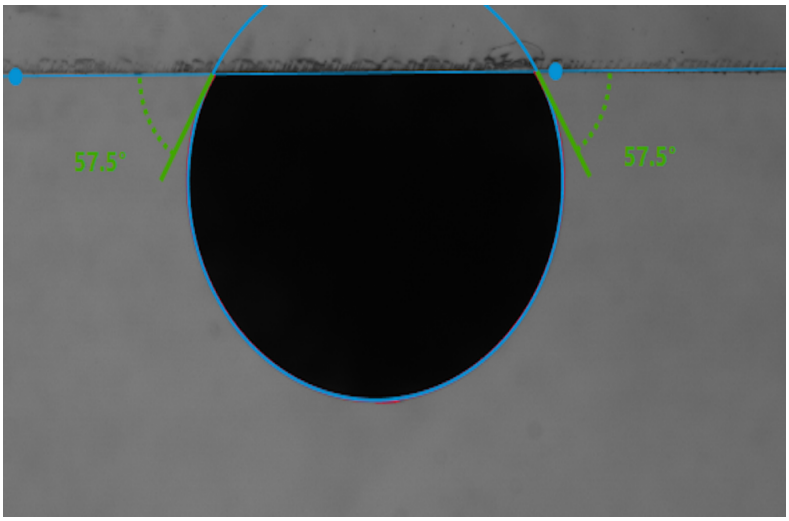


**Figure 5.2:** Photo of the captive bubble at the end of the experiment. Droplet of crude oil C surrounded by 0.1 wt% NaCl.

### 5.4.2 1 % CNC and crude oil C

Figure 5.3 shows the contact angle over a period of 12 hours for a droplet of crude oil C surrounded by CNC. Figure 5.4 shows a photo of of the droplet at the end of the experiment.

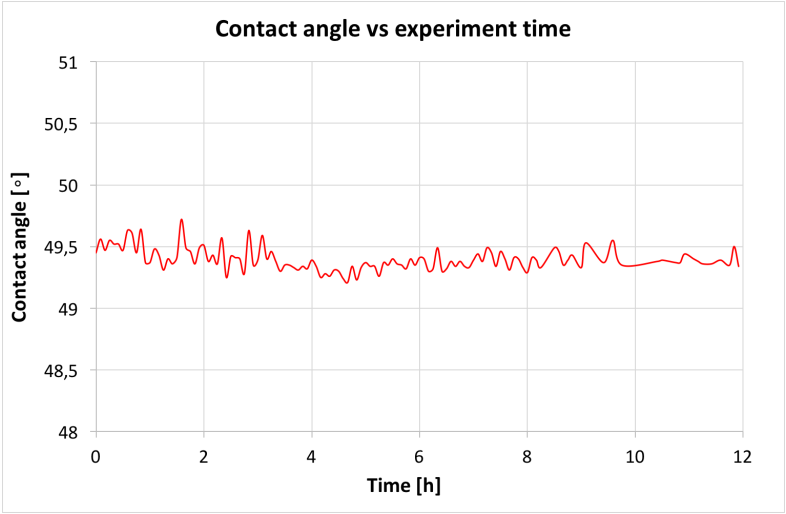


**Figure 5.3:** Contact angle vs experiment time for crude oil C and 1 % CNC.

**Figure 5.4:** Photo of the captive bubble at the end of the experiment. Droplet of crude oil C surrounded by 1 % CNC.

### 5.4.3 0.1 % TEMPO-CNF and crude oil C

Figure 5.5 shows the contact angle for a droplet of crude oil C surrounded by TEMPO-CNF over a time period of 12 hours. Figure 5.6 shows a photo of the oil droplet some hours past the end of the experiment, showing that the angle went slightly down from the end measurement.

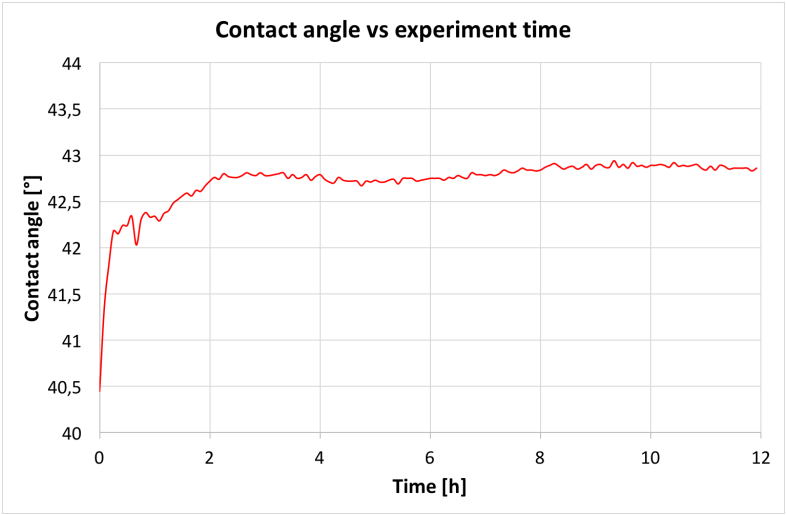


**Figure 5.5:** Contact angle vs experiment time for crude oil C and 0.1 % TEMPO-CNF.

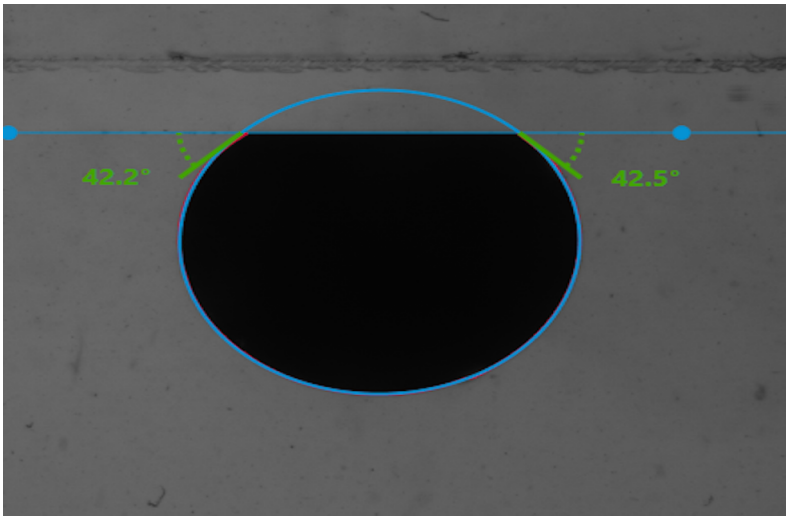


**Figure 5.6:** Photo of the captive bubble after the experiment. Droplet of crude oil C surrounded by 0.1 % TEMPO-CNF.

## 5.5 Interfacial tension

### 5.5.1 0.1 wt% NaCl and crude oil C

Figure 5.7 shows the interfacial tension for a droplet of crude oil C in 0.1 wt% NaCl over a period of 12 hours. Figure 5.8 shows a photo of the oil droplet at the end of the experiment.

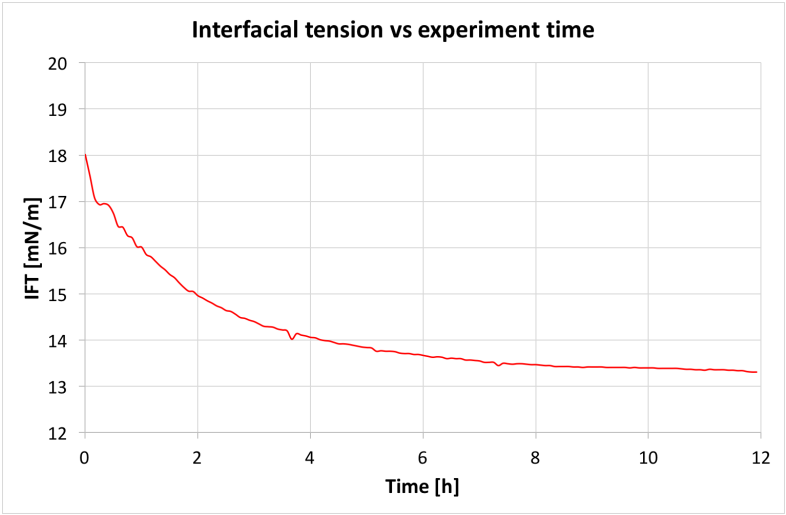


**Figure 5.7:** IFT vs experiment time for crude oil C and 0.1 wt% NaCl.

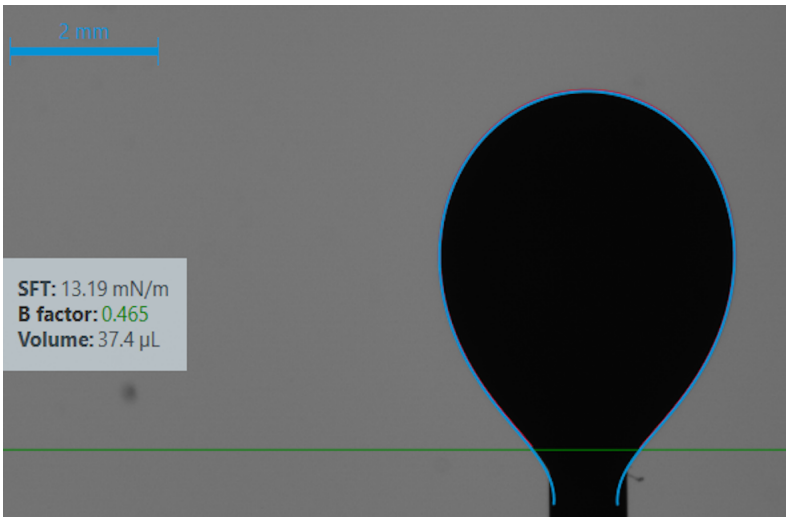


**Figure 5.8:** Photo of the oil droplet at the end of the experiment. Droplet of crude oil C surrounded by 0.1 wt% NaCl.

### 5.5.2 1 % CNC and crude oil C

Figure 5.9 shows the interfacial tension for a droplet of crude oil C surrounded by CNC over a period of 12 hours. Figure 5.10 shows a photo of the oil droplet at the end of the experiment.

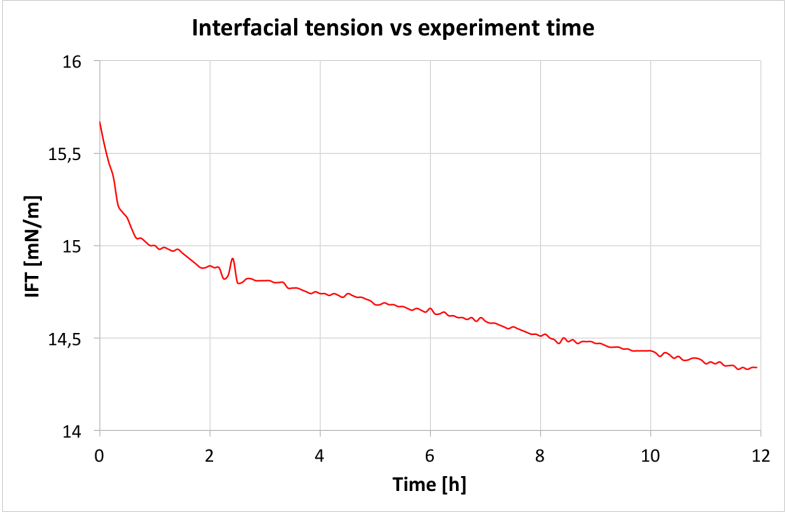


**Figure 5.9:** IFT vs experiment time for crude oil C and 1 % CNC.

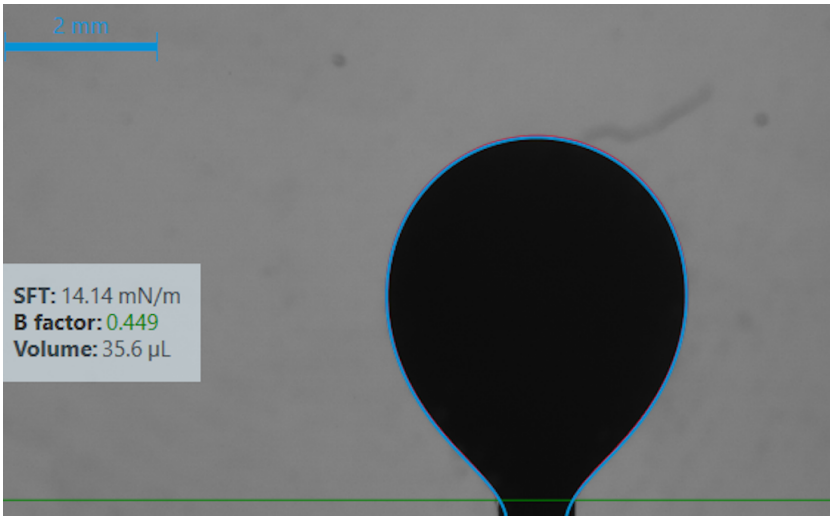


**Figure 5.10:** Photo of the oil droplet at the end of the experiment. Droplet of crude oil C surrounded by 1 % CNC.

### 5.5.3 0.1 % TEMPO-CNF and crude oil C

Figure 5.11 shows the interfacial tension for a droplet of crude oil C surrounded by TEMPO-CNF over a period of 12 hours. Figure 5.12 shows a photo of the oil droplet at the end of the experiment.

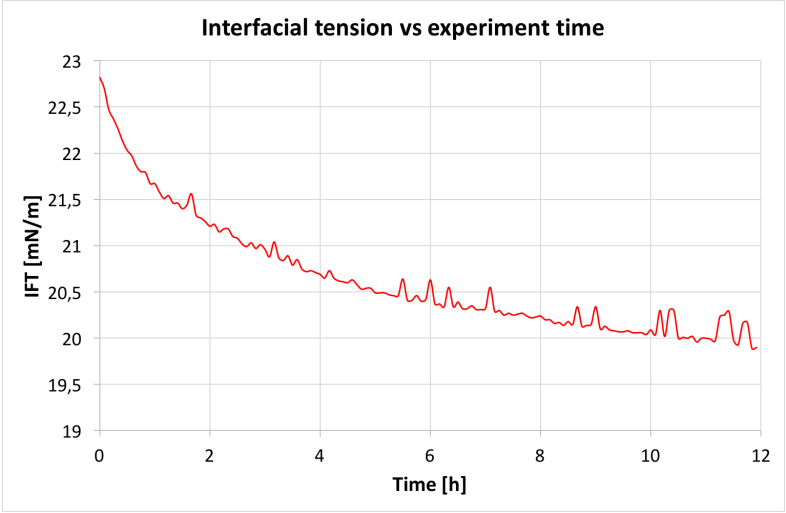


**Figure 5.11:** IFT vs experiment time for crude oil C and 0.1 % TEMPO-CNF.

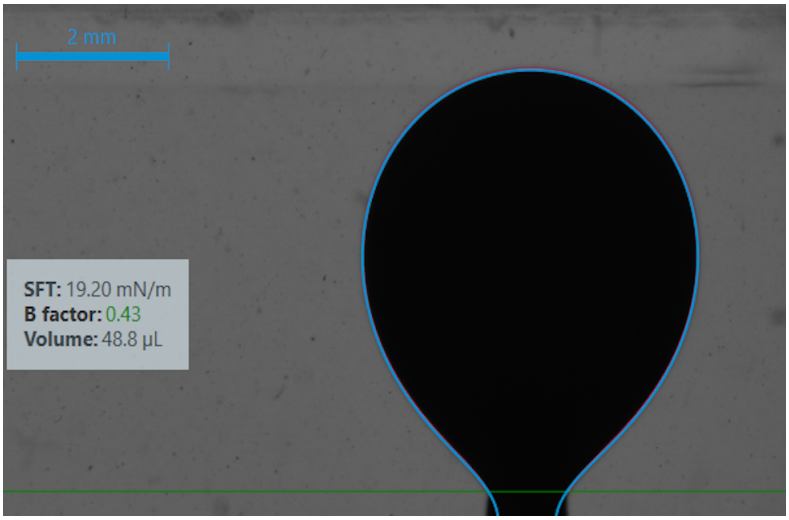


**Figure 5.12:** Photo of the oil droplet at the end of the experiment. Droplet of crude oil C surrounded by 0.1 wt% TEMPO-CNF.

## 5.6 Testing of rates

Figure 5.13a, 5.14a and 5.15a shows the oil saturation vs pore volume injected for test 1, 2 and 3 respectively. Figure 5.13b, 5.14b and 5.15b shows the oil saturation vs experiment time for test 1, 2 and 3 respectively.

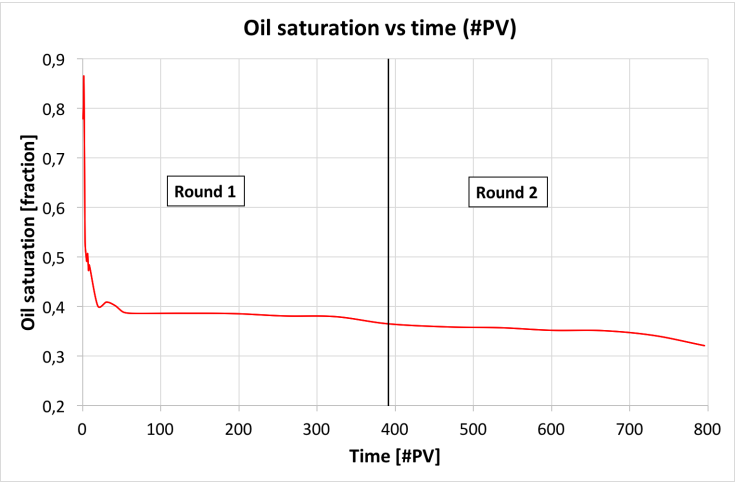


**(a)**

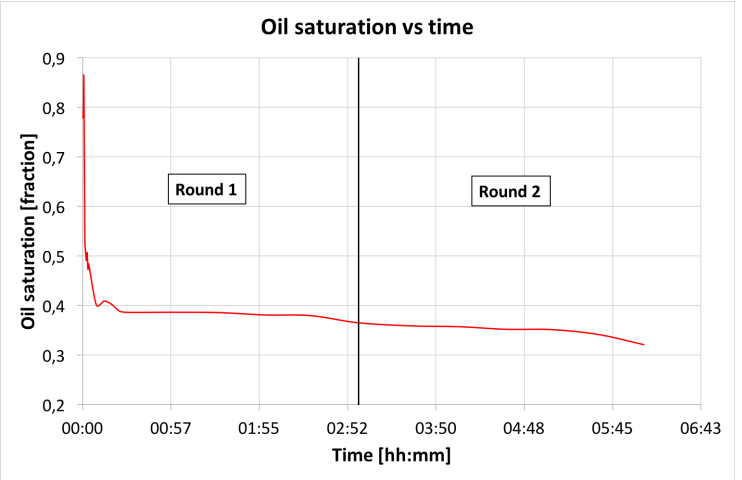


**(b)**

**Figure 5.13:** (a) Oil saturation versus pore volume injected for test 1. (b) Oil saturation versus injection time for test 1.

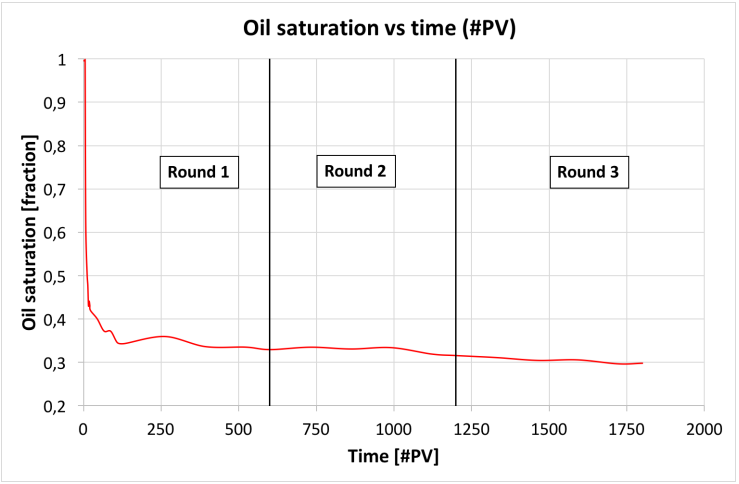


**(a)**

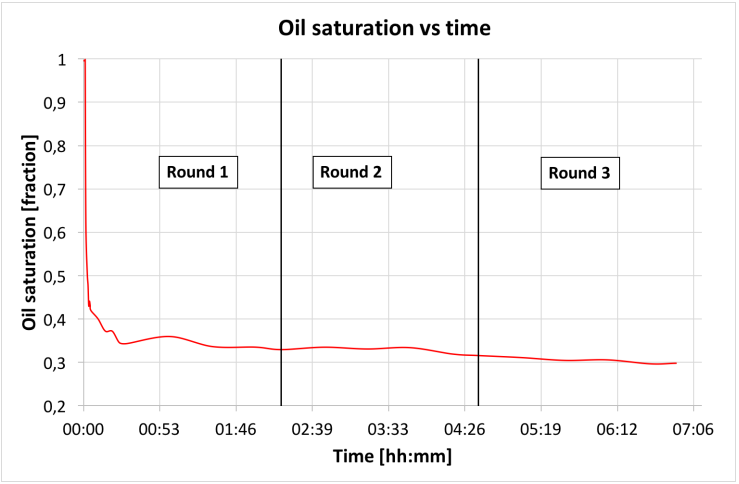


**(b)**

**Figure 5.14:** (a) Oil saturation versus pore volume injected for test 2. (b) Oil saturation versus injection time for test 2.

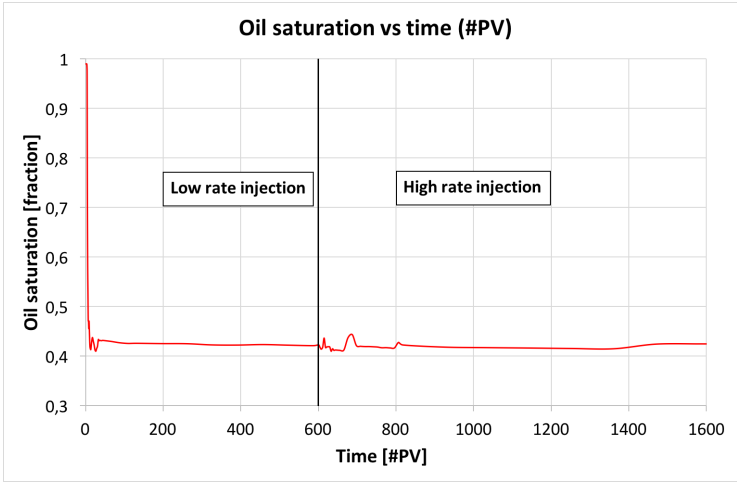


**(a)**

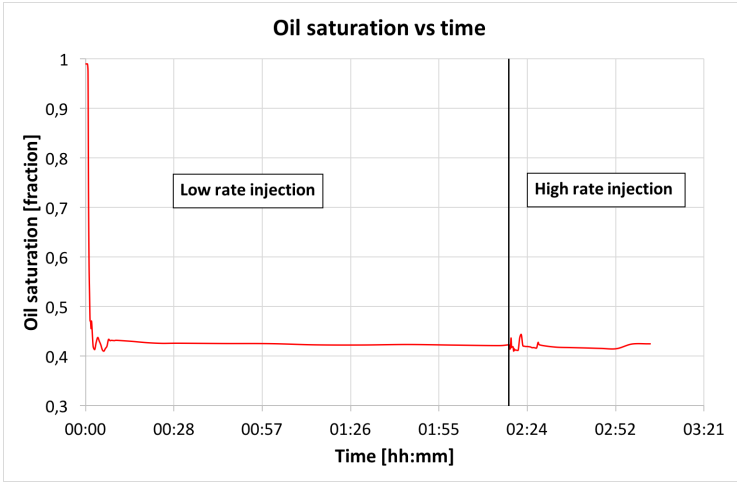


**(b)**

**Figure 5.15:** (a) Oil saturation versus pore volume injected for test 3. (b) Oil saturation versus injection time for test 3.

## 5.7 Secondary flooding

Figure 5.16a shows a water filled microchip, while 5.16b shows a water and oil filled microchip prior to flooding. These photos are approximately the same for all microfluidics experiments but might vary somewhat individually.

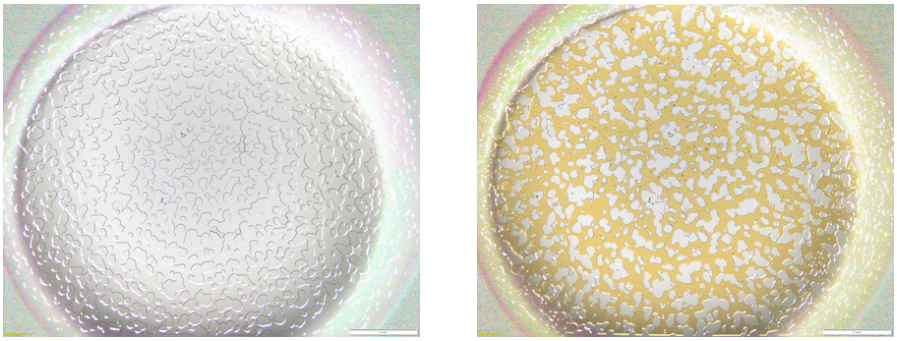

**(a)** **(b)**

**Figure 5.16:** (a) Microchip saturated with water prior to flooding. (b) Microchip saturated with water and oil prior to flooding.

### 5.7.1 1 % CNC

Table 5.9 shows the time and oil saturation for the figures in figure 5.17.

**Table 5.9:** Time, oil saturation and figures for different stages of the secondary flooding of CNC.

| Time [hh:mm:ss] | Describtion | Oil saturation [fraction] | Figure |
|---|---|---|---|
| 00:03:20 | Drop in oil saturation | 0,77 | 5.17a |
| 00:03:30 | Drop in oil saturation | 0,50 | 5.17b |
| 02:18:00 | End of low rate flooding | 0,33 | 5.17c |
| 03:04:00 | End of high rate flooding | 0,31 | 5.17d |

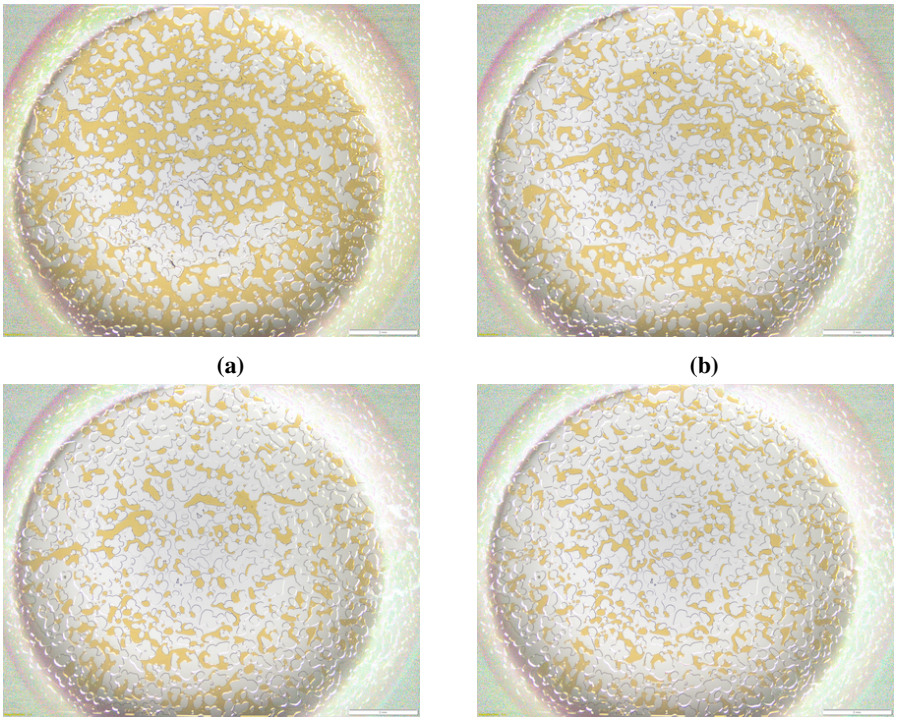

**(a)** **(b)**

**(c)** **(d)**

**Figure 5.17:** Secondary flooding of CNC. (a) Microchip after 3 minutes and 20 seconds, after a drop in oil saturation during the low rate flooding. (b) Microchip after 3 minutes and 30 seconds, after more drop in oil saturation during the low rate flooding. (c) Microchip at the end of the low rate flooding. (d) Microchip at the end of the high rate flooding.

Figure 5.18a shows the oil saturation as a function of pore volume injected for the secondary flooding of CNC, while figure 5.18b shows the oil saturation versus time.

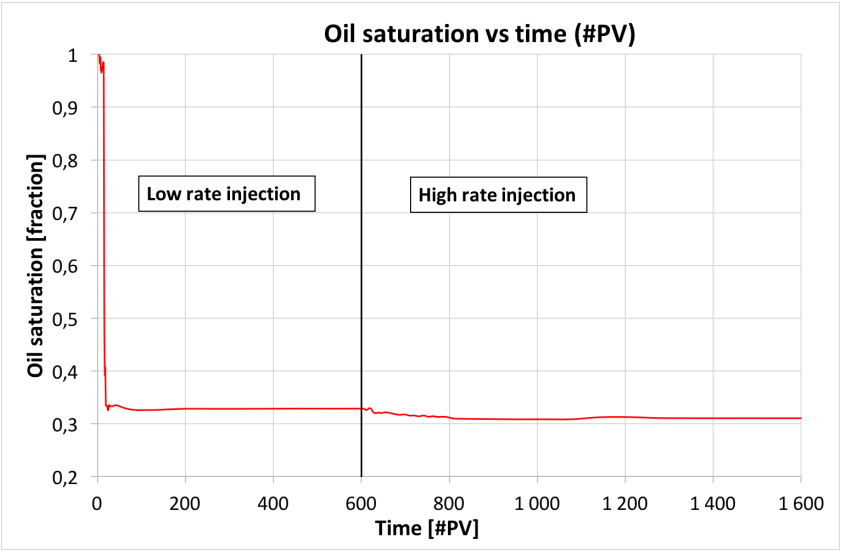


**(a)**

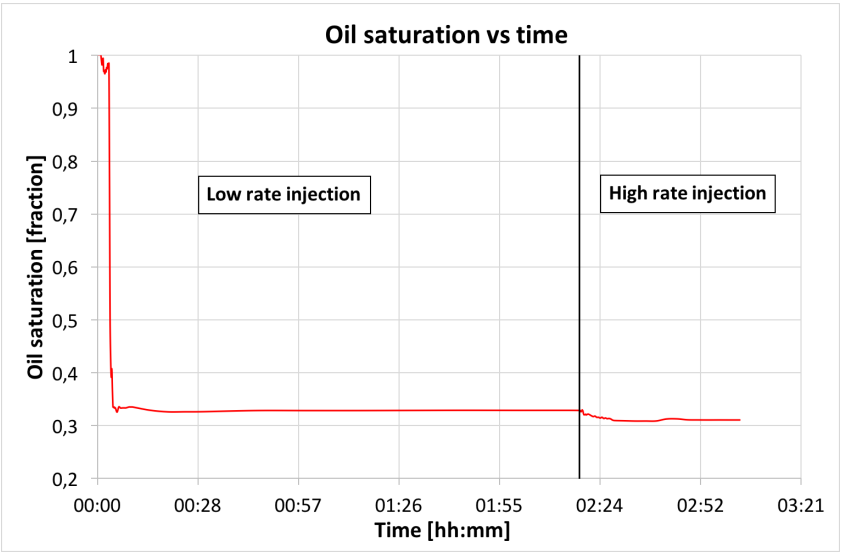


**(b)**

**Figure 5.18:** (a) Oil saturation versus pore volume injected for secondary flooding with CNC. (b) Oil saturation versus injection time for secondary flooding with CNC.

### 5.7.2 0.1 % TEMPO-CNF

Table 5.10 shows the time and oil saturation for the figures presented in figure 5.19

**Table 5.10:** Time, oil saturation and figures for different stages of the secondary flooding of TEMPO-CNF.

| Time [hh:mm:ss] | Description | Oil saturation [fraction] | Figure |
|---|---|---|---|
| 00:00:20 | Drop in oil saturation | 0,53 | 5.19a |
| 02:18:00 | End of low rate flooding | 0,22 | 5.19b |
| 02:18:50 | Drop in oil saturation | 0,16 | 5.19c |
| 03:04:00 | End of high rate flooding | 0,12 | 5.19d |

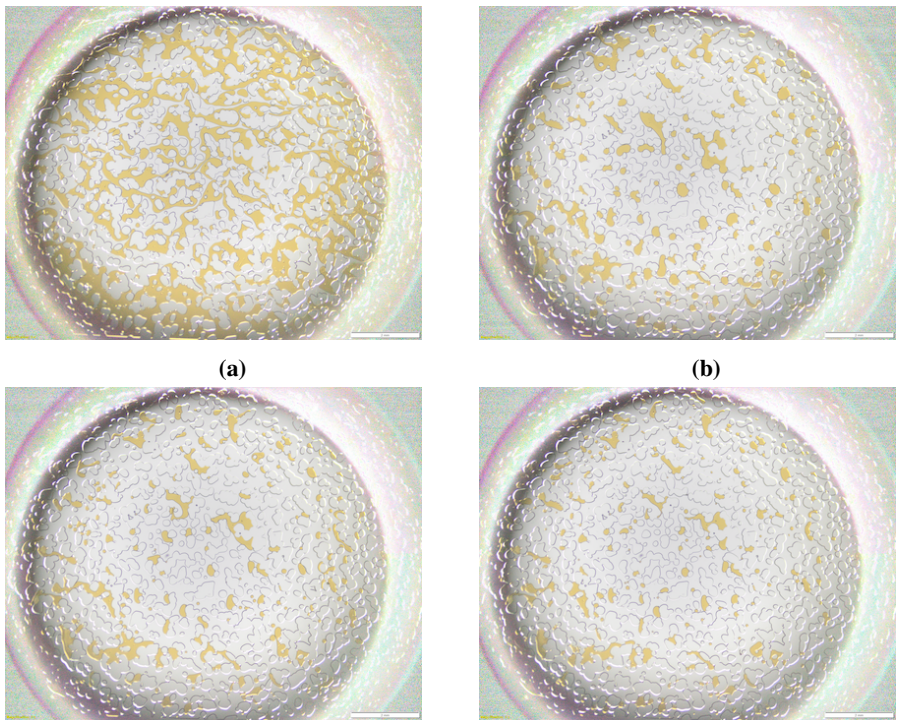

**(a)** **(b)**

**(c)** **(d)**

**Figure 5.19:** Secondary flooding of TEMPO-CNF. (a) Microchip after 20 seconds, after a drop in oil saturation during the low rate flooding. (b) Microchip at the end of the low rate flooding. (c) Microchip 50 seconds into the high rate flooding, after a drop in oil saturation. (d) Microchip at the end of the high rate flooding.

Figure 5.20a shows the oil saturation versus pore volume injected for the secondary flooding of TEMPO-CNF, while figure 5.20b shows the oil saturation vs time.

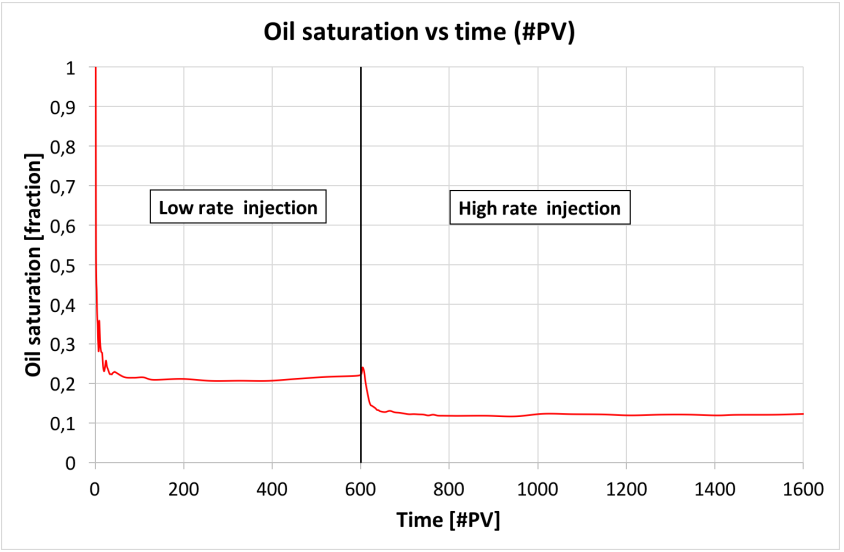


**(a)**

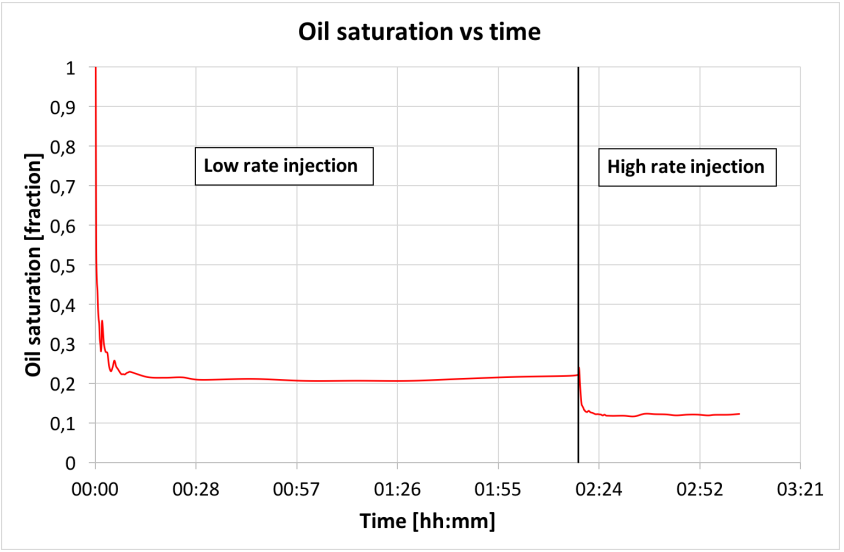


**(b)**

**Figure 5.20:** (a) Oil saturation versus pore volume injected for secondary flooding with TEMPO-CNF. (b) Oil saturation versus injection time for secondary flooding with TEMPO-CNF.

## 5.8 Tertiary flooding

### 5.8.1 1 % CNC, old setup

#### Waterflooding

Table 5.11 shows the time and oil saturation for figure 5.21.

**Table 5.11:** Time, oil saturation and figures for different stages of the waterflooding prior to the tertiary flooding of CNC, old setup.

| Time [hh:mm:ss] | Description | Oil saturation [fraction] | Figure |
|---|---|---|---|
| 00:01:00 | Drop in oil saturation | 0,62 | 5.21a |
| 00:02:30 | Drop in oil saturation | 0,50 | 5.21b |
| 02:18:00 | End of low rate flooding | 0,34 | 5.21c |
| 03:04:00 | End of high rate flooding | 0,32 | 5.21d |

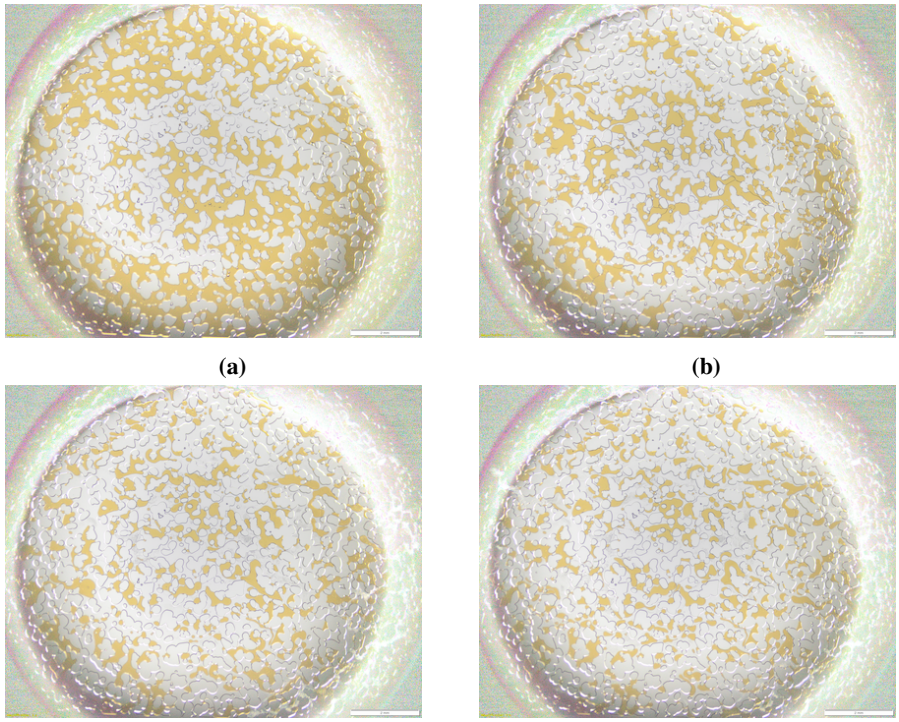

**(a)** **(b)** **(c)** **(d)**

**Figure 5.21:** Waterflooding prior to tertiary flooding of CNC, old setup. (a) Microchip after 1 minute, after a drop in oil saturation during the low rate waterflooding. (b) Microchip after 2 minutes and 30 seconds, after more drop in oil saturation during the low rate waterflooding. (c) Microchip at the end of low rate waterflooding. (d) Microchip at the end of the high rate waterflooding.

### Nanoflooding

Table 5.12 shows the time and oil saturation for the figures presented in figure 5.22.

**Table 5.12:** Time, oil saturation and figures for different stages of the tertiary flooding of CNC, old setup.

| Time [hh:mm:ss] | Description | Oil saturation [fraction] | Figure |
|---|---|---|---|
| 00:15:00 | Drop in oil saturation | 0,27 | 5.22a |
| 00:45:00 | Drop in oil saturation | 0,15 | 5.22b |
| 02.18:00 | End of low rate flooding | 0,09 | 5.22c |
| 03:04:00 | End of high rate flooding | 0,04 | 5.22d |

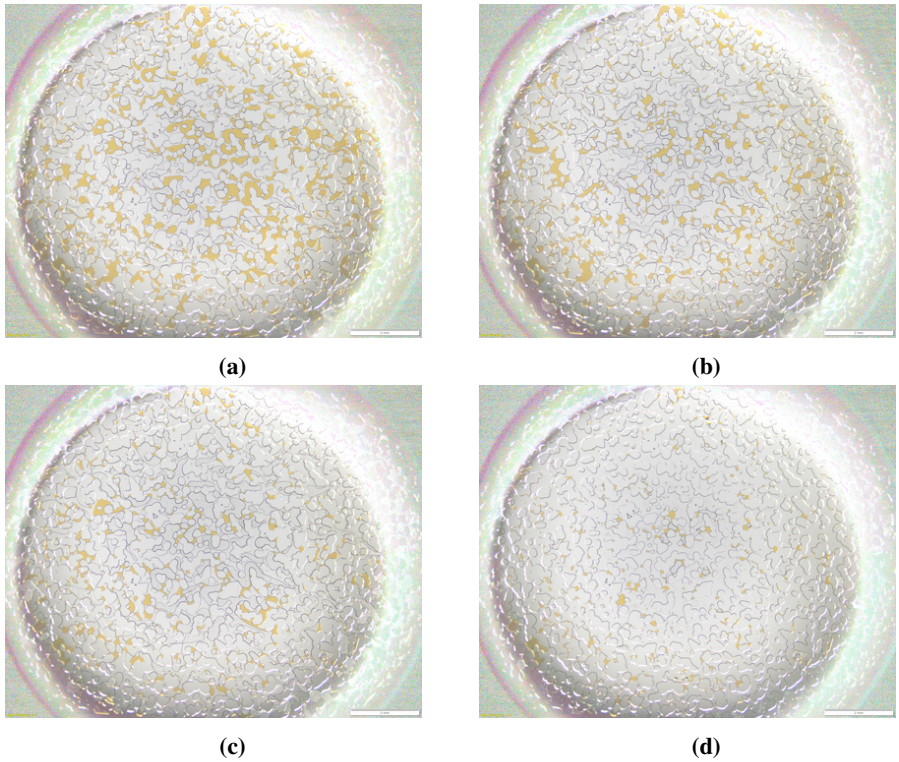

**(a)** **(b)** **(c)** **(d)**

**Figure 5.22:** Nanoflooding during tertiary flooding of CNC, old setup. (a) Microchip 15 minutes into the low rate flooding , after a drop in oil saturation. (b) Microchip 45 minutes into the low rate flooding, after more drop in oil saturation. (c) Microchip at the end of the low rate flooding. (d) Microchip at the end of the high rate flooding.

Figure 5.23a shows the oil saturation vs pore volume for the tertiary flooding of CNC using the old setup. Figure 5.23b shows the oil saturation vs time.

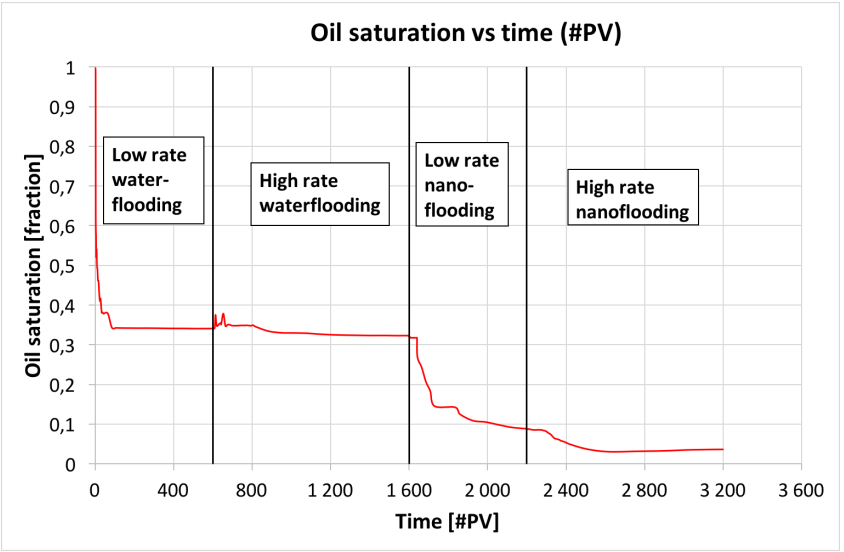


**(a)**

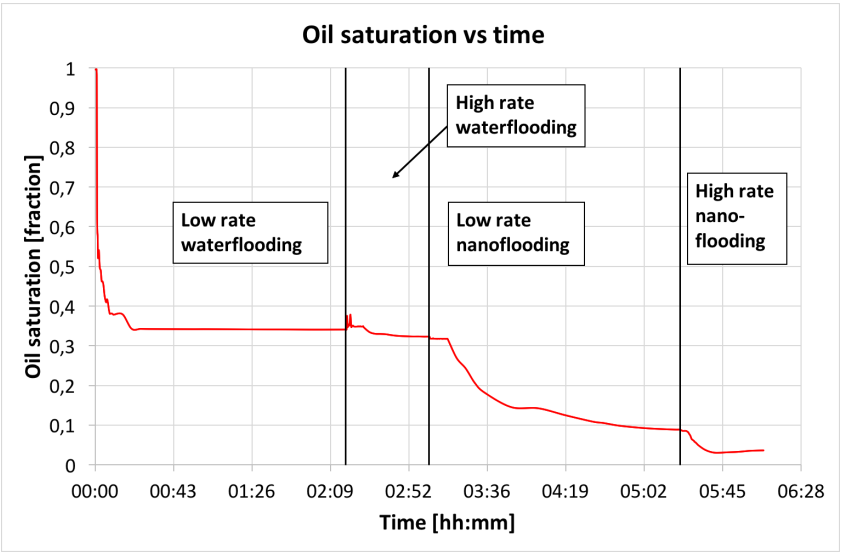


**(b)**

**Figure 5.23:** (a) Oil saturation versus pore volume injected for tertiary flooding with CNC, old setup. (b) Oil saturation versus injection time for tertiary flooding with CNC, old setup.

### 5.8.2 1 % CNC, new setup

#### Waterflooding

Table 5.13 shows the oil saturation and time for the figures presented in figure 5.24.

**Table 5.13:** Time, oil saturation and figures for different stages of the waterflooding prior to the tertiary flooding of CNC, new setup.

| Time [hh:mm:ss] | Description | Oil saturation [fraction] | Figure |
|---|---|---|---|
| 00:00:20 | Drop in oil saturation | 0,74 | 5.24a |
| 02:18:00 | End of low rate flooding | 0,35 | 5.24b |
| 02:18:20 | Drop in oil saturation | 0,32 | 5.24c |
| 03:04:00 | End of high rate flooding | 0,35 | 5.24d |

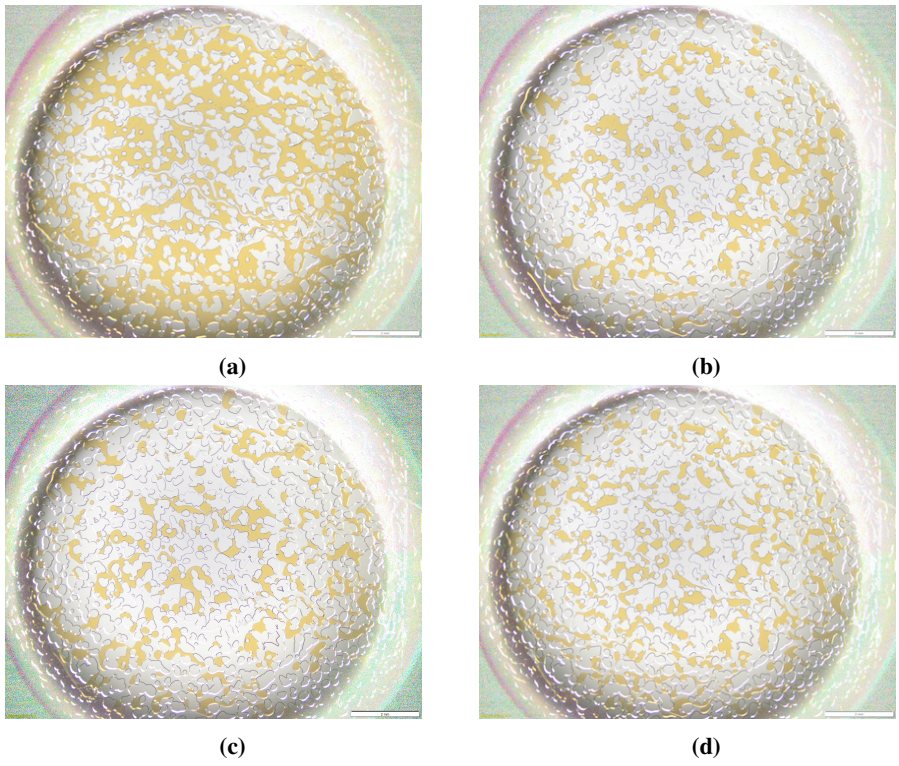

**(a)** **(b)** **(c)** **(d)**

**Figure 5.24:** Waterflooding prior to tertiary flooding of CNC, new setup. (a) Microchip after 20 seconds, after a drop in oil saturation in the low rate waterflooding. (b) Microchip at the end of the low rate waterflooding. (c) Microchip 20 seconds into the high rate waterflooding, after a drop in oil saturation (d) Microchip at the end of the high rate waterflooding.

### Nanoflooding

Table 5.14 shows the time and oil saturation for the figures presented in figure 5.25.

**Table 5.14:** Time, oil saturation and figures for different stages of the tertiary flooding of CNC, new setup.

| Time [hh:mm:ss] | Description | Oil saturation [fraction] | Figure |
|---|---|---|---|
| 00:00:10 | First photo of low rate flooding | 0,35 | 5.25a |
| 02:18:00 | End of low rate flooding | 0,35 | 5.25b |
| 02:18:10 | First photo of high rate flooding | 0,35 | 5.25c |
| 03:04:00 | End of high rate flooding | 0,34 | 5.25d |

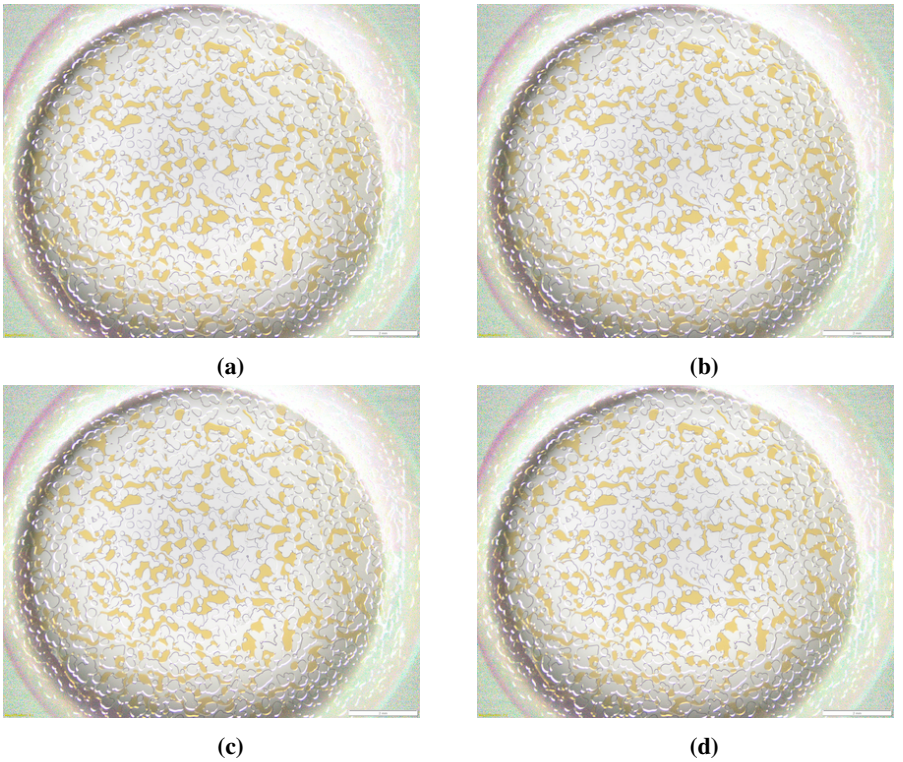

**(a)** **(b)** **(c)** **(d)**

**Figure 5.25:** Nanoflooding during tertiary flooding of CNC, new setup. (a) Microchip 10 seconds into the low rate flooding. (b) Microchip at the end of the low rate flooding. (c) Microchip 10 seconds into the high rate flooding. (d) Microchip at the end of the high rate flooding.

Figure 5.26a shows the oil saturation as a function of pore volume injected for the tertiary flooding of CNC, using the new setup. Figure 5.26b shows the oil saturation vs time.

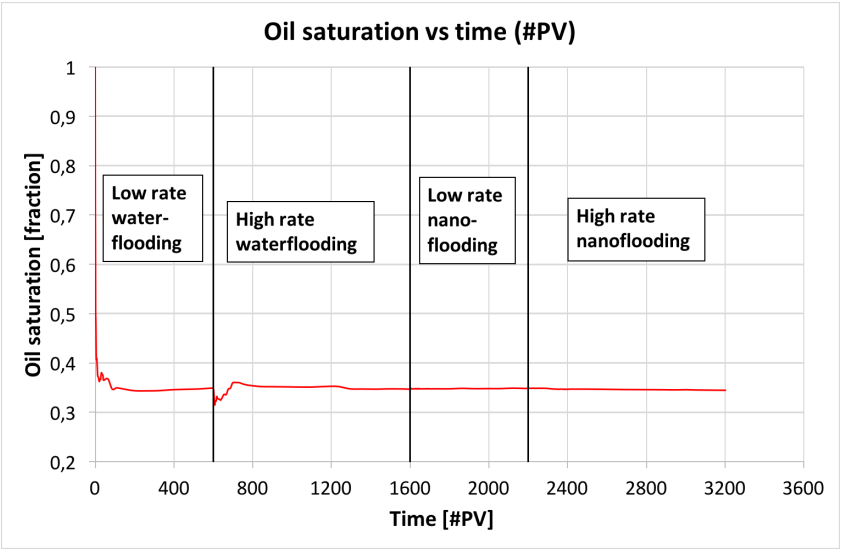


**(a)**

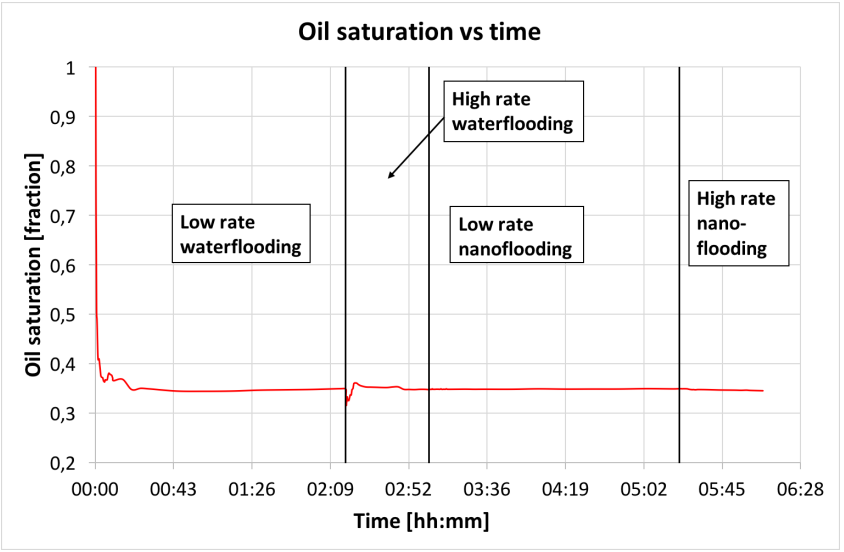


**(b)**

**Figure 5.26:** (a) Oil saturation versus pore volume injected for tertiary flooding with CNC, new setup. (b) Oil saturation versus injection time for tertiary flooding with CNC, new setup.

### 5.8.3 0.1 wt% NaCl as both secondary and tertiary fluid

#### First round of waterflooding

Table 5.15 shows the time and oil saturation for the figures in figure 5.27.

**Table 5.15:** Time, oil saturation and figures for different stages of the first round of waterflooding.

| Time [hh:mm:ss] | Description | Oil saturation [fraction] | Figure |
|---|---|---|---|
| 00:00:40 | Drop in oil saturation | 0,63 | 5.27a |
| 00:03:00 | Drop in oil saturation | 0,39 | 5.27b |
| 02:18:00 | End of low rate flooding | 0,27 | 5.27c |
| 03:04:00 | End of high rate flooding | 0,26 | 5.27d |

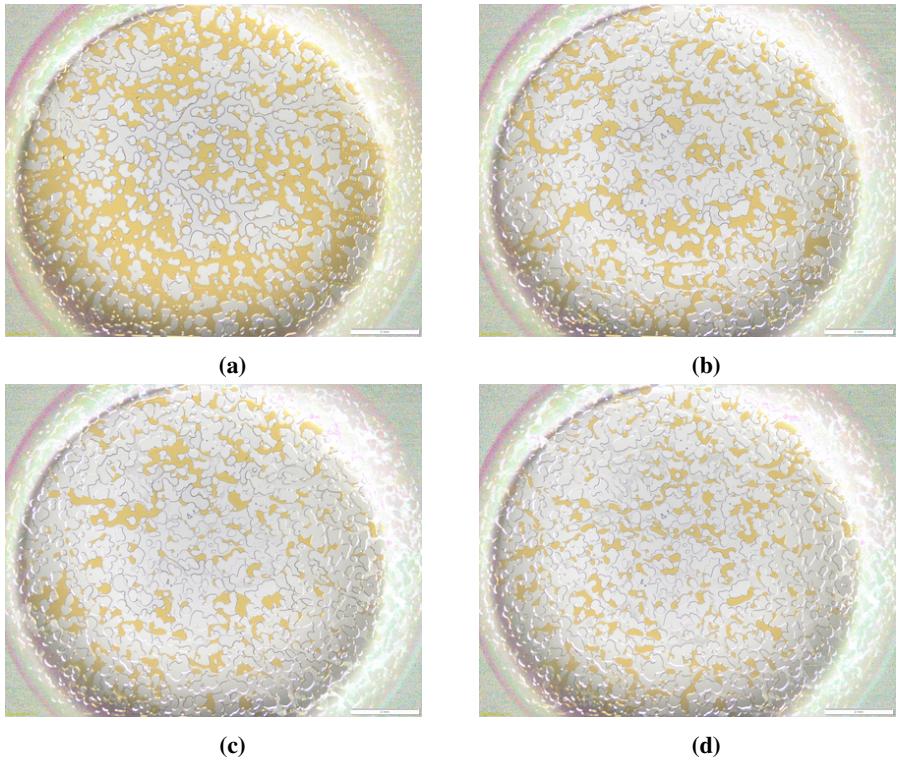

**(a)** **(b)** **(c)** **(d)**

**Figure 5.27:** First round of waterflooding during tertiary flooding of 0.1 wt% NaCl. (a) Microchip after 40 second, after a drop in oil saturation in the low rate waterflooding. (b) Microchip 3 minutes into the low rate waterflooding, after more drop in oil saturation. (c) Microchip at the end of the low rate waterflooding. (d) Microchip at the end of the high rate waterflooding.

### Second round of waterflooding

Table 5.16 shows the time and oil saturation for the figures presented in figure 5.28.

**Table 5.16:** Time, oil saturation and figures for different stages of the second round of waterflooding.

| Time [hh:mm:ss] | Description | Oil saturation [fraction] | Figure |
|---|---|---|---|
| 00:05:30 | No change in oil saturation | 0,27 | 5.28a |
| 02:18:00 | End of low rate flooding | 0,26 | 5.28b |
| 02:18:30 | Small drop in oil saturation | 0,24 | 5.28c |
| 03:40:00 | End of high rate flooding | 0,23 | 5.28d |

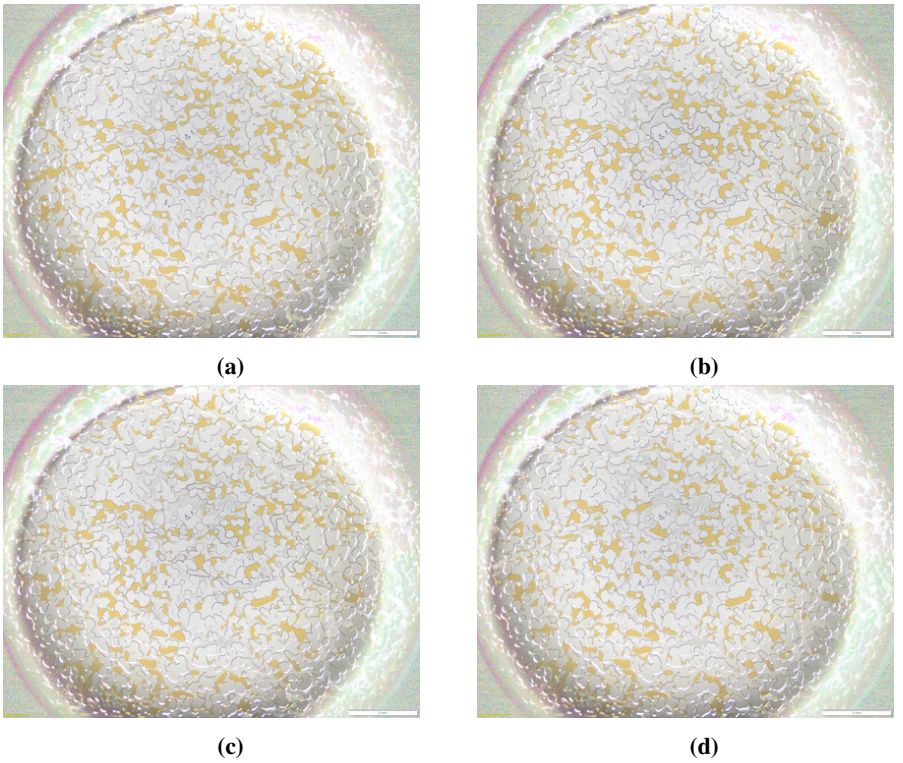

**(a)** **(b)** **(c)** **(d)**

**Figure 5.28:** Second round of waterflooding during tertiary flooding of 0.1 wt% NaCl. (a) Microchip 5 minutes and 30 second into the low rate waterflooding. (b) Microchip at the end of the low rate waterflooding. (c) Microchip 30 seconds into the high rate waterflooding, after a small drop in oil saturation. (d) Microchip at the end of the high rate waterflooding.

Figure 5.29a shows the oil saturation vs pore volume injected for the tertiary flooding of 0.1 wt% NaCl. Figure 5.29b shows the oil saturation vs time.

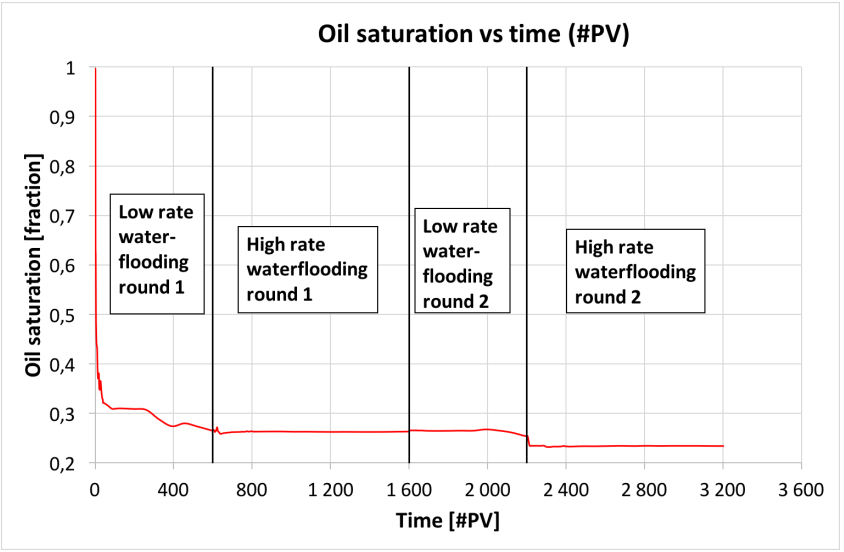


**(a)**

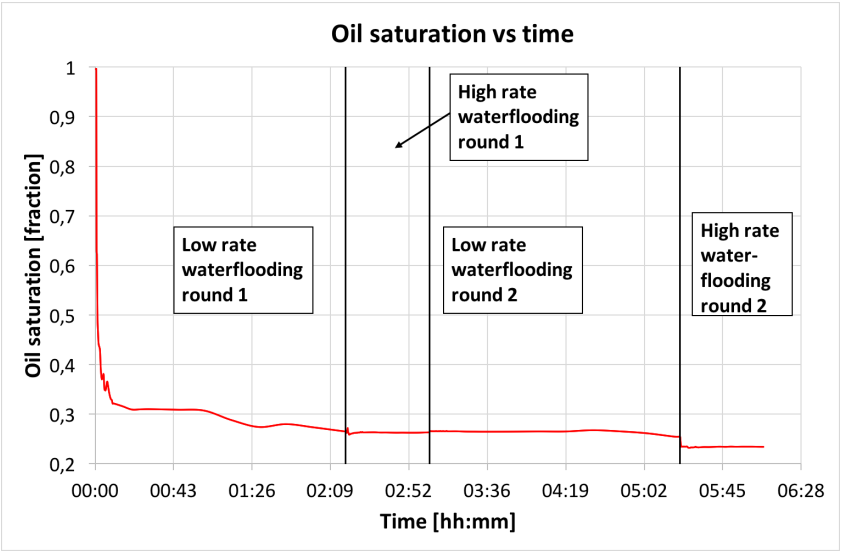


**(b)**

**Figure 5.29:** (a) Oil saturation versus pore volume injected for flooding with water. (b) Oil saturation versus injection time for flooding with water.

### 5.8.4 1 % CNC heated to 120°$C$

#### Waterflooding

Table 5.17 shows the time and oil saturation for the figures presented in figure 5.30.

**Table 5.17:** Time, oil saturation and figures for different stages of the waterflodding prior to the tertiary flooding of CNC heated to 120°$C$.

| Time [hh:mm:ss] | Description | Oil saturation [fraction] | Figure |
|---|---|---|---|
| 00:00:30 | Drop in oil saturation | 0,48 | 5.30a |
| 02:18:00 | End of low rate flooding | 0,25 | 5.30b |
| 02:18:10 | First photo of high rate flooding | 0,24 | 5.30c |
| 03:04:00 | End of high rate flooding | 0,26 | 5.30d |

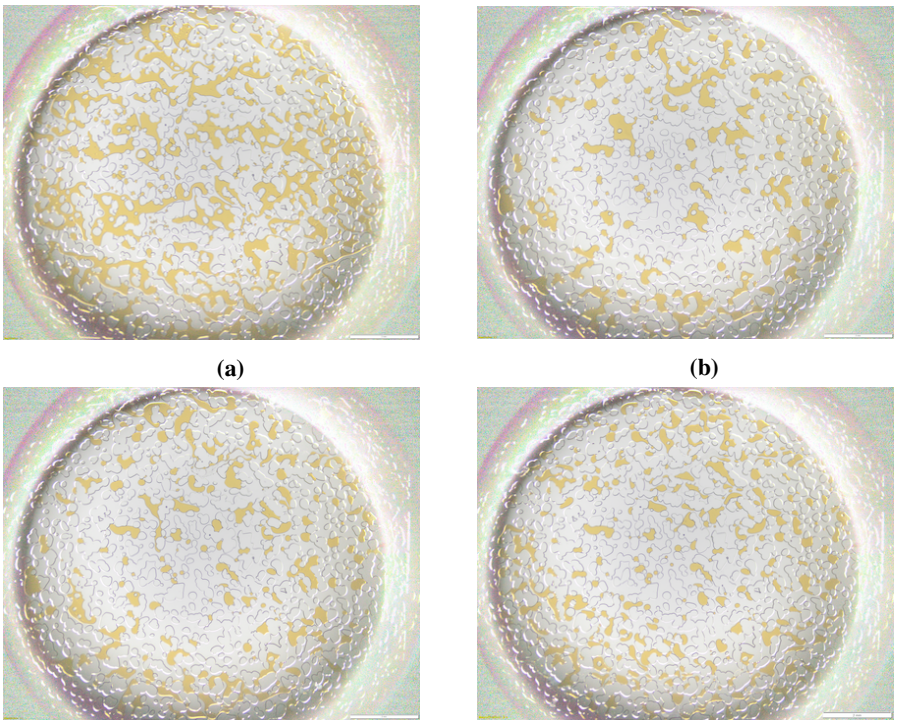

**(a)** **(b)** **(c)** **(d)**

**Figure 5.30:** Waterflooding prior to tertiary flooding of CNC heated to 120 °$C$. (a) Microchip after 30 seconds, after a drop in oil saturation in the low rate waterflooding. (b) Microchip at the end of the low rate waterflooding. (c) Microchip after 10 seconds of high rate waterflooding. (d) Microchip at the end of the high rate waterflooding.

### Nanoflooding

Table 5.18 shows the time and oil saturation for the figures presented in figure 5.31.

**Table 5.18:** Time, oil saturation and figures for different stages of the tertiary flooding of CNC heated to 120$^{\circ}C$.

| Time [hh:mm:ss] | Description | Oil saturation [fraction] | Figure |
|---|---|---|---|
| 02:18:00 | End of low rate flooding | 0,27 | 5.31a |
| 02:22:00 | Start of small oil droplets | 0,24 | 5.31b |
| 02:28:00 | More small oil droplets | 0,26 | 5.31c |
| 00:03:04 | End of high rate flooding | 0,25 | 5.31d |

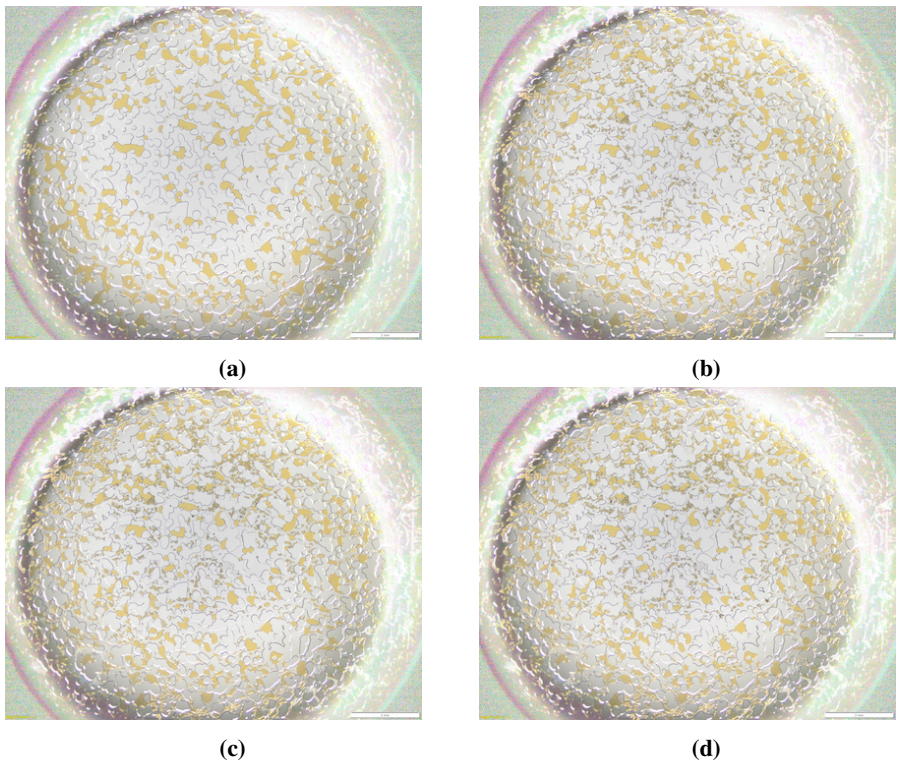

**(a)** **(b)** **(c)** **(d)**

**Figure 5.31:** Nanoflooding during tertiary flooding of CNC heated to 120 $^{\circ}C$. (a) Microchip at the end of the low rate flooding. (b) Microchip 4 minutes into the high rate flooding, when small droplets of oil starts to appear. (c) Microchip 10 minutes into the high rate flooding, when more small droplets of oil form. (d) Microchip at the end of the high rate flooding.

Figure 5.32a shows the oil saturation as a function of pore volume injected for the tertiary flooding of CNC heated to 120°$C$, while figure 5.32b shows the oil saturation vs time.

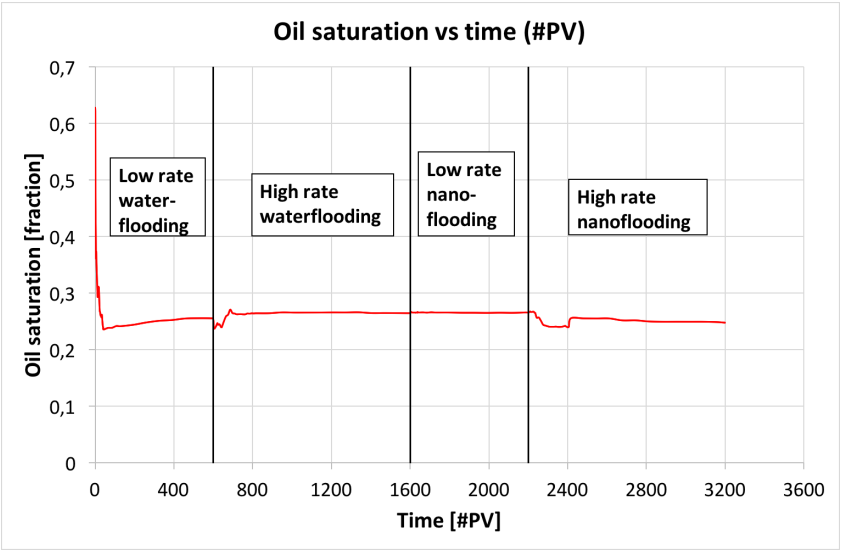


**(a)**

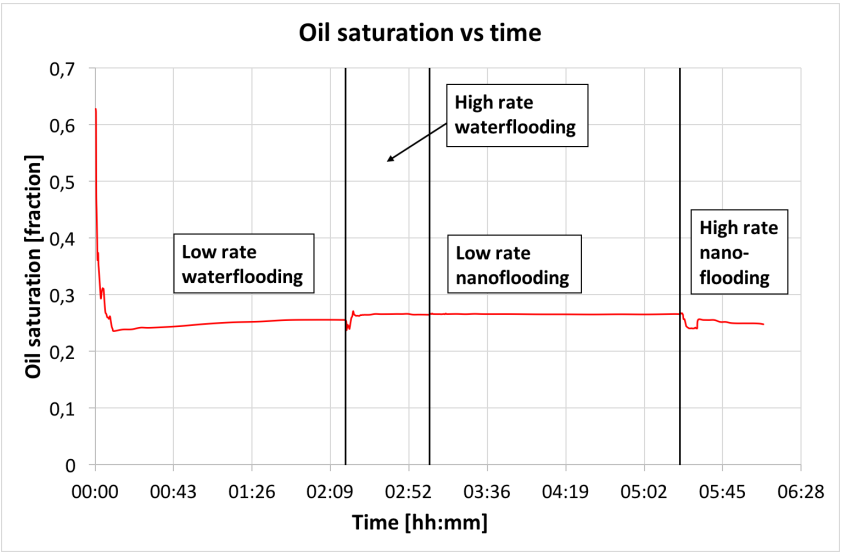


**(b)**

**Figure 5.32:** (a) Oil saturation versus pore volume injected for the tertiary flooding of CNC heated to 120°$C$. (b) Oil saturation versus injection time for the tertiary flooding of CNC heated to 120°$C$.

### 5.8.5 0.1 % TEMPO-CNF

#### Waterflooding

Table 5.19 shows the time and oil saturation for the figures presented in figure 5.33.

**Table 5.19:** Time, oil saturation and figures for different stages of the waterflooding prior to the tertiary flooding of TEMPO-CNF.

| Time [hh:mm:ss] | Description | Oil saturation [fraction] | Figure |
|---|---|---|---|
| 00:01:10 | Drop in oil saturation | 0,68 | 5.33a |
| 02:18:00 | End of low rate flooding | 0,43 | 5.33b |
| 02:18:10 | First photo of high rate flooding | 0,39 | 5.33c |
| 03:04:00 | End of high rate flooding | 0,39 | 5.33d |

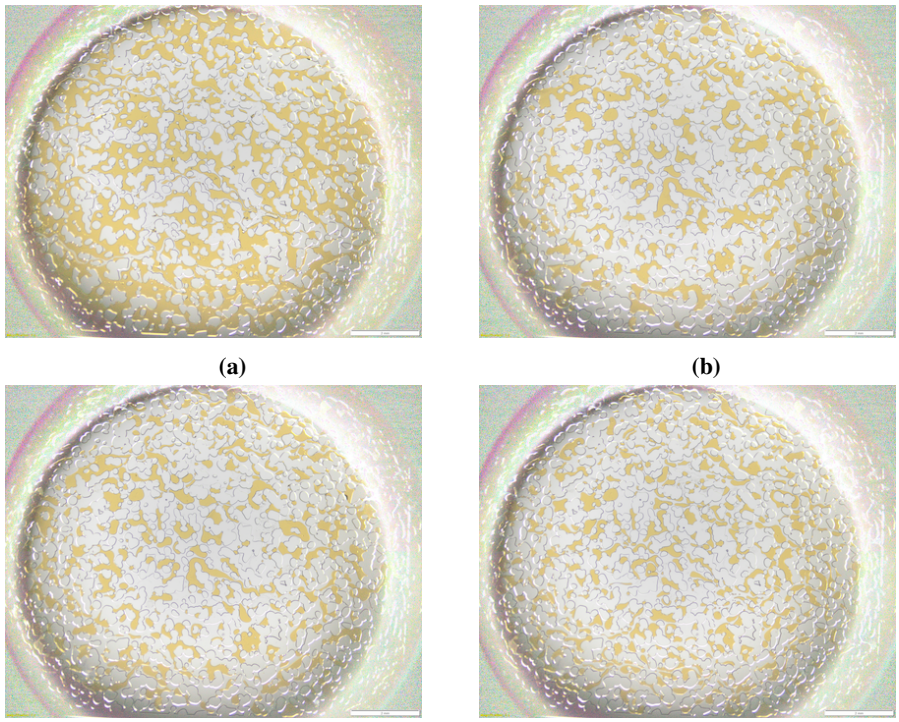

**(a)** **(b)** **(c)** **(d)**

**Figure 5.33:** Waterflooding prior to tertiary flooding of TEMPO-CNF. (a) Microchip after 1 minute and 10 seconds, after a drop in oil saturation in the low rate waterflooding. (b) Microchip at the end of the low rate waterflooding. (c) Microchip 10 seconds into the high rate waterflooding. (d) Microchip at the end of the high rate waterflooding.

### Nanoflooding

Table 5.20 shows the oil saturation and time for the different figures presented in figure 5.34.

**Table 5.20:** Time, oil saturation and figures for different stages of the tertiary flooding of TEMPO-CNF.

| Time [hh:mm:ss] | Description | Oil saturation [fraction] | Figure |
|---|---|---|---|
| 00:00:10 | First photo of low rate flooding | 0,39 | 5.34a |
| 02:18:00 | End of low rate flooding | 0,39 | 5.34b |
| 02:18:10 | First photo of high rate flooding | 0,39 | 5.34c |
| 03:04:00 | End of high rate flooding | 0,38 | 5.34d |

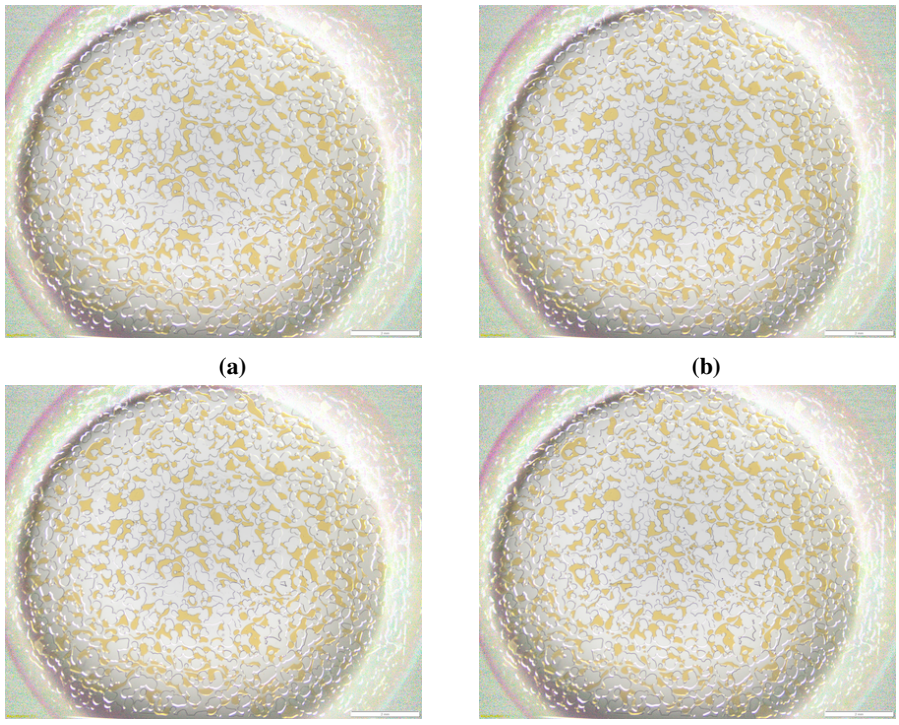

**(a)** **(b)**

**(c)** **(d)**

**Figure 5.34:** Nanoflooding during tertiary flooding of TEMPO-CNF. (a) Microchip after 10 seconds into the low rate flooding. (b) Microchip at the end of the low rate flooding. (c) Microchip 10 seconds into the high rate flooding. (d) Microchip at the end of the high rate flooding.

Figure 5.35a shows the oil saturation as a function of pore volume injected for the tertiary flooding of TEMPO-CNF, while figure 5.35b shows the oil saturation vs time.

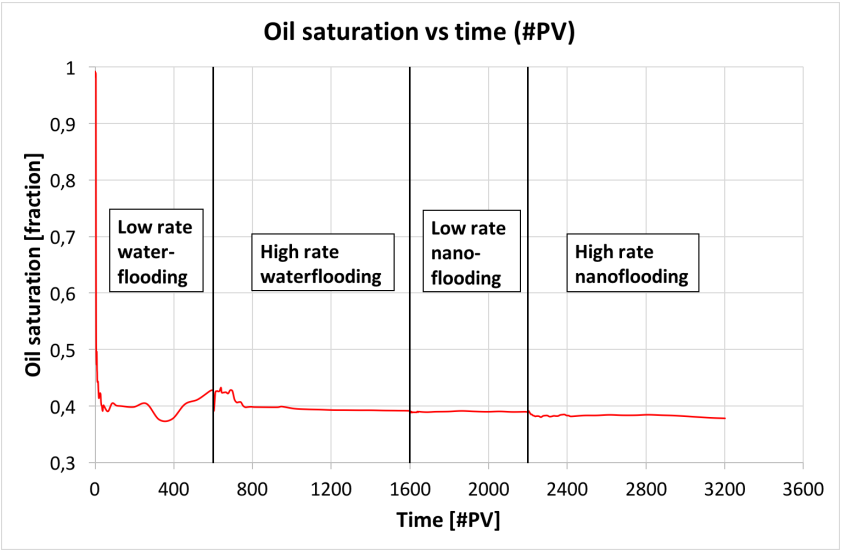


**(a)**

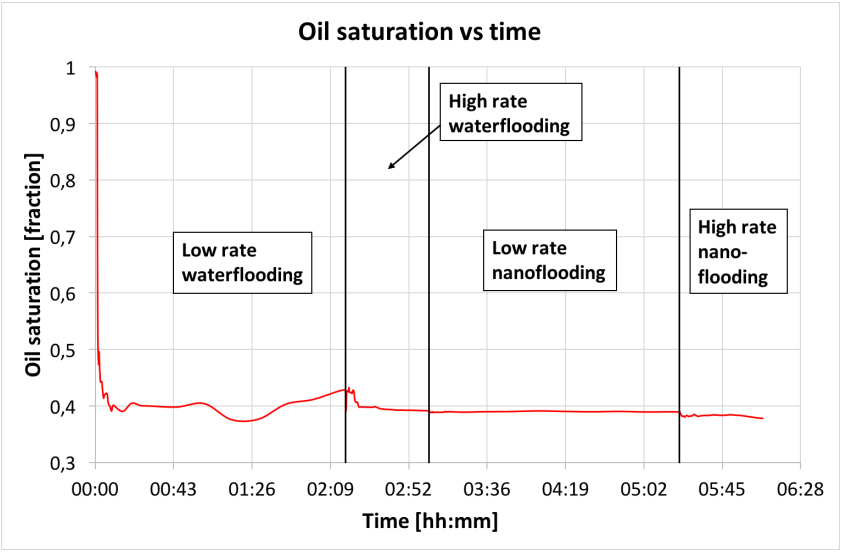


**(b)**

**Figure 5.35:** (a) Oil saturation versus pore volume injected for the tertiary flooding of TEMPO-CNF. (b) Oil saturation versus injection time for the tertiary flooding of TEMPO-CNF.

### 5.8.6 1 % CNC, low rate flooding

Table 5.21 shows the time and oil saturation for the figures presented in figure 5.36.

**Table 5.21:** Time, oil saturation and figures for different stages of the tertiary flooding of CNC using only low rates.

| Time [hh:mm:ss] | Description | Oil saturation [fraction] | Figure |
|---|---|---|---|
| 00:00:40 | Drop in oil saturation | 0,50 | 5.36a |
| 02:18:00 | End of waterflooding | 0,34 | 5.36b |
| 02:18:10 | First photo of nanoflooding | 0,33 | 5.36c |
| 04:36:00 | End of nanoflooding | 0,34 | 5.36d |

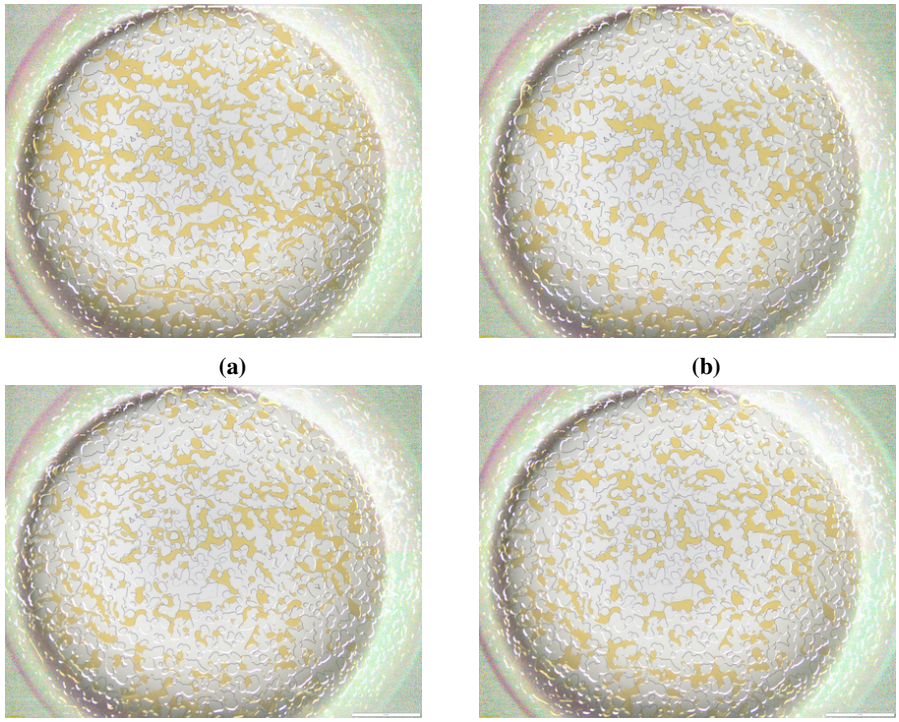

**(a)** **(b)**

**(c)** **(d)**

**Figure 5.36:** Tertiary flooding of CNC using low rates. (a) Microchip after 40 seconds into the low rate waterflooding. (b) Microchip at the end of the low rate waterflooding. (c) Microchip 10 seconds into the low rate flooding of CNC. (d) Microchip at the end of the low rate flooding of CNC.

Figure 5.37a shows the oil saturation as a function of pore volume injected for the tertiary flooding of CNC using only low rates, while figure 5.37b shows the oil saturation vs time.

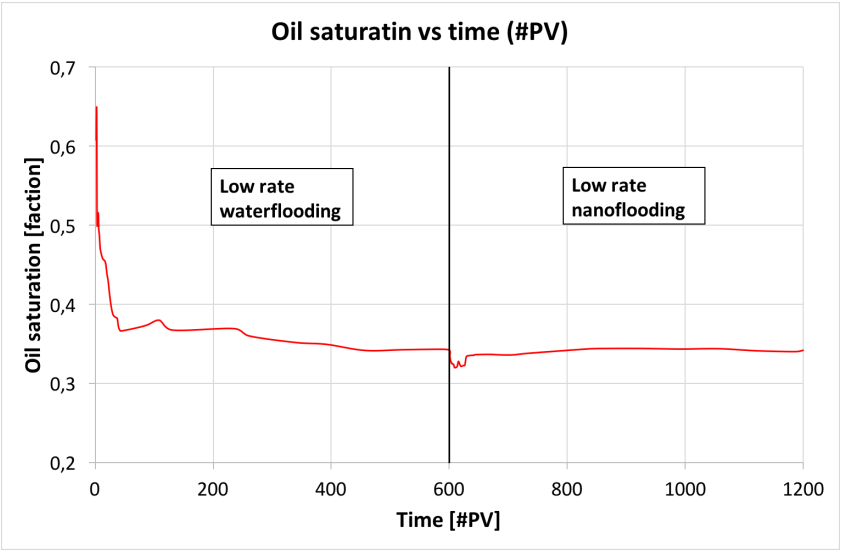


**(a)**

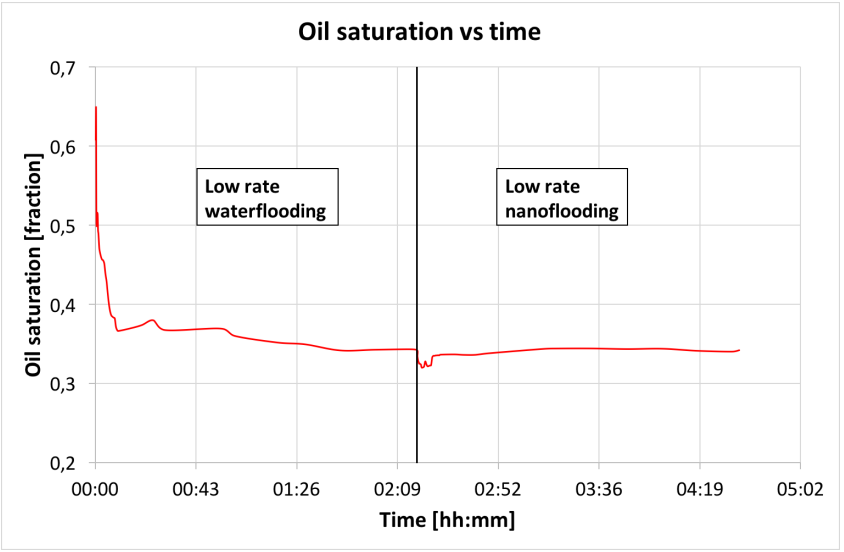


**(b)**

**Figure 5.37:** (a) Oil saturation versus pore volume injected for the tertiary flooding of CNC, using only low rates. (b) Oil saturation versus injection time for the tertiary flooding of CNC, using only low rates.

## 5.9 Comparison and error calculations of waterflooding

Figure 5.38a compares the oil saturation during the waterflooding prior to the two tertiary floodings using the old experimental setup in figure 4.4a. Figure 5.38b compares the oil saturation of the waterflooding using the new experimental setup in figure 4.4c

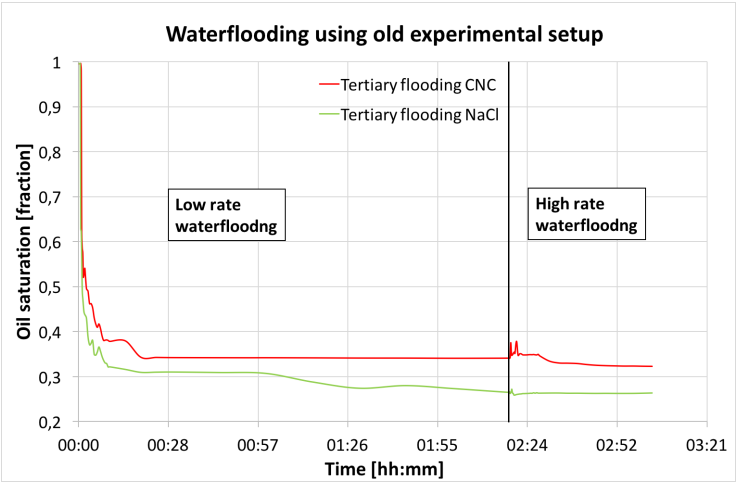


**(a)**

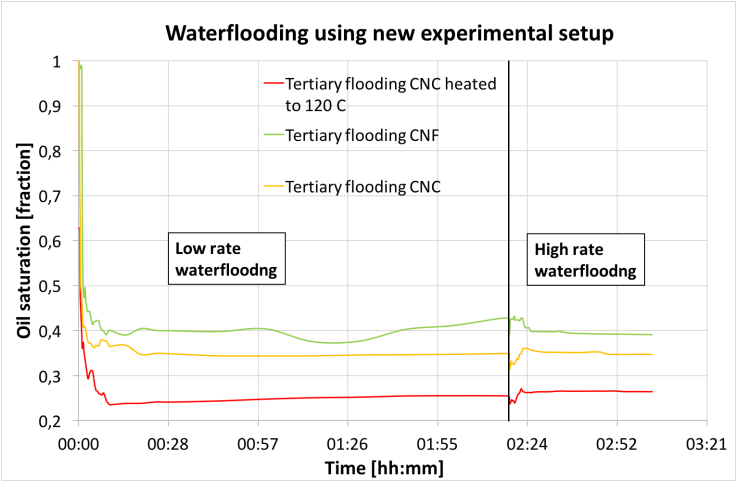


**(b)**

**Figure 5.38:** (a) Oil saturation versus time for the waterflooding prior to the tertiary flooding of CNC and NaCl, using the old experimental setup. (b) Oil saturation versus time for the waterflooding prior to the tertiary flooding of CNC, CNC heated to 120 $^{\circ}C$ and CNF, using the new experimental setup.

Table 5.22 shows the error calculations for the waterflooding using the old experimental setup. The end oil saturation for the low and high rate flooding is compared for the two experiments. The error is calculated using the equations presented in section 3.8. Table 5.23 shows the error calculations for the waterfloding using the new experimental setup.

**Table 5.22:** Error calculations for the waterflooding using the old experimental setup.

| Experiment | End saturation low rate [fraction] | End saturation high rate [fraction] |
|---|---|---|
| **Tertiary flooding with 1 % CNC** | 0,34 | 0,32 |
| **Tertiary flooding with 0.1 wt% NaCl as both secondary and tertiary fluid** | 0,27 | 0,26 |
| | | |
| | Low rate waterflooding | High rate waterflooding |
| **Variation in oil saturation between experiments [%]** | 7,53 | 5,86 |
| **Standard deviation [%]** | 5,33 | 4,15 |
| **Error [%]** | 3,77 | 2,93 |

**Table 5.23:** Error calculations for the waterflooding using the new experimental setup.

| Experiment | End saturation low rate [fraction] | End saturation high rate [fraction] |
|---|---|---|
| **Tertiary flooding with 1 % CNC** | 0,35 | 0,35 |
| **Tertiary flooding with 1 % CNC, heated to 120 C** | 0,25 | 0,26 |
| **Tertiary flooding with 0.1 % CNF** | 0,43 | 0,39 |
| | | |
| | Low rate waterflooding | High rate waterflooding |
| **Variation in oil saturation between experiments [%]** | 17,19 | 12,65 |
| **Standard deviation [%]** | 8,61 | 3,71 |
| **Error [%]** | 4,97 | 3,71 |

Chapter 6

# Discussion

## 6.1 Structure of discussion

This discussion chapter will first give some important notes on the equipment, method and experimental setup. Different parameters measured or calculated will then be addressed, before discussing the main results from the microfluidics experiments. The discussion of the contact angle, interfacial tension and microfluidics experiments is divided in the same way as the result chapter, by discussing each experiment and nanofluid separately. The results from this master thesis will then be compared to the findings in the literature presented in chapter 2. Finally, possible sources of error that could affect the results will be discussed, before giving some recommendations for future work.

## 6.2 Area of microchip viewed

As seen from the photos of the microchip in chapter 5, the snapshots are only able to capture a portion of the microchip. The microchip has a flow area of 20 mm x 10 mm, while the snapshots shows approximately 38% of this area. Hence, the observed variation in oil saturation can be due to oil moving in or out of the viewed area.

In addition to the snapshots minimizing the size of the microchip viewed, the MATLAB code further minimize this area. The MATLAB code analyzes an even smaller portion of the photo when calculating the oil saturation, as can be seen in figure 6.1a and 6.1b. The provided code calculates the oil saturation based on some coordinates that defines the area of the circle. This circle should avoid blurred areas and shadow, which is why the analyzed area is smaller than the snapshot.

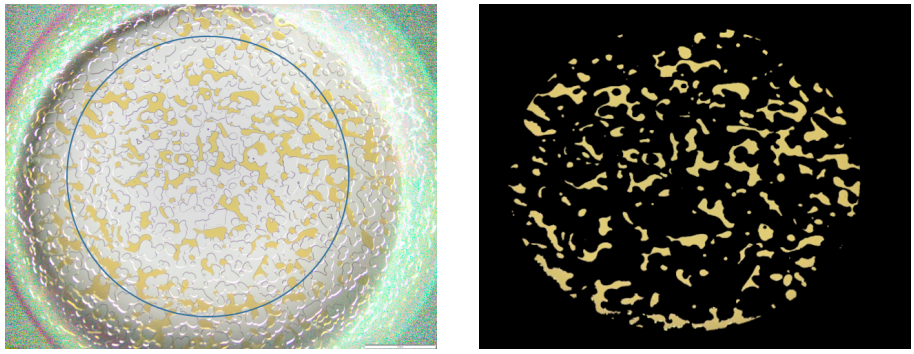

**(a)** **(b)**

**Figure 6.1:** (a) Photo showing area of snapshot used to calculate oil saturation. (b) MATLAB photo showing the circle used to calculate oil saturation.

Even though the circle that calculates the oil saturation should avoid the shadow and blurred areas, figure 6.1a shows that the circle could have been larger and still manage to avoid these areas. The area of the blue circle in figure 6.1a is only 25 % of the total flow area in the microchip. The area of the snapshot and this circle was calculated using the measurement tools in the Stream Basic program. The circle in figure 6.1a was added manually based on comparison with figure 6.1b, which adds some errors to the numbers. However, the numbers still give a good estimate of how small part of the microchip that is analyzed. Hence, the oil saturation calculated and presented in the graphs in chapter 5 represents only 25 % of the total flow area. This is a very small portion and brings a lot of uncertainty to the results.

## 6.3 Amount of pore volume injected

Since the rock pore volume of the microchip is only 2.3 $\mu$m, the amount of pore volumes injected becomes huge when injecting a total of 3.68 mL for each fluid. As seen from figure 5.23a, 3200 pore volumes are injected during the tertiary flooding. This topic is important to discuss as the pore volumes injected are so huge compared to both real conditions and core flooding.

These large pore volumes can raise questions to how valid this flooding with microfluidics is. The microchip represents a tiny portion of the reservoir, and the injected pore volume cannot be compared to injecting amounts of pore volumes of a reservoir. It could be reasonable to believe that several pore volumes are flushed through a small portion of 23 $\mu$m near the injector. However, 3200 pore volumes are still very large. When working with a system in the micrometer scale, the amount of fluid injected will quickly become several times larger than the pore volume of the model.

## 6.4 Experimental setup design

As described previously, a great part of this master thesis was to optimize the experimental setup, second to studying the oil saturation. The initial goal was to mainly use the microfluidics apparatus to study the possibilities of using nanocellulose to enhance recovery. However, it turned out that several changes could be made to improve the apparatus, and exclude factors that might affect the results.

The original setup in figure 4.4a had a line that went from the syringe and straight into the microchip. The syringe line for the water/nanofluids went through a three-way valve that could be used to bleed the lines. However, the injection line had to be removed from the microchip every time a new fluid was injected. There was a possibility of air entering the microchip every time this line was removed. In addition, the microchip had to be removed from the microscope to insert the injection line between each fluid change. Moving the microchip during each fluid change could disturb and move the fluids in the chip, which might affect the results.

The two-way valve in figure 4.4b was added near the microchip to avoid removing the injection line between the flooding of water and nanofluids. The injection line connected to the microchip would be connected to the microchip during the whole experiment, and hopefully minimize air in the system. The syringe lines would be bled with the fluid to be injected and placed in the two-way valve. However, it was not possible to bleed the valve connecting the syringe lines to the injection line, since the valve was a two-way valve. This means that the volume inside the valve would most likely be filled with air, and this air would enter the microchip during injection.

Finally, a three-way valve (originally four-way valve, but blocked in one direction so that it worked as a three-way valve) was provided, as seen in figure 4.4c. This made it possible to bleed the valve with each fluid prior to injection, so that the valve always would be filled with the injection fluid and not air. As described earlier, this setup was the one used for most of the experiments. The factors disturbing the microchip and allowing air to enter the system were eliminated as much as possible. An issue with this setup is the dead volume that is injected through the line connected to the microchip.

## 6.5 Dead volume injected

The extra injection line from the three-way valve to the microchip adds a dead volume to the total volume injected. The injection line will be filled with water prior to tertiary flooding of the nanofluids, as seen in figure 6.2. This volume of water will be injected during nanoflooding. Hence, the volume of nanofluids in the microchip will be less than the total volume injected. Equation 6.1 shows the total volume in the microchip, and there is no more fluid to be injected after nanoflooding. This logic applies to the waterflooding as well, as the injection line will be filled with oil prior to the flooding. However, the total volume of water injected will eventually equal the correct volume injected as seen from equation 6.1.

$$V_{total} = V_{injected} - V_{dead\ volume\ previous fluid} + V_{dead\ volume\ next\ fluid} \tag{6.1}$$

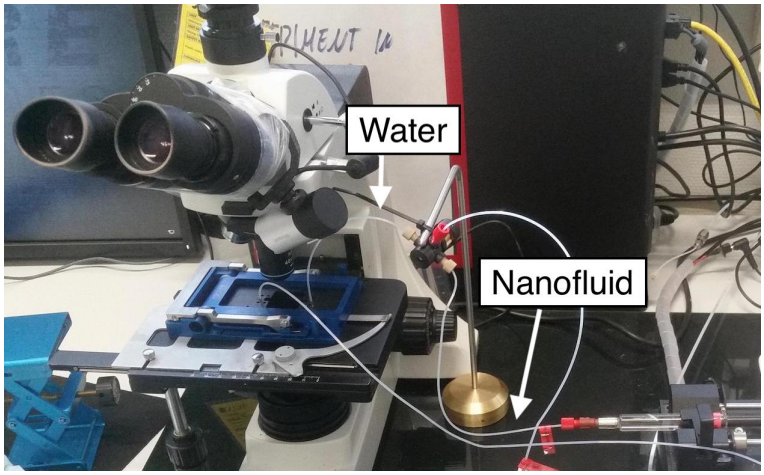


**Figure 6.2:** Photo showing the water filled injection line prior to tertiary nanoflooding.

The injection line is 16 cm long with an inner diameter of 0.08 cm, and the total dead volume equals 0.08 mL of fluid. A volume of 0.08 mL is less than 6 % of the total injected volume during low rate flooding, and less than 4% for the high rate flooding. This volume was injected after the nanofluid injection during one of the experiments to see if there were any effects. Since the volume is so small, no effects were seen. It is therefore considered reasonable not to add this volume after the end of each experiment.

To account for this dead volume, the experiments went on for a small amount of time before taking the snapshots. This time period was decided based on how long time it took the previously injected fluid to fully enter the microchip. Hence, the oil saturation calculated for each fluid should represent the fluid injected and not the previous fluid. However, it was harder to observe the front between water and nanofluids than between water and oil. The time period the oil used to enter the microfluidics was used as a reference for the nanofluid as well. This adds some uncertainty, and some of the early snapshots might represent a mix of water and nanofluid entering the microchip.

The inner volume of the three-way valve close to the microchip is 9.7 $\mu$m. However, this volume is not considered as a dead volume. The valve was filled with the fluid to be injected prior to each change of fluid. There might still be some amount of the previously injected fluid left inside the valve, but this volume is unknown. It is reasonable to assume that this volume is sufficiently small enough to ignore it.

## 6.6 Viscosity

There are some uncertainties related to the viscosity values converted to viscosity in the microfluidics system, as the viscosity versus RPM for the fluids was extrapolated to reach the RPM in the microfluidics system. These graphs are presented in figure A.1 and A.2 in Appendix A . The viscosity of both TEMPO-CNF and CNC heated to 120 $^{\circ}C$ decreased with increasing RPM, but CNC heated to 120 $^{\circ}C$ decreased much more. It is not known if the viscosity would continue with this trend for higher RPM values, and that is why the calculated viscosity in the microfluidics system is uncertain.

The results show that CNC heated to 120 $^{\circ}C$ is shear thinning, making the viscosity lower in the microfluidics system. TEMPO-CNF also shows a similar trend, but in a much smaller scale. Lowered viscosity of the fluids in the microfluidics system is not desirable for EOR, as the viscous effects will be reduced. However, the viscosity values are still larger than for water, except for CNC heated to 120 $^{\circ}C$ during the high rate flooding.

CNC at room temperature shows a different trend than the two other fluids measured in the Brookfield viscometer. These measurements were performed using two different spindle types. The appropriate spindle is chosen based on the assumed viscosity range of the fluid. It is believed that a torque around or above $10\%$ gives the most reliable results when using the Brookfield viscometer, but the torque should not be too high either. This implies that the viscosity values at 180 and 200 RPM using the S18 spindle, and the values at 100 and 120 RPM using the S30 spindle could be reliable. However, none of these values show a clear trend with respect to RPM, and it is not possible to transform the viscosity to microfluidics conditions. It is therefore assumed that CNC at room temperature is not shear thinning. It is then further assumed that the average measured viscosity of CNC remains the same in the microfluidics system.

## 6.7 Particle size

The Zetasizer nano ZS was able to measure the size of CNC and TEMPO-CNF. TEMPO-CNF are larger particles than CNC and would aggregate easier, so more measurements were needed. The size of CNC heated to 120 $^{\circ}C$ varied too much, and the apparatus was not able to report good result. The results presented in table 5.6 confirms that TEMPO-CNF are larger particles than CNC.

## 6.8 Capillary number

It was not possible to measure the interfacial tension and contact angle for CNC heated to 120 $^{\circ}C$, which will be discussed in the next section. Hence, the capillary number could not be calculated for this sample. Table 5.8 shows that the capillary numbers for all fluids injected are in the range of $10^{-5}$ to $10^{-4}$. All values are above $10^{-5}$, which implies that the flow is mostly dominated by viscous forces, as described in chapter 3.

The capillary number calculations also raise question to the rates used in these experiments. The rates used in the microfluidics experiments are larger than the total pore volume, which could be problematic. The unusually small pore volume makes the whole process special and several issues has to be addressed. If the rates were to be lowered more, the experiments would go on for a longer time. In addition, the experiment time would be long before a stable oil saturation could be observed.

The issue with these high rates was whether the rates were so high that the water would be able to sweep out too much oil during waterflooding. These high rates could possibly increase the capillary number so much that the flow would be completely dominated by viscous forces. If this was the case, there could be so small amounts of oil left in the microchip that the effect of the nanofluids would not apply. In addition, the enhanced oil recovery could simply be due to the high rates and not an effect of the fluids. However, a sensitivity study on the rates was performed in addition to calculating the capillary number for the rates used. This study showed that a huge change in the rate was needed for the capillary number to change significantly, which could imply that the relatively high rates were not an issue.

## 6.9 Contact angle

Since the Drop Shape Analyzer uses a camera to capture the oil droplet in the glass chamber, the camera must be able to separate the two fluids in the chamber. Both 1 $\%$ CNC and 0.1 $\%$ TEMPO-CNF is less transparent than water, making it harder for the camera to capture the oil droplet. This issue was solved by enhancing the brightness of the camera. However, 1 $\%$ CNC previously heated to 120 $^{\circ}C$ is too opaque for the camera to separate between the two fluids. Changing the brightness of the camera was not able to overcome this issue, and it was not possible to get measurements from this sample. The same issue applies for the interfacial tension measurements of 1 $\%$ CNC previously heated to 120 $^{\circ}C$. All contact angle and IFT measurements were performed over 12 hours to see if the value would change over time. Even though some of the measurements would continue to decrease after 12 hours, this time period was considered large enough to see a trend.

### 6.9.1 0.1 wt$\%$ NaCl and crude oil C

Figure 5.1 shows that the contact angle between 0.1 wt$\%$ NaCl and crude oil C remained stable around 57.6° for the entire experiment time. However, the measurements taken the first hour are somewhat lower than the rest. A contact angle of around 57° indicates that the wetting state between the glass plate, 0.1 wt$\%$ NaCl and crude oil C is water-wet. Since the oil droplet is not hanging from the needle as for the IFT measurements, it is harder to control the volume of the oil droplet. The volume is first measured when the oil droplet is placed under the glass plate. This makes the volumes vary between the experiments, which may affect the results and make them less comparable than the IFT measurements. Table B.1 in Appendix B shows that the volume of the droplet remained quite stable over the time period of 12 hours.

### 6.9.2 1 % CNC and crude oil C

Figure 5.3 shows that the contact angle between CNC and crude oil C remained stable around 49.4° for the entire experiment time. This value is about 8° lower than for 0.1 wt% NaCl and crude oil C, making the system more water-wet. This implies that the adding of CNC to low salinity water could lower the contact angle and change the system towards a more water-wet state, which could be favorable for the oil recovery as described in chapter 3. Table B.2 in Appendix B shows that the volume of the oil droplet is much higher than for water and crude oil C, and that the volume remains quite stable.

### 6.9.3 0.1 % TEMPO-CNF and crude oil C

Figure 5.5 shows that the contact angle between TEMPO-CNF and crude oil C remained stable between 42° and 43°, except for some lower values in the first hour of the experiment. This contact angle is about 15° lower than for 0.1 wt% NaCl and crude oil C, which means that adding TEMPO-CNF to water lowers the contact angle more than adding CNC does. Figure 5.6 shows that the contact angle varies a bit between the edges of the droplet. This might be due to the fact that the fit shown as a blue circle is not able to fit the droplet properly, which can be seen as a read line next to the green line measuring the contact angle. Table B.3 shows that the volume of the droplet is less than for both the experiments with CNC and water.

## 6.10 Interfacial tension

### 6.10.1 0.1 wt% NaCl and crude oil C

It can be seen from figure 5.7 that the interfacial tension between 0.1 wt% NaCl and crude oil C decreases from 18 mN/m to around 13 mN/m. The interfacial tension is somewhat stabilized at the end of the experiment time. Table C.1 in Appendix C shows that the volume of the droplet decreases somewhat during the experiment which will make the IFT decrease as well. The volume of the oil droplet was made approximately equal for all IFT measurements, which was done to make the experiments comparable.

### 6.10.2 1 % CNC and crude oil C

Figure 5.9 shows that the interfacial tension between CNC and crude oil C decreases from about 15.6 mN/m to 14.4 mN/m, which is a smaller decrease than for 0.1 wt% NaCl and crude oil C. However, the decline is more constant and continues to decrease during the entire experiment time. The interfacial tension is somewhat lower for CNC and crude oil C than for water and crude oil C in the beginning of the experiment, indicating that adding CNC could decrease the interfacial tension. However, the interfacial tension for water and crude oil C is decreased to 13 mN/m at the end of the experiment which is less than for CNC. Table C.2 in Appendix C shows that the volume of the droplet decreased during the experiment time.

### 6.10.3 0.1 % TEMPO-CNF and crude oil C

Figure 5.11 shows that the interfacial tension between TEMPO-CNF and crude oil C actually is higher than for 0.1 wt% NaCl and crude oil C, and remains higher during the entire experiment time. The adding of TEMPO-CNF to water increases the IFT between water and crude oil C, which is not favorable for the oil recovery. Figure 5.11 shows that the interfacial tension continues to decrease during the entire experiment time. Table C.3 in Appendix C shows that the volume of the droplet remained more stable than for CNC and water.

## 6.11 Testing of rates

As the goal was to see a stabilized oil saturation, the tests were continued until this result was obtained. A factor that should be discussed is at what accuracy the oil saturation should stabilize on, and for how long one should require the saturation to remain stable.

As discussed earlier, the oil saturation calculated represents only 25% of the flow area. This is why the changes in oil saturation has to be analyzed carefully. If the oil saturation stabilizes over a long period of time, one might assume that the oil saturation has stabilized in the entire microchip as well. However, this is an uncertainty that must be considered when analyzing the results. For these tests, the oil saturation was considered stable counting two significant digits.

As the oil saturation did not stabilize during the first injection in test 1, it was decided to inject the same volume of water immediately with the same rate. Figure 5.13a and 5.13b shows that the saturation still varied. Table D.1 in Appendix D shows all oil saturation values for test 1. Based on the results from test 1, it was decided to run another test with a higher rate. The injection was run three times, and the oil saturation continued to decrease during the third round of injection. It can be seen from table D.2 that the oil saturation did not vary much at the end. A change in oil saturation from 0.32 to 0.30 could be due to the fact that the whole microchip is not shown in the photo. However, a third test was run to see if the oil saturation could be more stabilized. Figure 5.15a, 5.15b and the tables D.3 and D.5 in Appendix D shows that the oil saturation stayed at 0.42 for over 40 minutes and for over 900 pore volumes injected. As the rates and volumes from test 3 showed the most stable oil saturation, these were the values used for the actual experiments.

## 6.12 Secondary flooding

### 6.12.1 1 % CNC

Figure 5.18a and 5.18b shows that the oil saturation went somewhat down when switching to the high rate, but only from 0.33 to 0.31. The oil saturation ended at 0.31, which is not much lower than the end saturation for waterflooding prior to tertiary flooding. Hence, no significant effect was seen during secondary flooding with CNC.

This experiment was performed using the experimental setup in figure 4.4b and not the final experimental setup, which might affect the results. It is believed that the final experimental setup is the best choice, and the experiments performed prior to these changes might be less valid.

### 6.12.2 0.1 % TEMPO-CNF

The effects of the secondary flooding of TEMPO-CNF were much more visible than for CNC, as can be seen from figure 5.20. This experiment was performed using the new experimental setup. A distinct decrease in oil saturation is shown when increasing the rate, and the end saturation of 0.12 is much lower than for the secondary flooding of CNC. As discussed previously, the results show that the interfacial tension is not lowered when adding TEMPO-CNF to water, and the wettability is changed towards more water-wet. A possible mechanism could be that a more water-wet system makes TEMPO-CNF able to enter the small pores throats and sweep more oil out.

## 6.13 Tertiary flooding

### 6.13.1 1 % CNC, old setup

This experiment was the first experiment to be performed, and the old setup in figure 4.4a was used. Figure 5.23a and 5.23b shows that the oil saturation went drastically down for the tertiary injection of CNC. There is a major difference between the tertiary flooding of CNC performed on the old experimental setup and the flooding with the new setup. This implies that there is something wrong with one of the experiments, most likely this experiment. If this experiment is less valid, it makes the other experiments performed using the old setup less reliable as well.

When switching the injection fluid from water to CNC, the nanofluid was not able to flow through the lines and the lines were replaced. Hence, different lines were used for the water and nanofluid injection. The nanofluid might have been unable to flow through the lines due to small twists or damages on the line. The water flows easier and could flow through the line, but would flow with a lower or uneven rate due to the damaged line. This means that the nanofluid would flow with a higher rate since the lines were switched. However, this is only one possible explanation to why the end saturation is so low.

Since this experiment was performed on the initial experimental setup, there was still a huge problem with air in the system. It can be seen from figure 5.22 that there might be some visible air, shown as areas with a darker outline. It can be hard to separate the air from the water when studying the photos of the microchip, but it is believed that air bubbles have darker outline. Since the microchip is water-wet, the water will surround the pores while air will form separate bubbles. The fluid that is left in the microchip at the end of the flooding might be a lot of air, and not much CNC. However, air should not be able to push out oil better than CNC.

This experiment is somewhat of a mystery as so much oil was swept out of the microcip. The exact explanation to why this happens is not clear, but these are some possible scenarios. These strange results further minimize the validity of the experiments performed using the old experimental setup.

### 6.13.2 1 % CNC, new setup

As discussed earlier, this experiments varies a lot from the same experiment performed using the old experimental setup. Figure 5.26a and 5.26b shows that the tertiary injection of CNC had no additional effect on the oil recovery. It is not possible to visually see any air bubbles in figure 5.25, which implies that there was not much air in the system. The results clearly shows that the effect of adding CNC to water does not increase the oil recovery. However, the validity of the micromodel has to be taken into account. Since the dimensions are so small, the system is different from core flooding and other factors has to be taken into account. CNC might still have potential as an EOR fluid, but this particular micromodel might not be a suitable tool to study the potential.

### 6.13.3 0.1 wt% NaCl as both secondary and tertiary fluid

This experiment was performed using the old experimental setup, which was previously discussed to be less reliable than the new experimental setup. The experiment was performed second to the tertiary flooding of CNC using the old setup. The goal was to see if the effect was due to CNC or simply an effect of time. This experiment showed that less oil was swept out, implying that the small amount of oil left in the microchip during the tertiary flooding of CNC was due to effects of the nanofluid. However, the tertiary flooding of CNC using the new setup erased some of the validness of the first experiment. Hence, this flooding with 0.1 wt% NaCl as both secondary and tertiary fluid is not of significant importance.

### 6.13.4 1 % CNC heated to 120 $^{\circ}C$

This experiment was performed because a core flooding of CNC heated to 120 $^{\circ}C$ was previously performed by a Ph.D candidate at NTNU. It was desirable to see how this fluid would behave in the microfluidics apparatus compared to core flooding. As it was not possible to heat up the microfluidics apparatus, the fluid was previously heated to 120 $^{\circ}C$ and cooled down to room temperature prior to the flooding. It was believed that the internal properties of the fluid would change at 120 $^{\circ}C$, and remain changed when cooled down.

Figure 5.32 shows that there was no significant effect on the oil saturation when injecting the nanofluid. However, figure 5.31 shows that small oil droplets appears during the high rate flooding of the nanofluid. Instead of pushing the oil out, the oil is split into smaller droplets but remains in the microchip. This effect is not seen for any of the other fluids, and could be due to the internal changes due to the heating. As discussed for the viscosity measurements, the viscosity of CNC heated to 120 $^{\circ}C$ seems to decrease with increasing RPM. The viscosity is lowered to less than the viscosity of water during the high rate injection. A possible explanation could be that the viscosity is too low for the nanofluid

to push the oil out. The nanofluid might instead go through and split the oil into small droplets. As this nanofluid was too opaque to get any measurements in the Drop Shape Analyzer, the IFT is unknown. If the IFT is sufficiently lowered, the two phases might blend and the oil droplets could be the beginning of emulsions. The IFT between two phases usually decreases with increasing temperature. If the change in internal properties of the nanofluid remains changed after cooling down to room temperature, the IFT might have been lowered. However, these are just possible explanations and not an absolute answer. A combination between the high rate and the properties of the heated fluid could be possible answers to the effect.

### 6.13.5 0.1 % TEMPO-CNF

Figure 5.34 shows that the tertiary flooding of TEMPO-CNF had no significant effect on the oil recovery. An important part of the discussion is why an effect was observed during the secondary flooding of TEMPO-CNF but not during the tertiary flooding. These results might imply that the effects of TEMPO-CNF only apply when there is a lot of oil left in the system. However, the comparison of the waterflooding showed that there are differences in the oil saturation for each experiment. The low end saturation for the secondary flooding of TEMPO-CNF could be due to errors in the microfluidics system, or an effect of TEMPO-CNF. However, no significant effect was observed during the tertiary flooding.

### 6.13.6 1 % CNC, low rate flooding

As there were some uncertainties concerning the high rate used in the experiments, a final experiment using only the low rate was performed. It was desirable to see if CNC was able to push more oil out when the water was previously injected with only the low rate. However, figure 5.37 shows that there was no significant change in oil saturation during the injection of CNC. These results might imply that the high rate was not an issue and a reason for the poor effects of the nanofluids. These results further support the conclusions made from the capillary number calculations.

## 6.14 Waterflooding

The comparison and error calculations of the waterflooding for all tertiary experiments were done to see how much these experiments varied. In theory, the end saturation for these experiments should be somewhat equal. The two experiments performed on the old experimental setup had a variation in end saturation of 7.33 % for the low rate flooding and 5.86 % for the high rate. The variation was higher for the three experiments performed on the new experimental setup. However, more experiments allow for larger errors. There are several factors that could explain why these waterflooding experiments vary. The initial oil saturation of the microchip could vary, and there could be errors on the pump making the rates vary. These factors will be further discussed under the section concerning sources of errors.

## 6.15 Comparison with findings in the literature

As presented in the literature review, Kusanagi et al. (2015) found that additional oil was recovered by tertiary flooding of CNF. The results from this master thesis shows that additional oil was recovered by secondary flooding of CNF but not by tertiary flooding. However, the results from both this thesis and the literature study shows that CNF could have the ability to push out additional oil from a porous media. The viscosity measurements from the Kusanagi et al. (2015) study showed similar results as this master thesis. CNF showed a clear shear thinning effect for concentrations above 0.1 %. This beginning effect was seen for the viscosity measurements performed in this master thesis as well, as the viscosity decreased slightly with increasing shear. This fact implies that the concentration of 0.1 % used in this master thesis was an appropriate choice. In addition, the electrolyte sensitivity of CNF was discussed in the Kusanagi et al. (2015) study. The brine used in this master thesis contains only NaCl and no other ions. Brine used in real situations in the oil industry would contain several electrolytes which could affect the stability of CNF.

Molnes et al. (2016) study on CNC showed that CNC had good colloidal stability, which was confirmed in this master thesis as well, by the size measurements and no observation of aggregates during flooding. Molnes et al. (2016) also found CNC to be independent of shear rate, which were the conclusions drawn from the results in this master thesis as well. The study by Wei et al. (2016) showed that the modified nanocellulose could reduce the IFT between oil and water significantly. This effect was not seen for the IFT measurements in this master thesis. However, the nanocellulose used in the study by Wei et al. (2016) and in this master thesis was different, which makes the results less comparable. No literature showing the IFT or contact angle between crude oil C, CNC and TEMPO-CNF was found.

Some of these studies presented in the literature review showed that microfluidics could be used to study the oil recovery. This master thesis showed that flooding in the microfluidics apparatus gave varying results and contained a lot of uncertainties. Microfluidics could have the potential as a tool to study the EOR potential of fluids. However, this particular micromodel needs further optimization.

## 6.16 Sources of error

### 6.16.1 Area of microchip viewed

As discussed previously, only 38% of the microchip is shown in the snapshots while the calculated oil saturation only represents 25% of the microchip. This is a huge disadvantage of the system and brings uncertainty to the results. The oil saturation in 75% of the microchip could possibly be different from the calculated value. However, if the saturation stabilizes over a long time, it is reasonable to assume that the oil saturation is stable in the rest of the microchip as well. It is still a disadvantage that such a small portion of the microchip is represented, and that the inlet cannot be seen.

### 6.16.2 Air in the system

Air in the system disturbs the results, as there are more than two phases present. The MATLAB code that analyzes the oil saturation is not able to separate between water and air, so it is sometimes hard to see how much air that has entered the system. This source of error was significantly minimized when improving the experimental setup. However, some air can still enter the system with the new experimental setup. Even though the three-way valve is flushed with the injection fluid, some air might still be trapped in small areas inside the valve. The vacuum procedure of the system could also have some errors, leaving some air left in the lines. A third way that air can enter the system is through the syringes. When filling the syringe with the injection fluid, it is important to avoid air bubbles in the fluid.

### 6.16.3 Fully oil saturated microchip

When initially saturating the microchip with oil, there is always some water in the microchip as well. The goal is to saturate the chip as much as possible with oil, but the success of this goal varies between the experiments. The MATLAB code that analyzes the oil saturation uses the "fully" oil saturated microchip as a reference of 100% oil saturation, and compares the rest of the photos to this reference. The code is not able to separate the water from the pores, but compares the yellow areas representing oil to the blank areas. This source of error could be a possible explanation to why the end saturation in the different waterflooding experiment varies. The initial oil saturation prior to the flooding varies between the experiments, making the final oil saturation vary as well.

### 6.16.4 Pump rates

The pump was tested prior to all experiment to see if the correct rates were pumped, and the results showed that the rates were correct. However, this might have changed during the experimental part of this master thesis. If the pump rate varies from the rate set on the computer, the rates used in each experiment could possibly vary. In addition, the rate might be uneven and pump the fluids in slugs. The pump has some limitations regarding maximum and minimum rates, and stops for some seconds before running again for high rates. In addition, there would often be a lag between starting the pump on the software and when the pump actually started. The whole uncertainty regarding the pump and the rates brings a source of error to the experiments.

### 6.16.5 Sensitivity of the Drop Shape Analyzer

The interfacial tension can be easily affected by small factors disturbing the sample to be measured. The system where the IFT and contact angle is measured is not a closed system, as can be seen from figure 4.3a. Hence, the measurements can be disturbed by dust/particles entering the sample. In addition, interfacial tension is strongly dependent on temperature. The room temperature in the laboratory is somewhat varying, which could affect the results. These factors could give some explanation to why the IFT measurements did not stabilize over 12 hours. Another source of error that could affect the results of

the values measured in the Drop Shape Analyzer is the volume of the oil droplet. As mentioned earlier, the volume of the droplet should be equal for all the experiments. In addition, the volume might vary during each experiment. The volume will decrease with time, making the IFT decrease as well. The volume of the droplet might decrease if the table under the apparatus is shaken or disturbed in some way during the experiment.

## 6.17 Recommendations for future work

A pump that is reliable and always pumps the correct rates should be used in future experiments. There were several errors caused by the pump during the experiments, and a new pump would minimize these errors. The rates were shortly tested prior to the experiments in this master thesis, but more time should be spent on choosing appropriate rates for the microfluidics system. A proper evaluation of the apparatus is needed prior to the experiments, so that the experiments are performed with appropriate rates.

The experimental setup of this master thesis was changed during the process, and the EOR aspect was considered simultaneously. A recommendation for future work is to spend more time on optimization prior to the experiments. The changes on the experimental setup should have been made prior to the experiments and not during the process, which would make all the results more comparable. A master thesis could in fact be to only focus on the microchip, appropriate rates and experimental setup design. There were a lot of errors and uncertainties associated with the microfluidics experiments, which were due to the fact that the apparatus was a relatively new addition to the laboratory, and lack of expertise on the model.

Many of the sources of errors regarding the experimental setup were minimized during the process. However, a more permanent setup for the three-way valve added near the microchip could be made. The valve was hanging loosely into a stand during the experiments. When changing the directions of the valve, the valve would move and could disturb the inlet line into the microchip. It is important that this line stays still so that the line does not jump out of the inlet hole of the microchip, or disturbs the microchip in other ways. The valve could be attached to a wall like the waste valve.

As discussed previously, the camera is only able to capture a portion of the microchip. A camera that is able to capture the whole microchip should definitely be used in future experiments. The MATLAB code should also be changed so that it captures more of the snapshots, and still avoid shadow and blurred areas. Another change that could be made to the MATLAB code is to change the code so that it can separate water from the pores. This would make it possible to see how much oil the microchip actually contains prior to flooding, instead of assuming 100% saturation. The MATLAB code was previously written and provided for use in this master thesis.

An interesting addition to the experiments performed in this thesis could be to change the wettability of the microchip. This possibility was addressed during the experimental work, but lack of equipment capable of handling the toxic fluid that would have to be injected

hindered the process. There exists a procedure that could change the wettability of the microchip to oil-wet, but it involves the injection of some toxic fluids. However, it could be interesting to see the effects on an oil-wet porous medium as well. The possibility of measuring pressure over the microchip was also discussed during the experimental work of this master thesis. However, this equipment was never installed. Measuring pressure could give more information, and could be done in future experiments.

The contact angle and IFT measurements could be performed using a temperature program. The temperature would then be forced to stay at 21 $^{\circ}C$ during the entire experiment, and would not vary depending on the temperature in the laboratory. In addition, a more closed setup around the fluid sample would be favorable, to minimize factors that can disturb the results.

The results showed that there are a lot of uncertainty and errors related to the microfluidics apparatus. Microfluidics might work better as a tool to study flow mechanisms and patterns than as an alternative to core flooding. The major advantage of microfluidics is in fact the visualization of the flow, and this advantage should be used more in future experiments. This part was not used that much in this master thesis, as the focus was to study the oil saturation.

Chapter 7

# Conclusion

- No significant effect on the oil saturation was observed during secondary and tertiary flooding with CNC, nor for the solution heated to 120°$C$.
- The oil saturation was significantly lowered during secondary flooding with TEMPO-CNF. However, the tertiary flooding showed no significant effect.
- Both CNC and TEMPO-CNF contributes to a more water-wet system, but the effect of TEMPO-CNF is more significant.
- Neither CNC nor TEMPO-CNF contributes to an effect that would significantly decrease the IFT and enhance oil recovery.
- The viscosity of brine was altered when adding both CNC and TEMPO-CNF. The viscosity of TEMPO-CNF and CNC heated to 120 °$C$ decreased with increasing shear rate. However, all viscosity values converted to the shear rate conditions in the microfluidics apparatus were still higher than the viscosity of brine, except for CNC heated to 120 °$C$ during the high rate flooding.
- There was a lot of uncertainty related to the microfluidics model as identical experiments showed varying results. Further optimization is needed to minimize uncertainties and errors. However, microfluidics is a promising method for visualization of fluid flow. The apparatus might work better as an addition to conventional core flooding rather than a replacement.

# References


Al-Zahrani, S. M., 1997. A generalized rheological model for shear thinning fluids. Journal of Petroleum Science and Engineering 17 (3-4), 211–215.

Andreassen, L., 2015. Nanoparticle effect on interfacial properties related to enhanced oil recovery. Master's thesis, NTNU.

Arab, D., Pourafshary, P., 2013. Nanoparticles-assisted surface charge modification of the porous medium to treat colloidal particles migration induced by low salinity water flooding. Colloids and Surfaces A: Physicochemical and Engineering Aspects 436, 803–814.

Atencia, J., Beebe, D. J., 2004. Controlled microfluidic interfaces. Nature 437 (7059), 648.

Aurland, K., 2015. Using nanofluids to enhance oil recovery. Accessed on 11/20/2017.
URL http://www.ntnutechzone.no/en/2015/05/using-nanofluids-to-enhance-oil-recovery/

Avraam, D., Payatakes, A., 1995. Flow regimes and relative permeabilities during steady-state two-phase flow in porous media. Journal of Fluid Mechanics 293, 207–236.

Bhattacharjee, S., 2016. Dls and zeta potential–what they are and what they are not? Journal of Controlled Release 235, 337–351.

Chatzis, I., Morrow, N. R., et al., 1984. Correlation of capillary number relationships for sandstone. Society of Petroleum Engineers Journal 24 (05), 555–562.

Darcy, H., 1856. Les fontaines publiques de la ville de Dijon: exposition et application... Victor Dalmont.

Das, S. K., Choi, S. U., Yu, W., Pradeep, T., 2007. Nanofluids: science and technology. John Wiley & Sons.

DataPhysics, 2018. Pendant drop method - optical determination of the surface/interfacial tension. Accessed on 12/05/2017.
URL http://www.dataphysics.de/2/start/understanding-interfaces/drop-shape-analysis/pendant-drop-method/

DOE, U., 2017. Us energy government, oil and gas research, enhanced oil recovery. Accessed on 11/05/2017.
URL https://energy.gov/fe/science-innovation/oil-gas-research/enhanced-oil-recovery

Dufresne, A., 2013. Nanocellulose: a new ageless bionanomaterial. Materials Today 16 (6), 220–227.

Gong, H., Li, Y., Dong, M., Ma, S., Liu, W., 2016. Effect of wettability alteration on enhanced heavy oil recovery by alkaline flooding. Colloids and Surfaces A: Physicochemical and Engineering Aspects 488, 28–35.

Hendraningrat, L., Li, S., Torsæter, O., 2013a. A coreflood investigation of nanofluid enhanced oil recovery. Journal of Petroleum Science and Engineering 111, 128–138.

Hendraningrat, L., Li, S., Torsater, O., et al., 2013b. Effect of some parameters influencing enhanced oil recovery process using silica nanoparticles: An experimental investigation. In: SPE Reservoir Characterization and Simulation Conference and Exhibition. Society of Petroleum Engineers.

Kapusta, S., Balzano, L., Te Riele, P. M., et al., 2011. Nanotechnology applications in oil and gas exploration and production. In: International Petroleum Technology Conference. International Petroleum Technology Conference.

Kenney, F., Keeping, E. S., 1951. Mathematics of statistics-part two. D. Van Nostrand Company, Inc Princeton,; New Jersey; Toronto; New York; London.

Khezrnejad, A., James, L., Johansen, T., 2015. Nanofluid enhanced oil recovery–mobility ratio, surface chemistry, or both. In: Int. Symp. of the Society of Core Analysts. pp. 16–21.

KRÜSS, 2017a. Drop shape analyzer dsa100. Accessed on 12/03/2017.
URL https://www.kruss.de/products/contact-angle/dsa100/drop-shape-analyzer-dsa100/?gclid=EAIaIQobChMIhpOqtebF1wIVE0kZCh13pQP0EAAYASAAEgIOQPD_BwE

KRÜSS, 2017b. Pendant drop. Accessed on 12/03/2017.
URL https://www.kruss.de/services/education-theory/glossary/pendant-drop/

KRÜSS, 2017c. Sessile drop. Accessed on 12/03/2017.
URL https://www.kruss.de/services/education-theory/glossary/sessile-drop/

KRÜSS, 2017d. Zetasizer nano zs for size, zeta potential, protein mobility and microrheology. Accessed on 12/03/2017.
URL https://www.malvern.com/en/products/product-range/zetasizer-range/zetasizer-nano-range/zetasizer-nano-zs

Kusanagi, K., Murata, S., Goi, Y., Sabi, M., Zinno, K., Kato, Y., Togashi, N., Matsuoka, T., Liang, Y., et al., 2015. Application of cellulose nanofiber as environment-friendly polymer for oil development. In: SPE/IATMI Asia Pacific Oil & Gas Conference and Exhibition. Society of Petroleum Engineers.

Lake, L. W., et al., 1989. Enhanced oil recovery.

Micronit, 2018. 3-pack enhanced oil recovery chips with random network. Accessed on 02/12/18.
URL https://store.micronit.com/microfluidic-chips/enhanced-oil-recovery-chips/3-pack-eor-chips-random-network

Molnes, S. N., Torrijos, I. P., Strand, S., Paso, K. G., Syverud, K., 2016. Sandstone injectivity and salt stability of cellulose nanocrystals (cnc) dispersionspremises for use of cnc in enhanced oil recovery. Industrial Crops and Products 93, 152–160.

Negin, C., Ali, S., Xie, Q., 2016. Application of nanotechnology for enhancing oil recovery–a review. Petroleum.

Npd, 2018a. Gode muligheter for å få ut mer olje. Accessed on 12/09/2017.
URL http://www.npd.no/tema/okt-utvinning/temaartikler/gode-muligheter-for-a-fa-ut-mer-olje/

Npd, 2018b. Storage options with eor. Accessed on 12/09/2017.
URL http://www.npd.no/en/Publications/Reports/Compiled-CO2-atlas/8-Storage-options-with-EOR/

Npd, 2018c. Store mengder olje fra gassinjeksjon. Accessed on 12/09/2017.
URL http://www.npd.no/no/Tema/Okt-utvinning/Temaartikler/Store-mengder-olje-fra-gassinjeksjon/

Npd, 2018d. Verkty for økt utvinning. Accessed on 12/09/2017.
URL http://www.npd.no/no/Tema/Okt-utvinning/Temaartikler/Verktoy-for-okt-utvinning-/

Ogolo, N., Olafuyi, O., Onyekonwu, M., et al., 2012. Enhanced oil recovery using nanoparticles. In: SPE Saudi Arabia section technical symposium and exhibition. Society of Petroleum Engineers.

Onyekonwu, M. O., Ogolo, N. A., et al., 2010. Investigating the use of nanoparticles in enhancing oil recovery. In: Nigeria Annual international conference and exhibition. Society of Petroleum Engineers.

Petrowiki, 2017. Interfacial tension. Accessed on 11/20/2017.
URL http://petrowiki.org/Interfacial_tension

Psaltis, D., Quake, S. R., Yang, C., 2006. Developing optofluidic technology through the fusion of microfluidics and optics. Nature 442 (7101), 381.

Rajagopalan, R., Hiemenz, P. C., 1997. Principles of colloid and surface chemistry. Marcel Dekker, New-York, 3e édition, ISBN 0 8247 (9397), 8.

Salas, C., Nypelö, T., Rodriguez-Abreu, C., Carrillo, C., Rojas, O. J., 2014. Nanocellulose properties and applications in colloids and interfaces. Current Opinion in Colloid & Interface Science 19 (5), 383–396.

Salvesen, S. H., 2017. Specialization project: Nanocellulose for enhanced oil recovery.

Schlumberger, 2018a. Enhanced oil recovery. Accessed on 11/12/2017.
URL http://www.glossary.oilfield.slb.com/Disciplines/Enhanced-Oil-Recovery.aspx

Schlumberger, 2018b. Enhanced oil recovery (eor). Accessed on 11/05/2017.
URL http://www.slb.com/services/technical_challenges/enhanced_oil_recovery.aspx

Schlumberger, 2018c. Wettability. Accessed on 11/20/2017.
URL http://www.glossary.oilfield.slb.com/Terms/w/wettability.aspx

Selle, O. M., Fischer, H., Standnes, D. C., Auflem, I. H., Lambertsen, A. M., Svela, P. E., Mebratu, A. A., Gundersen, E. B., Melien, I., et al., 2013. Offshore polymer/lps injectivity test with focus on operational feasibility and near wellbore response in a heidrun injector. In: SPE Annual Technical Conference and Exhibition. Society of Petroleum Engineers.

Sheng, J., 2010. Modern chemical enhanced oil recovery: theory and practice. Gulf Professional Publishing.

SINTEF, Apr 2011. Interfacial tension measurement. Accessed on 11/05/2017.
URL https://www.sintef.no/globalassets/upload/petroleumsforskning/brosjyrer/ift.pdf

Skår, H., 2014. Simulation of surfactant eor in a mechanistic model with fracture and ekofisk properties. Master's thesis, Institutt for petroleumsteknologi og anvendt geofysikk.

Stone, H. A., Stroock, A. D., Ajdari, A., 2004. Engineering flows in small devices: microfluidics toward a lab-on-a-chip. Annu. Rev. Fluid Mech. 36, 381–411.

Torsæter, O., Abtahi, M., 2003. Experimental reservoir engineering laboratory workbook. Norwegian University of Science and Technology.

Wasan, D., Nikolov, A., Kondiparty, K., 2011. The wetting and spreading of nanofluids on solids: Role of the structural disjoining pressure. Current Opinion in Colloid & Interface Science 16 (4), 344–349.

Wei, B., Li, Q., Jin, F., Li, H., Wang, C., 2016. The potential of a novel nanofluid in enhancing oil recovery. Energy & Fuels 30 (4), 2882–2891.

Xu, K., Zhu, P., Huh, C., Balhoff, M. T., 2015. Microfluidic investigation of nanoparticles role in mobilizing trapped oil droplets in porous media. Langmuir 31 (51), 13673–13679.

Youssif, M. I., El-Maghraby, R. M., Saleh, S. M., Elgibaly, A., 2017. Silica nanofluid flooding for enhanced oil recovery in sandstone rocks. Egyptian Journal of Petroleum.

Zhao, B., MacMinn, C. W., Juanes, R., 2016. Wettability control on multiphase flow in patterned microfluidics. Proceedings of the National Academy of Sciences 113 (37), 10251–10256.

# Appendix A

# Viscosity

## A.1 % CNC heated to 120°C

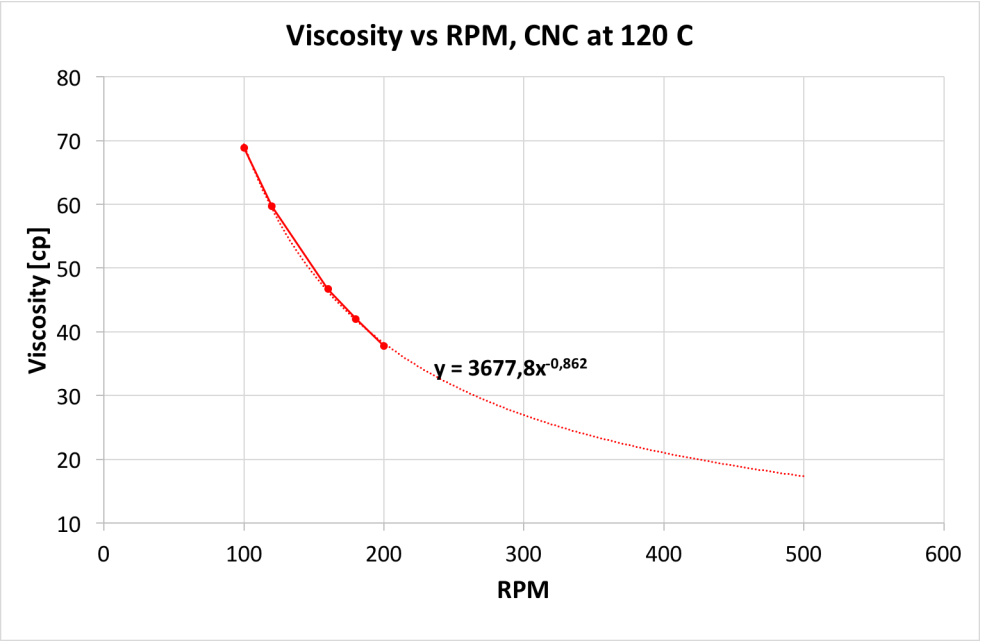


**Figure A.1:** Viscosity vs RPM for CNC heated to 120 °C, showing the extrapolation line used to calculate the viscosity at microfluidcs conditions.

## A.2 0.1 % TEMPO-CNF

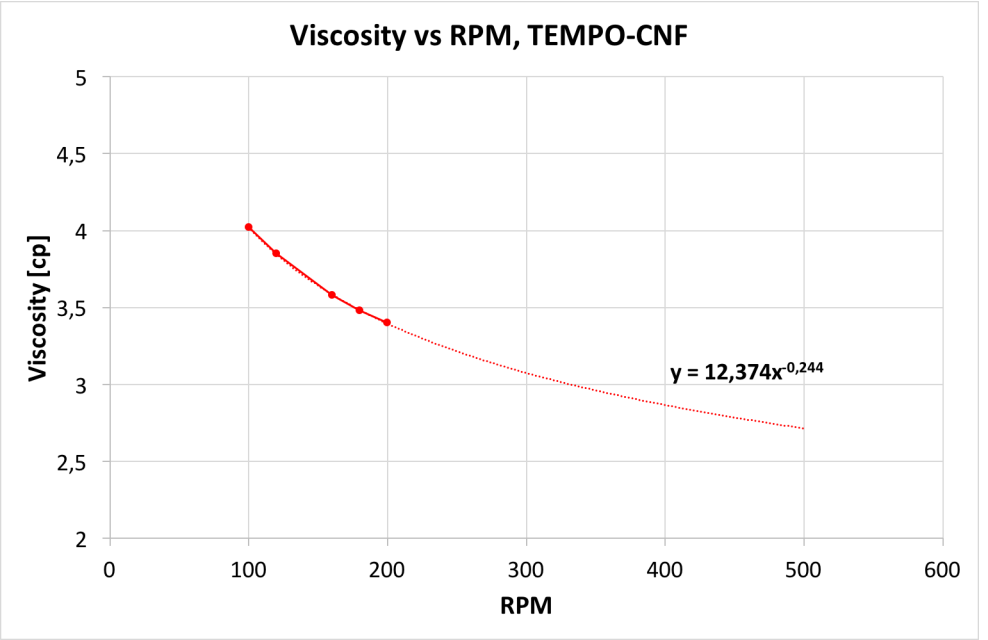


**Figure A.2:** Viscosity vs RPM for TEMPO-CNF, showing the extrapolation line used to calculate the viscosity at microfluidcs conditions.

# Appendix B

# Contact angle

## B.1 0.1 wt% NaCl and crude oil C

**Table B.1:** Average contact angle for each 30 minute of measurements for 0.1 wt% NaCl and crude oil C.

| Time [hh:mm] | Average contact angle [°] | Volume of oil drop [$\mu$L] |
|---|---|---|
| 00:30 | 56,92 | 46,4 |
| 01:00 | 57,61 | 46,2 |
| 01:30 | 57,78 | 46,1 |
| 02:00 | 57,78 | 46,0 |
| 02:30 | 57,81 | 46,0 |
| 03:00 | 57,79 | 45,9 |
| 03:30 | 57,78 | 45,9 |
| 04:00 | 57,76 | 45,9 |
| 04:30 | 57,72 | 45,9 |
| 05:00 | 57,71 | 45,9 |
| 05:30 | 57,69 | 45,9 |
| 06:00 | 57,67 | 45,8 |
| 06:30 | 57,65 | 45,8 |
| 07:00 | 57,66 | 45,8 |
| 07:30 | 57,68 | 45,8 |
| 08:00 | 57,66 | 45,7 |
| 08:30 | 57,65 | 45,7 |
| 09:00 | 57,64 | 45,7 |
| 09:30 | 57,65 | 45,7 |
| 10:00 | 57,65 | 45,7 |
| 10:30 | 57,65 | 45,7 |
| 11:00 | 57,65 | 45,7 |
| 11:30 | 57,65 | 45,7 |
| 12:00 | 57,65 | 45,7 |

## B.2 1% CNC and crude oil C

**Table B.2:** Average contact angle for each 30 minute of measurements for 1% CNC in 0.1 wt% NaCl and crude oil C.

| Time [hh:mm] | Average contact angle [° ] | Volume of oil drop[$\mu$L] |
|---|---|---|
| 00:30 | 49,51 | 81,23 |
| 01:00 | 49,51 | 80,92 |
| 01:30 | 49,40 | 80,65 |
| 02:00 | 49,51 | 80,60 |
| 02:30 | 49,40 | 80,42 |
| 03:00 | 49,41 | 80,34 |
| 03:30 | 49,41 | 80,28 |
| 04:00 | 49,34 | 80,18 |
| 04:30 | 49,29 | 80,08 |
| 05:00 | 49,29 | 80,00 |
| 05:30 | 49,34 | 80,00 |
| 06:00 | 49,37 | 79,90 |
| 06:30 | 49,36 | 79,84 |
| 07:00 | 49,36 | 79,75 |
| 07:30 | 49,43 | 79,74 |
| 08:00 | 49,36 | 79,63 |
| 08:30 | 49,41 | 79,61 |
| 09:00 | 49,39 | 79,55 |
| 09:30 | 49,45 | 79,55 |
| 10:00 | 50,07 | 79,96 |
| 10:30 | 49,95 | 85,52 |
| 11:00 | 49,85 | 83,97 |
| 11:30 | 49,38 | 79,33 |
| 12:00 | 49,40 | 79,33 |

## B.3 0.1 % TEMPO-CNF and crude oil C

**Table B.3:** Average contact angle for each 30 minute of measurements for 0.1% TEMPO-CNF in 0.1 wt% NaCl and crude oil C.

| Time [hh:mm] | Average contact angle [°] | Volume of oil drop [$\mu$L] |
|---|---|---|
| 00:30 | 41,77 | 28,76 |
| 01:00 | 42,29 | 28,76 |
| 01:30 | 42,44 | 28,73 |
| 02:00 | 42,63 | 28,72 |
| 02:30 | 42,77 | 28,71 |
| 03:00 | 42,79 | 28,69 |
| 03:30 | 42,79 | 28,68 |
| 04:00 | 42,77 | 28,67 |
| 04:30 | 42,73 | 28,65 |
| 05:00 | 42,71 | 28,64 |
| 05:30 | 42,72 | 28,64 |
| 06:00 | 42,74 | 28,65 |
| 06:30 | 42,75 | 28,64 |
| 07:00 | 42,78 | 28,64 |
| 07:30 | 42,81 | 28,63 |
| 08:00 | 42,84 | 28,63 |
| 08:30 | 42,88 | 28,63 |
| 09:00 | 42,87 | 28,62 |
| 09:30 | 42,89 | 28,63 |
| 10:00 | 42,89 | 28,63 |
| 10:30 | 42,89 | 28,63 |
| 11:00 | 42,88 | 28,63 |
| 11:30 | 42,87 | 28,63 |
| 12:00 | 42,85 | 28,63 |

# Appendix C

# Interfacial tension

## C.1 0.1 wt% NaCl and crude oil C

**Table C.1:** Average interfacial tension for each 30 minute of measurements for 0.1 wt% NaCl and crude oil C.

| Time [hh:mm] | Average IFT [mN/m] | Volume [$\mu$L] |
|---|---|---|
| 00:30 | 17,17 | 40,82 |
| 01:00 | 16,23 | 40,74 |
| 01:30 | 15,65 | 40,71 |
| 02:00 | 15,13 | 40,68 |
| 02:30 | 14,77 | 40,61 |
| 03:00 | 14,50 | 40,51 |
| 03:30 | 14,28 | 40,48 |
| 04:00 | 14,10 | 40,40 |
| 04:30 | 13,98 | 40,32 |
| 05:00 | 13,88 | 40,23 |
| 05:30 | 13,77 | 40,12 |
| 06:00 | 13,70 | 39,97 |
| 06:30 | 13,63 | 39,87 |
| 07:00 | 13,58 | 39,76 |
| 07:30 | 13,50 | 39,61 |
| 08:00 | 13,48 | 39,46 |
| 08:30 | 13,44 | 39,33 |
| 09:00 | 13,42 | 39,23 |
| 09:30 | 13,41 | 39,08 |
| 10:00 | 13,40 | 38,96 |
| 10:30 | 13,39 | 38,86 |
| 11:00 | 13,37 | 38,75 |
| 11:30 | 13,36 | 38,62 |
| 12:00 | 13,32 | 38,50 |

## C.2 1% CNC and crude oil C

**Table C.2:** Average interfacial tension for each 30 minute of measurements for 1% CNC in 0.1 wt% NaCl and crude oil C.

| Time [hh:mm] | Average IFT [mN/m] | Volume [$\mu$L] |
|---|---|---|
| 00:30 | 15,41 | 41,43 |
| 01:00 | 15,03 | 41,24 |
| 01:30 | 14,98 | 41,01 |
| 02:00 | 14,90 | 40,75 |
| 02:30 | 14,86 | 40,50 |
| 03:00 | 14,81 | 40,24 |
| 03:30 | 14,79 | 40,01 |
| 04:00 | 14,75 | 39,81 |
| 04:30 | 14,73 | 39,64 |
| 05:00 | 14,71 | 39,44 |
| 05:30 | 14,68 | 39,24 |
| 06:00 | 14,65 | 39,08 |
| 06:30 | 14,63 | 38,92 |
| 07:00 | 14,60 | 38,84 |
| 07:30 | 14,57 | 38,82 |
| 08:00 | 14,53 | 38,74 |
| 08:30 | 14,49 | 38,64 |
| 09:00 | 14,48 | 38,53 |
| 09:30 | 14,45 | 38,42 |
| 10:00 | 14,43 | 38,32 |
| 10:30 | 14,41 | 38,22 |
| 11:00 | 14,38 | 38,11 |
| 11:30 | 14,36 | 38,02 |
| 12:00 | 14,34 | 37,93 |

## C.3 0.1 % TEMPO-CNF and crude oil C

**Table C.3:** Average interfacial tension for each 30 minute of measurements for 0.1 % TEMPO-CNF in 0.1 wt% NaCl and crude oil C.

| Time [hh:mm] | Average IFT [mN/m] | Volume [$\mu$L] |
|---|---|---|
| 00:30 | 22,40 | 49,07 |
| 01:00 | 21,79 | 49,08 |
| 01:30 | 21,49 | 49,06 |
| 02:00 | 21,35 | 49,06 |
| 02:30 | 21,15 | 49,04 |
| 03:00 | 21,00 | 49,04 |
| 03:30 | 20,89 | 49,07 |
| 04:00 | 20,74 | 49,07 |
| 04:30 | 20,64 | 49,05 |
| 05:00 | 20,55 | 49,02 |
| 05:30 | 20,50 | 48,97 |
| 06:00 | 20,46 | 48,92 |
| 06:30 | 20,39 | 48,88 |
| 07:00 | 20,32 | 48,83 |
| 07:30 | 20,32 | 48,90 |
| 08:00 | 20,24 | 48,87 |
| 08:30 | 20,18 | 48,86 |
| 09:00 | 20,21 | 48,87 |
| 09:30 | 20,09 | 48,83 |
| 10:00 | 20,07 | 48,85 |
| 10:30 | 20,16 | 48,85 |
| 11:00 | 20,00 | 48,81 |
| 11:30 | 20,12 | 48,82 |
| 12:00 | 20,01 | 48,80 |

# Appendix D

# Testing of rates

## D.1 Test 1

**Table D.1:** Oil saturation, time and pore volume for test 1. The bold font represents the end of the first run.

| Time [hh:mm:ss] | PV injected | Oil saturation [fraction] |
|---|---|---|
| 00:00:15 | 0,54 | 0,78 |
| 00:00:30 | 1,09 | 0,80 |
| 00:00:45 | 1,63 | 0,87 |
| 00:01:00 | 2,17 | 0,78 |
| 00:01:30 | 3,26 | 0,53 |
| 00:02:00 | 4,35 | 0,51 |
| 00:02:30 | 5,43 | 0,49 |
| 00:03:00 | 6,52 | 0,51 |
| 00:03:30 | 7,61 | 0,47 |
| 00:04:00 | 8,70 | 0,48 |
| 00:09:00 | 19,57 | 0,40 |
| 00:14:00 | 30,43 | 0,41 |
| 00:19:00 | 41,30 | 0,40 |
| 00:24:00 | 52,17 | 0,39 |
| 00:29:00 | 63,04 | 0,39 |
| 00:59:00 | 128,26 | 0,39 |
| 01:29:00 | 193,48 | 0,39 |
| 01:59:00 | 258,70 | 0,38 |
| 02:29:00 | 323,91 | 0,38 |
| **03:00:00** | **391,30** | **0,36** |
| 03:36:00 | 469,57 | 0,36 |
| 04:06:00 | 534,78 | 0,36 |
| 04:36:00 | 600,00 | 0,35 |
| 05:06:00 | 665,22 | 0,35 |
| 05:36:00 | 730,43 | 0,34 |
| 06:06:00 | 795,65 | 0,32 |

## D.2 Test 2

**Table D.2:** Oil saturation, time and pore volume for test 2. The bold fonts represents the end of each run.

| Time [hh:mm:ss] | PV injected | Oil saturation [fraction] |
|---|---|---|
| 00:00:10 | 0,72 | 1,00 |
| 00:00:20 | 1,45 | 1,00 |
| 00:00:30 | 2,17 | 1,00 |
| 00:00:40 | 2,90 | 1,00 |
| 00:00:50 | 3,62 | 1,00 |
| 00:01:00 | 4,35 | 1,00 |
| 00:01:30 | 6,52 | 0,61 |
| 00:02:30 | 10,87 | 0,50 |
| 00:03:00 | 13,04 | 0,48 |
| 00:03:30 | 15,22 | 0,43 |
| 00:04:00 | 17,39 | 0,44 |
| 00:04:30 | 19,57 | 0,43 |
| 00:05:00 | 21,74 | 0,42 |
| 00:10:00 | 43,48 | 0,40 |
| 00:15:00 | 65,22 | 0,37 |
| 00:20:00 | 86,96 | 0,37 |
| 00:25:00 | 108,70 | 0,34 |
| 00:30:00 | 130,43 | 0,34 |
| 01:00:00 | 260,87 | 0,36 |
| 01:30:00 | 391,30 | 0,34 |
| 02:00:00 | 521,74 | 0,33 |
| **02:18:00** | **600,00** | **0,33** |
| 02:48:00 | 730,43 | 0,33 |
| 03:18:00 | 860,87 | 0,33 |
| 03:48:00 | 991,30 | 0,33 |
| 04:18:00 | 1121,74 | 0,32 |
| **04:36:00** | **1200,00** | **0,32** |
| 05:06:00 | 1330,43 | 0,31 |
| 05:36:00 | 1460,87 | 0,30 |
| 06:06:00 | 1591,30 | 0,31 |
| 06:36:00 | 1721,74 | 0,30 |
| 06:54:00 | 1800,00 | 0,30 |

## D.3 Test 3

**Table D.3:** Oil saturation, time and pore volume for the first rate of test 3, part 1

| Time [hh:mm:ss] | PV injected | Oil saturation [fraction] |
|---|---|---|
| 00:00:10 | 0,72 | 0,99 |
| 00:00:20 | 1,45 | 0,99 |
| 00:00:30 | 2,17 | 0,99 |
| 00:00:40 | 2,90 | 0,99 |
| 00:00:50 | 3,62 | 0,97 |
| 00:01:00 | 4,35 | 0,73 |
| 00:01:10 | 5,07 | 0,59 |
| 00:01:20 | 5,80 | 0,53 |
| 00:01:30 | 6,52 | 0,47 |
| 00:01:40 | 7,25 | 0,47 |
| 00:01:50 | 7,97 | 0,46 |
| 00:02:00 | 8,70 | 0,47 |
| 00:02:30 | 10,87 | 0,42 |
| 00:03:00 | 13,04 | 0,41 |
| 00:03:30 | 15,22 | 0,43 |
| 00:04:00 | 17,39 | 0,44 |
| 00:04:30 | 19,57 | 0,43 |
| 00:05:00 | 21,74 | 0,42 |
| 00:05:30 | 23,91 | 0,41 |
| 00:06:00 | 26,09 | 0,41 |

**Table D.4:** Oil saturation, time and pore volume for the first rate of test 3, part 2

| Time [hh:mm:ss] | PV injected | Oil saturation [fraction] |
|---|---|---|
| 00:06:30 | 28,26 | 0,42 |
| 00:07:00 | 30,43 | 0,42 |
| 00:07:30 | 32,61 | 0,43 |
| 00:08:00 | 34,78 | 0,43 |
| 00:08:30 | 36,96 | 0,43 |
| 00:09:00 | 39,13 | 0,43 |
| 00:09:30 | 41,30 | 0,43 |
| 00:10:00 | 43,48 | 0,43 |
| 00:15:00 | 65,22 | 0,43 |
| 00:20:00 | 86,96 | 0,43 |
| 00:25:00 | 108,70 | 0,43 |
| 00:30:00 | 130,43 | 0,43 |
| 00:45:00 | 195,65 | 0,43 |
| 01:00:00 | 260,87 | 0,43 |
| 01:15:00 | 326,09 | 0,42 |
| 01:30:00 | 391,30 | 0,42 |
| 01:45:00 | 456,52 | 0,42 |
| 02:00:00 | 521,74 | 0,42 |
| 02:15:00 | 586,96 | 0,42 |
| 02:18:00 | 600,00 | 0,42 |

**Table D.5:** Oil saturation, time and pore volume for the second rate of test 3.

| Time [hh:mm:ss] | PV injected | Oil saturation [fraction] |
|---|---|---|
| 02:18:10 | 603,62 | 0,42 |
| 02:18:20 | 607,25 | 0,41 |
| 02:18:30 | 610,87 | 0,42 |
| 02:18:40 | 614,49 | 0,44 |
| 02:18:50 | 618,12 | 0,42 |
| 02:19:00 | 621,74 | 0,42 |
| 02:19:10 | 625,36 | 0,42 |
| 02:19:20 | 628,99 | 0,42 |
| 02:19:30 | 632,61 | 0,41 |
| 02:19:40 | 636,23 | 0,41 |
| 02:19:50 | 639,86 | 0,41 |
| 02:20:00 | 643,48 | 0,41 |
| 02:20:30 | 654,35 | 0,41 |
| 02:21:00 | 665,22 | 0,41 |
| 02:21:30 | 676,09 | 0,44 |
| 02:22:00 | 686,96 | 0,44 |
| 02:22:30 | 697,83 | 0,42 |
| 02:23:00 | 708,70 | 0,42 |
| 02:23:30 | 719,57 | 0,42 |
| 02:24:00 | 730,43 | 0,42 |
| 02:24:30 | 741,30 | 0,42 |
| 02:25:00 | 752,17 | 0,42 |
| 02:25:30 | 763,04 | 0,42 |
| 02:26:00 | 773,91 | 0,42 |
| 02:26:30 | 784,78 | 0,42 |
| 02:27:00 | 795,65 | 0,42 |
| 02:27:30 | 806,52 | 0,43 |
| 02:28:00 | 817,39 | 0,42 |
| 02:33:00 | 926,09 | 0,42 |
| 02:38:00 | 1034,78 | 0,42 |
| 02:43:00 | 1143,48 | 0,42 |
| 02:48:00 | 1252,17 | 0,42 |
| 02:53:00 | 1360,87 | 0,42 |
| 02:58:00 | 1469,57 | 0,42 |
| 03:03:00 | 1578,26 | 0,42 |
| 03:04:00 | 1600,00 | 0,42 |

# Appendix E

# Secondary flooding

## E.1 1% CNC

**Table E.1:** Oil saturation, time and pore volume for the low rate secondary flooding of CNC. First part.

| Time [hh:mm:ss] | PV injected | Oil saturation [fraction] |
|---|---|---|
| 00:00:10 | 0,72 | 1,00 |
| 00:00:20 | 1,45 | 1,00 |
| 00:00:30 | 2,17 | 1,00 |
| 00:00:40 | 2,90 | 1,00 |
| 00:00:50 | 3,62 | 1,00 |
| 00:01:10 | 5,07 | 0,98 |
| 00:01:20 | 5,80 | 0,99 |
| 00:01:30 | 6,52 | 0,99 |
| 00:01:40 | 7,25 | 0,97 |
| 00:01:50 | 7,97 | 0,97 |
| 00:02:00 | 8,70 | 0,97 |
| 00:02:10 | 9,42 | 0,97 |
| 00:02:20 | 10,14 | 0,97 |
| 00:02:30 | 10,87 | 0,98 |
| 00:02:40 | 11,59 | 0,97 |
| 00:02:50 | 12,32 | 0,98 |
| 00:03:00 | 13,04 | 0,98 |
| 00:03:10 | 13,77 | 0,99 |
| 00:03:20 | 14,49 | 0,77 |
| 00:03:30 | 15,22 | 0,50 |
| 00:03:40 | 15,94 | 0,42 |
| 00:03:50 | 16,67 | 0,39 |
| 00:04:00 | 17,39 | 0,41 |
| 00:04:10 | 18,12 | 0,37 |
| 00:04:20 | 18,84 | 0,34 |

**Table E.2:** Oil saturation, time and pore volume for the low rate secondary flooding of CNC. Second part.

| Time [hh:mm:ss] | PV injected | Oil saturation [fraction] |
|---|---|---|
| 00:04:30 | 19,57 | 0,33 |
| 00:04:40 | 20,29 | 0,34 |
| 00:04:50 | 21,01 | 0,33 |
| 00:05:00 | 21,74 | 0,33 |
| 00:05:30 | 23,91 | 0,33 |
| 00:06:00 | 26,09 | 0,34 |
| 00:06:30 | 28,26 | 0,33 |
| 00:07:00 | 30,43 | 0,33 |
| 00:07:30 | 32,61 | 0,33 |
| 00:08:00 | 34,78 | 0,33 |
| 00:08:30 | 36,96 | 0,33 |
| 00:09:00 | 39,13 | 0,34 |
| 00:09:30 | 41,30 | 0,34 |
| 00:10:00 | 43,48 | 0,34 |
| 00:15:00 | 65,22 | 0,33 |
| 00:20:00 | 86,96 | 0,33 |
| 00:25:00 | 108,70 | 0,33 |
| 00:30:00 | 130,43 | 0,33 |
| 00:45:00 | 195,65 | 0,33 |
| 01:00:00 | 260,87 | 0,33 |
| 01:15:00 | 326,09 | 0,33 |
| 01:30:00 | 391,30 | 0,33 |
| 01:45:00 | 456,52 | 0,33 |
| 02:00:00 | 521,74 | 0,33 |
| 02:15:00 | 586,96 | 0,33 |
| 02:18:00 | 600,00 | 0,33 |

**Table E.3:** Oil saturation, time and pore volume for the high rate secondary flooding of CNC.

| Time [hh:mm:ss] | PV injected | Oil saturation [fraction] |
|---|---|---|
| 02:18:10 | 603,62 | 0,33 |
| 02:18:20 | 607,25 | 0,33 |
| 02:18:30 | 610,87 | 0,33 |
| 02:18:40 | 614,49 | 0,33 |
| 02:18:50 | 618,12 | 0,33 |
| 02:19:00 | 621,74 | 0,33 |
| 02:19:10 | 625,36 | 0,32 |
| 02:19:20 | 628,99 | 0,32 |
| 02:19:30 | 632,61 | 0,32 |
| 02:19:40 | 636,23 | 0,32 |
| 02:19:50 | 639,86 | 0,32 |
| 02:20:00 | 643,48 | 0,32 |
| 02:20:30 | 654,35 | 0,32 |
| 02:21:00 | 665,22 | 0,32 |
| 02:21:30 | 676,09 | 0,32 |
| 02:22:00 | 686,96 | 0,32 |
| 02:22:30 | 697,83 | 0,32 |
| 02:23:00 | 708,70 | 0,32 |
| 02:23:30 | 719,57 | 0,32 |
| 02:24:00 | 730,43 | 0,31 |
| 02:24:30 | 741,30 | 0,32 |
| 02:25:00 | 752,17 | 0,31 |
| 02:25:30 | 763,04 | 0,31 |
| 02:26:00 | 773,91 | 0,31 |
| 02:26:30 | 784,78 | 0,31 |
| 02:27:00 | 795,65 | 0,31 |
| 02:27:30 | 806,52 | 0,31 |
| 02:28:00 | 817,39 | 0,31 |
| 02:31:00 | 882,61 | 0,31 |
| 02:34:00 | 947,83 | 0,31 |
| 02:37:00 | 1013,04 | 0,31 |
| 02:40:00 | 1078,26 | 0,31 |
| 02:43:00 | 1143,48 | 0,31 |
| 02:46:00 | 1208,70 | 0,31 |
| 02:49:00 | 1273,91 | 0,31 |
| 02:52:00 | 1339,13 | 0,31 |
| 02:55:00 | 1404,35 | 0,31 |
| 02:58:00 | 1469,57 | 0,31 |
| 03:01:00 | 1534,78 | 0,31 |
| 03:04:00 | 1600,00 | 0,31 |

## E.2 0.1% TEMPO-CNF

**Table E.4:** Oil saturation, time and pore volume for the low rate secondary flooding of TEMPO-CNF, part 1.

| Time [hh:mm:ss] | PV injected | Oil saturation [fraction] |
|---|---|---|
| 00:00:10 | 0,72 | 1,00 |
| 00:00:20 | 1,45 | 0,53 |
| 00:00:30 | 2,17 | 0,46 |
| 00:00:40 | 2,90 | 0,43 |
| 00:00:50 | 3,62 | 0,39 |
| 00:01:00 | 4,35 | 0,36 |
| 00:01:10 | 5,07 | 0,35 |
| 00:01:20 | 5,80 | 0,31 |
| 00:01:30 | 6,52 | 0,30 |
| 00:01:40 | 7,25 | 0,28 |
| 00:01:50 | 7,97 | 0,30 |
| 00:02:00 | 8,70 | 0,36 |
| 00:02:30 | 10,87 | 0,30 |
| 00:03:00 | 13,04 | 0,28 |
| 00:03:30 | 15,22 | 0,28 |
| 00:04:00 | 17,39 | 0,24 |
| 00:04:30 | 19,57 | 0,23 |

**Table E.5:** Oil saturation, time and pore volume for the low rate secondary flooding of TEMPO-CNF, part 2.

| Time [hh:mm:ss] | PV injected | Oil saturation [fraction] |
|---|---|---|
| 00:05:00 | 21,74 | 0,24 |
| 00:05:30 | 23,91 | 0,26 |
| 00:06:00 | 26,09 | 0,24 |
| 00:06:30 | 28,26 | 0,24 |
| 00:07:00 | 30,43 | 0,23 |
| 00:07:30 | 32,61 | 0,22 |
| 00:08:00 | 34,78 | 0,22 |
| 00:08:30 | 36,96 | 0,22 |
| 00:09:00 | 39,13 | 0,23 |
| 00:09:30 | 41,30 | 0,23 |
| 00:10:00 | 43,48 | 0,23 |
| 00:15:00 | 65,22 | 0,22 |
| 00:20:00 | 86,96 | 0,21 |
| 00:25:00 | 108,70 | 0,22 |
| 00:30:00 | 130,43 | 0,21 |
| 00:45:00 | 195,65 | 0,21 |
| 01:00:00 | 260,87 | 0,21 |
| 01:15:00 | 326,09 | 0,21 |
| 01:30:00 | 391,30 | 0,21 |
| 01:45:00 | 456,52 | 0,21 |
| 02:00:00 | 521,74 | 0,22 |
| 02:15:00 | 586,96 | 0,22 |
| 02:18:00 | 600,00 | 0,22 |

**Table E.6:** Oil saturation, time and pore volume for the high rate secondary flooding of TEMPO-CNF.

| Time [hh:mm:ss] | PV injected | Oil saturation [fraction] |
|---|---|---|
| 02:18:10 | 603,62 | 0,24 |
| 02:18:20 | 607,25 | 0,23 |
| 02:18:30 | 610,87 | 0,20 |
| 02:18:50 | 618,12 | 0,16 |
| 02:19:00 | 621,74 | 0,15 |
| 02:19:10 | 625,36 | 0,14 |
| 02:19:30 | 632,61 | 0,14 |
| 02:19:40 | 636,23 | 0,13 |
| 02:19:50 | 639,86 | 0,13 |
| 02:20:00 | 643,48 | 0,13 |
| 02:20:30 | 654,35 | 0,13 |
| 02:21:00 | 665,22 | 0,13 |
| 02:21:30 | 676,09 | 0,13 |
| 02:22:00 | 686,96 | 0,13 |
| 02:22:30 | 697,83 | 0,12 |
| 02:23:00 | 708,70 | 0,12 |
| 02:23:30 | 719,57 | 0,12 |
| 02:24:00 | 730,43 | 0,12 |
| 02:24:30 | 741,30 | 0,12 |
| 02:25:00 | 752,17 | 0,12 |
| 02:25:30 | 763,04 | 0,12 |
| 02:26:00 | 773,91 | 0,12 |
| 02:26:30 | 784,78 | 0,12 |
| 02:27:00 | 795,65 | 0,12 |
| 02:27:30 | 806,52 | 0,12 |
| 02:28:00 | 817,39 | 0,12 |
| 02:31:00 | 882,61 | 0,12 |
| 02:34:00 | 947,83 | 0,12 |
| 02:37:00 | 1013,04 | 0,12 |
| 02:40:00 | 1078,26 | 0,12 |
| 02:43:10 | 1147,10 | 0,12 |
| 02:46:00 | 1208,70 | 0,12 |
| 02:49:12 | 1278,26 | 0,12 |
| 02:52:00 | 1339,13 | 0,12 |
| 02:55:00 | 1404,35 | 0,12 |
| 02:57:00 | 1447,83 | 0,12 |
| 03:01:00 | 1534,78 | 0,12 |
| 03:04:00 | 1600,00 | 0,12 |

# Appendix F

# Tertiary flooding

## F.1 1% CNC, old setup

**Table F.1:** Oil saturation, time and pore volume for the low rate waterflooding prior to the tertiary flooding of CNC, old setup, part 1

| Time [hh:mm:ss] | PV injected | Oil saturation [fraction] |
|---|---|---|
| 00:00:10 | 0,72 | 1,00 |
| 00:00:20 | 1,45 | 1,00 |
| 00:00:30 | 2,17 | 1,00 |
| 00:00:40 | 2,90 | 1,00 |
| 00:00:50 | 3,62 | 0,98 |
| 00:01:00 | 4,35 | 0,62 |
| 00:01:10 | 5,07 | 0,58 |
| 00:01:20 | 5,80 | 0,58 |
| 00:01:30 | 6,52 | 0,52 |
| 00:01:40 | 7,25 | 0,52 |
| 00:01:50 | 7,97 | 0,54 |
| 00:02:00 | 8,70 | 0,54 |
| 00:02:30 | 10,87 | 0,50 |
| 00:03:00 | 13,04 | 0,49 |
| 00:03:30 | 15,22 | 0,46 |
| 00:04:00 | 17,39 | 0,46 |
| 00:04:30 | 19,57 | 0,45 |
| 00:05:00 | 21,74 | 0,43 |
| 00:05:30 | 23,91 | 0,42 |
| 00:06:00 | 26,09 | 0,41 |
| 00:06:30 | 28,26 | 0,42 |

**Table F.2:** Oil saturation, time and pore volume for the low rate waterflooding prior to the tertiary flooding of CNC, old setup, part 2.

| Time [hh:mm:ss] | PV injected | Oil saturation [fraction] |
|---|---|---|
| 00:07:00 | 30,43 | 0,41 |
| 00:07:30 | 32,61 | 0,39 |
| 00:08:00 | 34,78 | 0,38 |
| 00:08:30 | 36,96 | 0,38 |
| 00:09:00 | 39,13 | 0,38 |
| 00:09:30 | 41,30 | 0,38 |
| 00:10:00 | 43,48 | 0,38 |
| 00:15:00 | 65,22 | 0,38 |
| 00:20:00 | 86,96 | 0,34 |
| 00:25:00 | 108,70 | 0,34 |
| 00:30:00 | 130,43 | 0,34 |
| 00:54:00 | 234,78 | 0,34 |
| 01:00:00 | 260,87 | 0,34 |
| 01:15:00 | 326,09 | 0,34 |
| 01:30:00 | 391,30 | 0,34 |
| 01:45:00 | 456,52 | 0,34 |
| 02:00:00 | 521,74 | 0,34 |
| 02:15:00 | 586,96 | 0,34 |
| 02:18:00 | 600,00 | 0,34 |

**Table F.3:** Oil saturation, time and pore volume for the high rate waterflooding prior to the tertiary flooding of CNC, old setup.

| Time [hh:mm:ss] | PV injected | Oil saturation [fraction] |
|---|---|---|
| 02:18:10 | 603,62 | 0,34 |
| 02:18:20 | 607,25 | 0,34 |
| 02:18:30 | 610,87 | 0,34 |
| 02:18:40 | 614,49 | 0,37 |
| 02:18:50 | 618,12 | 0,36 |
| 02:19:00 | 621,74 | 0,35 |
| 02:19:10 | 625,36 | 0,35 |
| 02:19:20 | 628,99 | 0,35 |
| 02:19:30 | 632,61 | 0,35 |
| 02:19:40 | 636,23 | 0,35 |
| 02:19:50 | 639,86 | 0,35 |
| 02:20:00 | 643,48 | 0,35 |
| 02:20:30 | 654,35 | 0,38 |
| 02:21:00 | 665,22 | 0,35 |
| 02:21:30 | 676,09 | 0,35 |
| 02:22:00 | 686,96 | 0,35 |
| 02:22:30 | 697,83 | 0,35 |
| 02:23:00 | 708,70 | 0,35 |
| 02:23:30 | 719,57 | 0,35 |
| 02:24:00 | 730,43 | 0,35 |
| 02:24:30 | 741,30 | 0,35 |
| 02:25:00 | 752,17 | 0,35 |
| 02:25:30 | 763,04 | 0,35 |
| 02:26:00 | 773,91 | 0,35 |
| 02:26:30 | 784,78 | 0,35 |
| 02:27:00 | 795,65 | 0,35 |
| 02:27:30 | 806,52 | 0,35 |
| 02:28:00 | 817,39 | 0,35 |
| 02:31:00 | 882,61 | 0,33 |
| 02:34:00 | 947,83 | 0,33 |
| 02:37:00 | 1013,04 | 0,33 |
| 02:40:00 | 1078,26 | 0,33 |
| 02:43:00 | 1143,48 | 0,33 |
| 02:46:00 | 1208,70 | 0,32 |
| 02:49:00 | 1273,91 | 0,32 |
| 02:52:00 | 1339,13 | 0,32 |
| 02:55:00 | 1404,35 | 0,32 |
| 02:58:00 | 1469,57 | 0,32 |
| 03:01:00 | 1534,78 | 0,32 |
| 03:04:00 | 1600,00 | 0,32 |

**Table F.4:** Oil saturation, time and pore volume for the low rate nanoflooding of the tertiary flooding of CNC, old setup.

| Time [hh:mm:ss] | PV injected | Oil saturation [fraction] |
|---|---|---|
| 00:00:10 | 0,72 | 0,32 |
| 00:00:30 | 2,17 | 0,32 |
| 00:00:40 | 2,90 | 0,32 |
| 00:00:50 | 3,62 | 0,32 |
| 00:01:00 | 4,35 | 0,32 |
| 00:01:10 | 5,07 | 0,32 |
| 00:01:20 | 5,80 | 0,32 |
| 00:01:30 | 6,52 | 0,32 |
| 00:01:40 | 7,25 | 0,32 |
| 00:01:50 | 7,97 | 0,32 |
| 00:02:00 | 8,70 | 0,32 |
| 00:02:30 | 10,87 | 0,32 |
| 00:03:00 | 13,04 | 0,32 |
| 00:03:30 | 15,22 | 0,32 |
| 00:04:00 | 17,39 | 0,32 |
| 00:04:30 | 19,57 | 0,32 |
| 00:05:00 | 21,74 | 0,32 |
| 00:05:30 | 23,91 | 0,32 |
| 00:06:00 | 26,09 | 0,32 |
| 00:06:30 | 28,26 | 0,32 |
| 00:07:00 | 30,43 | 0,32 |
| 00:07:30 | 32,61 | 0,32 |
| 00:08:00 | 34,78 | 0,32 |
| 00:08:30 | 36,96 | 0,32 |
| 00:09:00 | 39,13 | 0,32 |
| 00:09:30 | 41,30 | 0,32 |
| 00:10:00 | 43,48 | 0,32 |
| 00:15:00 | 65,22 | 0,27 |
| 00:20:00 | 86,96 | 0,24 |
| 00:25:00 | 108,70 | 0,21 |
| 00:30:00 | 130,43 | 0,18 |
| 00:45:00 | 195,65 | 0,15 |
| 01:00:00 | 260,87 | 0,14 |
| 01:15:00 | 326,09 | 0,12 |
| 01:30:00 | 391,30 | 0,11 |
| 01:36:00 | 417,39 | 0,11 |
| 01:45:00 | 456,52 | 0,10 |
| 02:00:00 | 521,74 | 0,09 |
| 02:15:00 | 586,96 | 0,09 |
| 02:18:00 | 600,00 | 0,09 |

**Table F.5:** Oil saturation, time and pore volume for the high rate nanoflooding of the tertiary flooding of CNC, old setup

| Time [hh:mm:ss] | PV injected | Oil saturation [fraction] |
|---|---|---|
| 02:18:10 | 603,62 | 0,09 |
| 02:18:20 | 607,25 | 0,09 |
| 02:18:30 | 610,87 | 0,09 |
| 02:18:40 | 614,49 | 0,09 |
| 02:18:50 | 618,12 | 0,09 |
| 02:19:00 | 621,74 | 0,09 |
| 02:19:10 | 625,36 | 0,09 |
| 02:19:20 | 628,99 | 0,09 |
| 02:19:30 | 632,61 | 0,09 |
| 02:19:40 | 636,23 | 0,09 |
| 02:19:50 | 639,86 | 0,09 |
| 02:20:00 | 643,48 | 0,09 |
| 02:20:30 | 654,35 | 0,09 |
| 02:21:00 | 665,22 | 0,09 |
| 02:21:30 | 676,09 | 0,09 |
| 02:22:00 | 686,96 | 0,08 |
| 02:22:30 | 697,83 | 0,08 |
| 02:23:00 | 708,70 | 0,08 |
| 02:23:40 | 719,57 | 0,07 |
| 02:24:00 | 730,43 | 0,07 |
| 02:24:30 | 741,30 | 0,06 |
| 02:25:00 | 752,17 | 0,06 |
| 02:25:40 | 763,04 | 0,06 |
| 02:26:00 | 773,91 | 0,06 |
| 02:26:40 | 784,78 | 0,06 |
| 02:27:00 | 795,65 | 0,05 |
| 02:27:30 | 806,52 | 0,05 |
| 02:28:00 | 817,39 | 0,05 |
| 02:31:00 | 882,61 | 0,04 |
| 02:34:00 | 947,83 | 0,03 |
| 02:37:00 | 1013,04 | 0,03 |
| 02:40:00 | 1078,26 | 0,03 |
| 02:43:10 | 1143,48 | 0,03 |
| 02:46:00 | 1208,70 | 0,03 |
| 02:49:00 | 1273,91 | 0,03 |
| 02:53:00 | 1339,13 | 0,03 |
| 02:56:00 | 1404,35 | 0,04 |
| 02:59:00 | 1469,57 | 0,04 |
| 03:02:00 | 1534,78 | 0,04 |
| 03:04:00 | 1600,00 | 0,04 |

## F.2 1% CNC, new setup

**Table F.6:** Oil saturation, time and pore volume for the low rate waterflooding prior to the tertiary flooding og CNC, new setup, part 1

| Time [hh:mm:ss] | PV injected | Oil saturation [fraction] |
|---|---|---|
| 00:00:10 | 0,72 | 1,01 |
| 00:00:20 | 1,45 | 0,74 |
| 00:00:30 | 2,17 | 0,64 |
| 00:00:40 | 2,90 | 0,50 |
| 00:00:50 | 3,62 | 0,49 |
| 00:01:00 | 4,35 | 0,47 |
| 00:01:10 | 5,07 | 0,44 |
| 00:01:20 | 5,80 | 0,42 |
| 00:01:30 | 6,52 | 0,41 |
| 00:01:40 | 7,25 | 0,41 |
| 00:01:50 | 7,97 | 0,41 |
| 00:02:00 | 8,70 | 0,41 |
| 00:02:30 | 10,87 | 0,39 |
| 00:03:00 | 13,04 | 0,37 |
| 00:03:30 | 15,22 | 0,37 |
| 00:04:00 | 17,39 | 0,37 |
| 00:04:30 | 19,57 | 0,36 |
| 00:05:00 | 21,74 | 0,36 |
| 00:05:30 | 23,91 | 0,37 |

**Table F.7:** Oil saturation, time and pore volume for the low rate waterflooding prior to the tertiary flooding of CNC, new setup, part 2

| Time [hh:mm:ss] | PV injected | Oil saturation [fraction] |
|---|---|---|
| 00:06:00 | 26,09 | 0,37 |
| 00:06:30 | 28,26 | 0,37 |
| 00:07:00 | 30,43 | 0,38 |
| 00:07:30 | 32,61 | 0,38 |
| 00:08:00 | 34,78 | 0,38 |
| 00:08:30 | 36,96 | 0,38 |
| 00:09:00 | 39,13 | 0,38 |
| 00:09:30 | 41,30 | 0,37 |
| 00:10:00 | 43,48 | 0,37 |
| 00:15:00 | 65,22 | 0,37 |
| 00:20:00 | 86,96 | 0,35 |
| 00:25:00 | 108,70 | 0,35 |
| 00:30:00 | 130,43 | 0,35 |
| 00:45:00 | 195,65 | 0,34 |
| 01:00:00 | 260,87 | 0,34 |
| 01:15:00 | 326,09 | 0,34 |
| 01:30:00 | 391,30 | 0,35 |
| 01:45:00 | 456,52 | 0,35 |
| 02:00:00 | 521,74 | 0,35 |
| 02:15:00 | 586,96 | 0,35 |
| 02:18:00 | 600,00 | 0,35 |

**Table F.8:** Oil saturation, time and pore volume for the high rate waterflooding prior to the tertiary flooding of CNC, new setup.

| Time [hh:mm:ss] | PV injected | Oil saturation [fraction] |
|---|---|---|
| 02:18:10 | 603,62 | 0,33 |
| 02:18:20 | 607,25 | 0,32 |
| 02:18:30 | 610,87 | 0,32 |
| 02:18:40 | 614,49 | 0,32 |
| 02:18:50 | 618,12 | 0,33 |
| 02:19:00 | 621,74 | 0,33 |
| 02:19:10 | 625,36 | 0,33 |
| 02:19:20 | 628,99 | 0,33 |
| 02:19:30 | 632,61 | 0,33 |
| 02:19:40 | 636,23 | 0,32 |
| 02:20:00 | 643,48 | 0,33 |
| 02:20:30 | 654,35 | 0,34 |
| 02:21:00 | 665,22 | 0,34 |
| 02:21:30 | 676,09 | 0,35 |
| 02:22:00 | 686,96 | 0,35 |
| 02:22:30 | 697,83 | 0,36 |
| 02:23:00 | 708,70 | 0,36 |
| 02:23:30 | 719,57 | 0,36 |
| 02:24:00 | 730,43 | 0,36 |
| 02:24:30 | 741,30 | 0,36 |
| 02:25:00 | 752,17 | 0,36 |
| 02:25:30 | 763,04 | 0,36 |
| 02:26:00 | 773,91 | 0,36 |
| 02:29:00 | 839,13 | 0,35 |
| 02:32:00 | 904,35 | 0,35 |
| 02:35:10 | 973,19 | 0,35 |
| 02:38:00 | 1034,78 | 0,35 |
| 02:41:00 | 1100,00 | 0,35 |
| 02:44:00 | 1165,22 | 0,35 |
| 02:47:00 | 1230,43 | 0,35 |
| 02:50:00 | 1295,65 | 0,35 |
| 02:53:00 | 1360,87 | 0,35 |
| 02:56:00 | 1426,09 | 0,35 |
| 02:59:00 | 1491,30 | 0,35 |
| 03:02:00 | 1556,52 | 0,35 |
| 03:04:00 | 1600,00 | 0,35 |

**Table F.9:** Oil saturation, time and pore volume for the low rate nanoflooding of the tertiary flooding og CNC, new setup.

| Time [hh:mm:ss] | PV injected | Oil saturation [fraction] |
|---|---|---|
| 00:00:10 | 0,72 | 0,35 |
| 00:00:30 | 2,17 | 0,35 |
| 00:00:40 | 2,90 | 0,35 |
| 00:00:50 | 3,62 | 0,35 |
| 00:01:00 | 4,35 | 0,35 |
| 00:01:10 | 5,07 | 0,35 |
| 00:01:20 | 5,80 | 0,35 |
| 00:01:30 | 6,52 | 0,35 |
| 00:01:40 | 7,25 | 0,35 |
| 00:01:50 | 7,97 | 0,35 |
| 00:02:00 | 8,70 | 0,35 |
| 00:02:30 | 10,87 | 0,35 |
| 00:03:00 | 13,04 | 0,35 |
| 00:03:30 | 15,22 | 0,35 |
| 00:04:00 | 17,39 | 0,35 |
| 00:04:30 | 19,57 | 0,35 |
| 00:05:00 | 21,74 | 0,35 |
| 00:05:30 | 23,91 | 0,35 |
| 00:06:00 | 26,09 | 0,35 |
| 00:06:30 | 28,26 | 0,35 |
| 00:07:00 | 30,43 | 0,35 |
| 00:07:30 | 32,61 | 0,35 |
| 00:08:00 | 34,78 | 0,35 |
| 00:08:30 | 36,96 | 0,35 |
| 00:09:00 | 39,13 | 0,35 |
| 00:09:30 | 41,30 | 0,35 |
| 00:10:00 | 43,48 | 0,35 |
| 00:15:00 | 65,22 | 0,35 |
| 00:20:00 | 86,96 | 0,35 |
| 00:25:00 | 108,70 | 0,35 |
| 00:30:00 | 130,43 | 0,35 |
| 00:46:00 | 200,00 | 0,35 |
| 01:00:00 | 260,87 | 0,35 |
| 01:15:00 | 326,09 | 0,35 |
| 01:30:00 | 391,30 | 0,35 |
| 01:45:00 | 456,52 | 0,35 |
| 02:00:00 | 521,74 | 0,35 |
| 02:15:00 | 586,96 | 0,35 |
| 02:18:00 | 600,00 | 0,35 |

**Table F.10:** Oil saturation, time and pore volume for the high rate nanoflooding of the tertiary flooding of CNC, new setup.

| Time [hh:mm:ss] | PV injected | Oil saturation [fraction] |
|---|---|---|
| 02:18:10 | 603,62 | 0,35 |
| 02:18:20 | 607,25 | 0,35 |
| 02:18:30 | 610,87 | 0,35 |
| 02:18:40 | 614,49 | 0,35 |
| 02:18:50 | 618,12 | 0,35 |
| 02:19:00 | 621,74 | 0,35 |
| 02:19:10 | 625,36 | 0,35 |
| 02:19:20 | 628,99 | 0,35 |
| 02:19:30 | 632,61 | 0,35 |
| 02:19:50 | 639,86 | 0,35 |
| 02:20:00 | 643,48 | 0,35 |
| 02:20:30 | 654,35 | 0,35 |
| 02:21:00 | 665,22 | 0,35 |
| 02:21:30 | 676,09 | 0,35 |
| 02:22:00 | 686,96 | 0,35 |
| 02:22:30 | 697,83 | 0,35 |
| 02:23:00 | 708,70 | 0,35 |
| 02:23:30 | 719,57 | 0,35 |
| 02:24:00 | 730,43 | 0,35 |
| 02:24:30 | 741,30 | 0,35 |
| 02:25:00 | 752,17 | 0,35 |
| 02:25:30 | 763,04 | 0,35 |
| 02:26:00 | 773,91 | 0,35 |
| 02:27:00 | 795,65 | 0,35 |
| 02:27:30 | 806,52 | 0,35 |
| 02:28:00 | 817,39 | 0,35 |
| 02:31:00 | 882,61 | 0,35 |
| 02:34:00 | 947,83 | 0,35 |
| 02:37:00 | 1013,04 | 0,35 |
| 02:40:00 | 1078,26 | 0,35 |
| 02:43:10 | 1147,10 | 0,35 |
| 02:46:00 | 1208,70 | 0,35 |
| 02:49:12 | 1278,26 | 0,35 |
| 02:52:00 | 1339,13 | 0,35 |
| 02:55:00 | 1404,35 | 0,35 |
| 02:57:00 | 1447,83 | 0,35 |
| 03:04:00 | 1600,00 | 0,34 |

## F.3 1% CNC heated to 120 °C

**Table F.11:** Oil saturation, time and pore volume for the low rate waterflooding prior to the tertiary flooding of CNC heated to 120 °C, part 1

| Time [hh:mm:ss] | PV injected | Oil saturation [fraction] |
|---|---|---|
| 00:00:10 | 0,72 | 0,63 |
| 00:00:20 | 1,45 | 0,62 |
| 00:00:30 | 2,17 | 0,48 |
| 00:00:40 | 2,90 | 0,45 |
| 00:00:50 | 3,62 | 0,42 |
| 00:01:00 | 4,35 | 0,39 |
| 00:01:10 | 5,07 | 0,36 |
| 00:01:30 | 6,52 | 0,37 |
| 00:01:40 | 7,25 | 0,36 |
| 00:01:50 | 7,97 | 0,35 |
| 00:02:00 | 8,70 | 0,34 |
| 00:02:30 | 10,87 | 0,31 |
| 00:03:00 | 13,04 | 0,29 |
| 00:03:30 | 15,22 | 0,30 |
| 00:04:00 | 17,39 | 0,31 |
| 00:04:30 | 19,57 | 0,31 |
| 00:05:00 | 21,74 | 0,29 |
| 00:05:30 | 23,91 | 0,27 |

**Table F.12:** Oil saturation, time and pore volume for the low rate waterflooding prior to the tertiary flooding of CNC heated to 120 $^{\circ}C$, part 2

| Time [hh:mm:ss] | PV injected | Oil saturation [fraction] |
|---|---|---|
| 00:06:00 | 26,09 | 0,27 |
| 00:06:30 | 28,26 | 0,26 |
| 00:07:00 | 30,43 | 0,26 |
| 00:07:30 | 32,61 | 0,26 |
| 00:08:00 | 34,78 | 0,26 |
| 00:08:30 | 36,96 | 0,25 |
| 00:09:00 | 39,13 | 0,24 |
| 00:09:30 | 41,30 | 0,24 |
| 00:10:00 | 43,48 | 0,24 |
| 00:15:00 | 65,22 | 0,24 |
| 00:20:00 | 86,96 | 0,24 |
| 00:25:00 | 108,70 | 0,24 |
| 00:30:00 | 130,43 | 0,24 |
| 00:45:00 | 195,65 | 0,24 |
| 01:00:00 | 260,87 | 0,25 |
| 01:15:00 | 326,09 | 0,25 |
| 01:30:00 | 391,30 | 0,25 |
| 01:45:00 | 456,52 | 0,26 |
| 02:00:00 | 521,74 | 0,26 |
| 02:15:00 | 586,96 | 0,26 |
| 02:18:00 | 600,00 | 0,25 |

**Table F.13:** Oil saturation, time and pore volume for the high rate waterflooding prior to the tertiary flooding of CNC heated to 120 $^{\circ}C$.

| Time [hh:mm:ss] | PV injected | Oil saturation [fraction] |
|---|---|---|
| 02:18:10 | 603,62 | 0,24 |
| 02:18:20 | 607,25 | 0,24 |
| 02:18:30 | 610,87 | 0,24 |
| 02:18:40 | 614,49 | 0,24 |
| 02:18:50 | 618,12 | 0,24 |
| 02:19:00 | 621,74 | 0,25 |
| 02:19:10 | 625,36 | 0,24 |
| 02:19:30 | 632,61 | 0,24 |
| 02:19:50 | 639,86 | 0,24 |
| 02:20:00 | 643,48 | 0,24 |
| 02:20:30 | 654,35 | 0,25 |
| 02:21:00 | 665,22 | 0,26 |
| 02:21:30 | 676,09 | 0,26 |
| 02:22:00 | 686,96 | 0,27 |
| 02:22:30 | 697,83 | 0,26 |
| 02:23:00 | 708,70 | 0,26 |
| 02:23:30 | 719,57 | 0,26 |
| 02:24:00 | 730,43 | 0,26 |
| 02:24:30 | 741,30 | 0,26 |
| 02:25:00 | 752,17 | 0,26 |
| 02:25:30 | 763,04 | 0,26 |
| 02:26:00 | 773,91 | 0,26 |
| 02:26:30 | 784,78 | 0,26 |
| 02:27:00 | 795,65 | 0,26 |
| 02:27:30 | 806,52 | 0,26 |
| 02:28:00 | 817,39 | 0,26 |
| 02:31:00 | 882,61 | 0,26 |
| 02:34:00 | 947,83 | 0,27 |
| 02:37:00 | 1013,04 | 0,27 |
| 02:40:00 | 1078,26 | 0,27 |
| 02:43:00 | 1143,48 | 0,27 |
| 02:46:00 | 1208,70 | 0,27 |
| 02:49:00 | 1273,91 | 0,27 |
| 02:52:00 | 1339,13 | 0,27 |
| 02:55:00 | 1404,35 | 0,26 |
| 02:58:00 | 1469,57 | 0,26 |
| 03:01:00 | 1534,78 | 0,26 |
| 03:04:00 | 1600,00 | 0,26 |

**Table F.14:** Oil saturation, time and pore volume for the low rate nanoflooding of the tertiary flooding of CNC heated to 120 $^{\circ}C$.

| Time [hh:mm:ss] | PV injected | Oil saturation [fraction] |
|---|---|---|
| 00:00:10 | 0,72 | 0,27 |
| 00:00:20 | 1,45 | 0,27 |
| 00:00:40 | 2,90 | 0,27 |
| 00:01:00 | 4,35 | 0,27 |
| 00:01:10 | 5,07 | 0,27 |
| 00:01:20 | 5,80 | 0,27 |
| 00:01:30 | 6,52 | 0,27 |
| 00:01:50 | 7,97 | 0,27 |
| 00:02:00 | 8,70 | 0,27 |
| 00:02:30 | 10,87 | 0,27 |
| 00:03:00 | 13,04 | 0,27 |
| 00:03:30 | 15,22 | 0,27 |
| 00:04:00 | 17,39 | 0,27 |
| 00:04:30 | 19,57 | 0,27 |
| 00:05:00 | 21,74 | 0,27 |
| 00:05:30 | 23,91 | 0,27 |
| 00:06:00 | 26,09 | 0,27 |
| 00:06:30 | 28,26 | 0,27 |
| 00:07:00 | 30,43 | 0,27 |
| 00:07:30 | 32,61 | 0,27 |
| 00:08:00 | 34,78 | 0,27 |
| 00:08:30 | 36,96 | 0,27 |
| 00:09:00 | 39,13 | 0,27 |
| 00:09:30 | 41,30 | 0,27 |
| 00:10:00 | 43,48 | 0,27 |
| 00:15:00 | 65,22 | 0,27 |
| 00:20:00 | 86,96 | 0,27 |
| 00:25:00 | 108,70 | 0,27 |
| 00:30:00 | 130,43 | 0,27 |
| 00:45:00 | 195,65 | 0,27 |
| 01:00:00 | 260,87 | 0,27 |
| 01:15:00 | 326,09 | 0,27 |
| 01:30:00 | 391,30 | 0,26 |
| 01:45:00 | 456,52 | 0,27 |
| 02:00:00 | 521,74 | 0,27 |
| 02:15:00 | 586,96 | 0,27 |
| 02:18:00 | 600 | 0,27 |

**Table F.15:** Oil saturation, time and pore volume for the high rate nanoflooding of the tertiary flooding of CNC heated to 120 $^{\circ}C$.

| Time [hh:mm:ss] | PV injected | Oil saturation [fraction] |
|---|---|---|
| 02:18:20 | 607,25 | 0,27 |
| 02:18:30 | 610,87 | 0,27 |
| 02:18:40 | 614,49 | 0,27 |
| 02:18:50 | 618,12 | 0,27 |
| 02:19:10 | 625,36 | 0,27 |
| 02:19:20 | 628,99 | 0,27 |
| 02:19:30 | 632,61 | 0,27 |
| 02:19:40 | 636,23 | 0,26 |
| 02:20:00 | 643,48 | 0,26 |
| 02:20:30 | 654,35 | 0,26 |
| 02:21:00 | 665,22 | 0,25 |
| 02:21:30 | 676,09 | 0,24 |
| 02:22:00 | 686,96 | 0,24 |
| 02:22:30 | 697,83 | 0,24 |
| 02:23:00 | 708,70 | 0,24 |
| 02:23:40 | 723,19 | 0,24 |
| 02:24:00 | 730,43 | 0,24 |
| 02:24:30 | 741,30 | 0,24 |
| 02:25:00 | 752,17 | 0,24 |
| 02:25:40 | 766,67 | 0,24 |
| 02:26:00 | 773,91 | 0,24 |
| 02:26:40 | 788,41 | 0,24 |
| 02:27:00 | 795,65 | 0,24 |
| 02:27:30 | 806,52 | 0,24 |
| 02:28:00 | 817,39 | 0,26 |
| 02:31:00 | 882,61 | 0,26 |
| 02:34:00 | 947,83 | 0,26 |
| 02:37:00 | 1013,04 | 0,26 |
| 02:40:00 | 1078,26 | 0,25 |
| 02:43:10 | 1147,10 | 0,25 |
| 02:46:00 | 1208,70 | 0,25 |
| 02:49:00 | 1273,91 | 0,25 |
| 02:53:00 | 1360,87 | 0,25 |
| 02:56:00 | 1426,09 | 0,25 |
| 02:59:00 | 1491,30 | 0,25 |
| 03:02:00 | 1556,52 | 0,25 |
| 03:04:00 | 1600,00 | 0,25 |

## F.4 0.1 % TEMPO-CNF

**Table F.16:** Oil saturation, time and pore volume for the low rate waterflooding prior to the tertiary flooding of TEMPO-CNF, part 1.

| Time [hh:mm:ss] | PV injected | Oil saturation [fraction] |
|---|---|---|
| 00:00:10 | 0,72 | 0,99 |
| 00:00:20 | 1,45 | 0,99 |
| 00:00:30 | 2,17 | 0,99 |
| 00:00:40 | 2,90 | 0,98 |
| 00:00:50 | 3,62 | 0,99 |
| 00:01:00 | 4,35 | 0,99 |
| 00:01:10 | 5,07 | 0,68 |
| 00:01:20 | 5,80 | 0,53 |
| 00:01:30 | 6,52 | 0,49 |
| 00:01:50 | 7,97 | 0,47 |
| 00:02:00 | 8,70 | 0,50 |
| 00:02:10 | 9,42 | 0,48 |
| 00:02:20 | 10,14 | 0,46 |
| 00:02:30 | 10,87 | 0,46 |
| 00:02:40 | 11,59 | 0,44 |
| 00:03:00 | 13,04 | 0,44 |
| 00:03:30 | 15,22 | 0,44 |
| 00:04:00 | 17,39 | 0,43 |
| 00:04:30 | 19,57 | 0,41 |
| 00:05:00 | 21,74 | 0,42 |
| 00:05:30 | 23,91 | 0,42 |

**Table F.17:** Oil saturation, time and pore volume for the low rate waterflooding prior to the tertiary flooding of TEMPO-CNF, part 2.

| Time [hh:mm:ss] | PV injected | Oil saturation [fraction] |
|---|---|---|
| 00:06:00 | 26,09 | 0,42 |
| 00:06:30 | 28,26 | 0,42 |
| 00:07:00 | 30,43 | 0,41 |
| 00:07:30 | 32,61 | 0,40 |
| 00:08:00 | 34,78 | 0,40 |
| 00:08:30 | 36,96 | 0,39 |
| 00:09:00 | 39,13 | 0,39 |
| 00:09:30 | 41,30 | 0,40 |
| 00:10:00 | 43,48 | 0,40 |
| 00:15:00 | 65,22 | 0,39 |
| 00:20:00 | 86,96 | 0,40 |
| 00:25:00 | 108,70 | 0,40 |
| 00:30:00 | 130,43 | 0,40 |
| 00:45:00 | 195,65 | 0,40 |
| 01:00:00 | 260,87 | 0,40 |
| 01:15:00 | 326,09 | 0,38 |
| 01:30:00 | 391,30 | 0,38 |
| 01:45:00 | 456,52 | 0,40 |
| 02:00:00 | 521,74 | 0,41 |
| 02:15:00 | 586,96 | 0,43 |
| 02:18:00 | 600,00 | 0,43 |

**Table F.18:** Oil saturation, time and pore volume for the high rate waterflooding prior to the tertiary flooding of TEMPO-CNF.

| Time [hh:mm:ss] | PV injected | Oil saturation [fraction] |
|---|---|---|
| 02:18:10 | 603,62 | 0,39 |
| 02:18:30 | 610,87 | 0,42 |
| 02:18:40 | 614,49 | 0,43 |
| 02:18:50 | 618,12 | 0,43 |
| 02:19:00 | 621,74 | 0,43 |
| 02:19:10 | 625,36 | 0,43 |
| 02:19:30 | 632,61 | 0,43 |
| 02:19:50 | 639,86 | 0,43 |
| 02:20:00 | 643,48 | 0,42 |
| 02:20:30 | 654,35 | 0,42 |
| 02:21:00 | 665,22 | 0,42 |
| 02:21:30 | 676,09 | 0,42 |
| 02:22:00 | 686,96 | 0,43 |
| 02:22:30 | 697,83 | 0,43 |
| 02:23:00 | 708,70 | 0,41 |
| 02:23:30 | 719,57 | 0,41 |
| 02:24:00 | 730,43 | 0,41 |
| 02:24:30 | 741,30 | 0,41 |
| 02:25:00 | 752,17 | 0,40 |
| 02:25:30 | 763,04 | 0,40 |
| 02:26:00 | 773,91 | 0,40 |
| 02:26:30 | 784,78 | 0,40 |
| 02:27:00 | 795,65 | 0,40 |
| 02:27:30 | 806,52 | 0,40 |
| 02:28:00 | 817,39 | 0,40 |
| 02:33:00 | 926,09 | 0,40 |
| 02:34:00 | 947,83 | 0,40 |
| 02:37:00 | 1013,04 | 0,40 |
| 02:40:00 | 1078,26 | 0,39 |
| 02:43:00 | 1143,48 | 0,39 |
| 02:46:00 | 1208,70 | 0,39 |
| 02:49:00 | 1273,91 | 0,39 |
| 02:52:00 | 1339,13 | 0,39 |
| 02:55:00 | 1404,35 | 0,39 |
| 02:58:00 | 1469,57 | 0,39 |
| 03:01:00 | 1534,78 | 0,39 |
| 03:04:00 | 1600,00 | 0,39 |

**Table F.19:** Oil saturation, time and pore volume for the low rate nanoflooding of the tertiary flooding of TEMPO-CNF.

| Time [hh:mm:ss] | PV injected | Oil saturation [fraction] |
|---|---|---|
| 00:00:10 | 0,72 | 0,39 |
| 00:00:20 | 1,45 | 0,39 |
| 00:00:30 | 2,17 | 0,39 |
| 00:00:40 | 2,90 | 0,39 |
| 00:00:50 | 3,62 | 0,39 |
| 00:01:00 | 4,35 | 0,39 |
| 00:01:10 | 5,07 | 0,39 |
| 00:01:20 | 5,80 | 0,39 |
| 00:01:30 | 6,52 | 0,39 |
| 00:01:40 | 7,25 | 0,39 |
| 00:01:50 | 7,97 | 0,39 |
| 00:02:00 | 8,70 | 0,39 |
| 00:02:30 | 10,87 | 0,39 |
| 00:03:00 | 13,04 | 0,39 |
| 00:03:30 | 15,22 | 0,39 |
| 00:04:00 | 17,39 | 0,39 |
| 00:04:30 | 19,57 | 0,39 |
| 00:05:00 | 21,74 | 0,39 |
| 00:05:30 | 23,91 | 0,39 |
| 00:06:00 | 26,09 | 0,39 |
| 00:06:30 | 28,26 | 0,39 |
| 00:07:00 | 30,43 | 0,39 |
| 00:07:30 | 32,61 | 0,39 |
| 00:08:00 | 34,78 | 0,39 |
| 00:08:30 | 36,96 | 0,39 |
| 00:09:00 | 39,13 | 0,39 |
| 00:09:30 | 41,30 | 0,39 |
| 00:10:00 | 43,48 | 0,39 |
| 00:15:00 | 65,22 | 0,39 |
| 00:20:00 | 86,96 | 0,39 |
| 00:25:00 | 108,70 | 0,39 |
| 00:30:00 | 130,43 | 0,39 |
| 00:45:00 | 195,65 | 0,39 |
| 01:00:00 | 260,87 | 0,39 |
| 01:15:00 | 326,09 | 0,39 |
| 01:30:00 | 391,30 | 0,39 |
| 01:45:00 | 456,52 | 0,39 |
| 02:00:00 | 521,74 | 0,39 |
| 02:15:00 | 586,96 | 0,39 |
| 02:18:00 | 600,00 | 0,39 |

**Table F.20:** Oil saturation, time and pore volume for the high rate nanoflooding of the tertiary flooding of TEMPO-CNF.

| Time [hh:mm:ss] | PV injected | Oil saturation [fraction] |
|---|---|---|
| 02:18:10 | 603,62 | 0,39 |
| 02:18:20 | 607,25 | 0,39 |
| 02:18:30 | 610,87 | 0,39 |
| 02:18:40 | 614,49 | 0,38 |
| 02:18:50 | 618,12 | 0,38 |
| 02:19:00 | 621,74 | 0,38 |
| 02:19:10 | 625,36 | 0,38 |
| 02:19:20 | 628,99 | 0,38 |
| 02:19:30 | 632,61 | 0,38 |
| 02:19:40 | 636,23 | 0,38 |
| 02:19:50 | 639,86 | 0,38 |
| 02:20:00 | 643,48 | 0,38 |
| 02:20:30 | 654,35 | 0,38 |
| 02:21:00 | 665,22 | 0,38 |
| 02:21:30 | 676,09 | 0,38 |
| 02:22:00 | 686,96 | 0,38 |
| 02:22:30 | 697,83 | 0,38 |
| 02:23:00 | 708,70 | 0,38 |
| 02:23:30 | 719,57 | 0,38 |
| 02:24:00 | 730,43 | 0,38 |
| 02:24:30 | 741,30 | 0,38 |
| 02:25:00 | 752,17 | 0,38 |
| 02:25:30 | 763,04 | 0,38 |
| 02:26:00 | 773,91 | 0,38 |
| 02:26:30 | 784,78 | 0,38 |
| 02:27:00 | 795,65 | 0,38 |
| 02:27:30 | 806,52 | 0,38 |
| 02:28:00 | 817,39 | 0,38 |
| 02:31:00 | 882,61 | 0,38 |
| 02:34:00 | 947,83 | 0,38 |
| 02:37:00 | 1013,04 | 0,38 |
| 02:40:00 | 1078,26 | 0,38 |
| 02:43:10 | 1147,10 | 0,38 |
| 02:46:00 | 1208,70 | 0,38 |
| 02:49:12 | 1278,26 | 0,38 |
| 02:52:00 | 1339,13 | 0,38 |
| 02:55:00 | 1404,35 | 0,38 |
| 02:57:00 | 1447,83 | 0,38 |
| 03:01:00 | 1534,78 | 0,38 |
| 03:04:00 | 1600,00 | 0,38 |

## F.5 0.1 wt% NaCl as both secondary and tertiary fluid

**Table F.21:** Oil saturation, time and pore volume for the first round of low rate injection of water. Part 1.

| Time [hh:mm:ss] | PV injected | Oil saturation [fraction] |
|---|---|---|
| 00:00:10 | 0,72 | 1,00 |
| 00:00:20 | 1,45 | 1,00 |
| 00:00:30 | 2,17 | 1,00 |
| 00:00:40 | 2,90 | 0,63 |
| 00:00:50 | 3,62 | 0,62 |
| 00:01:10 | 5,07 | 0,49 |
| 00:01:20 | 5,80 | 0,47 |
| 00:01:40 | 7,25 | 0,45 |
| 00:01:50 | 7,97 | 0,44 |
| 00:02:00 | 8,70 | 0,44 |
| 00:02:30 | 10,87 | 0,43 |
| 00:03:00 | 13,04 | 0,39 |
| 00:03:30 | 15,22 | 0,37 |
| 00:04:00 | 17,39 | 0,37 |
| 00:04:30 | 19,57 | 0,38 |
| 00:05:00 | 21,74 | 0,35 |
| 00:05:30 | 23,91 | 0,35 |

**Table F.22:** Oil saturation, time and pore volume for the first round of low rate injection of water. Part 2.

| Time [hh:mm:ss] | PV injected | Oil saturation [fraction] |
|---|---|---|
| 00:06:00 | 26,09 | 0,36 |
| 00:06:30 | 28,26 | 0,37 |
| 00:07:00 | 30,43 | 0,36 |
| 00:07:30 | 32,61 | 0,35 |
| 00:08:00 | 34,78 | 0,34 |
| 00:08:30 | 36,96 | 0,33 |
| 00:09:00 | 39,13 | 0,33 |
| 00:09:30 | 41,30 | 0,32 |
| 00:10:00 | 43,48 | 0,32 |
| 00:15:00 | 65,22 | 0,32 |
| 00:20:00 | 86,96 | 0,31 |
| 00:25:00 | 108,70 | 0,31 |
| 00:30:00 | 130,43 | 0,31 |
| 00:45:00 | 195,65 | 0,31 |
| 01:00:00 | 260,87 | 0,31 |
| 01:15:00 | 326,09 | 0,29 |
| 01:30:00 | 391,30 | 0,27 |
| 01:45:00 | 456,52 | 0,28 |
| 02:00:00 | 521,74 | 0,27 |
| 02:15:00 | 586,96 | 0,27 |
| 02:18:00 | 600,00 | 0,27 |

**Table F.23:** Oil saturation, time and pore volume for the first round of high rate injection of water.

| Time [hh:mm:ss] | PV injected | Oil saturation [fraction] |
|---|---|---|
| 02:18:10 | 603,62 | 0,27 |
| 02:18:20 | 607,25 | 0,27 |
| 02:18:30 | 610,87 | 0,26 |
| 02:18:40 | 614,49 | 0,26 |
| 02:18:50 | 618,12 | 0,27 |
| 02:19:00 | 621,74 | 0,27 |
| 02:19:10 | 625,36 | 0,27 |
| 02:19:20 | 628,99 | 0,26 |
| 02:19:30 | 632,61 | 0,26 |
| 02:19:40 | 636,23 | 0,26 |
| 02:19:50 | 639,86 | 0,26 |
| 02:20:00 | 643,48 | 0,26 |
| 02:20:30 | 654,35 | 0,26 |
| 02:21:00 | 665,22 | 0,26 |
| 02:21:30 | 676,09 | 0,26 |
| 02:22:00 | 686,96 | 0,26 |
| 02:22:30 | 697,83 | 0,26 |
| 02:23:00 | 708,70 | 0,26 |
| 02:23:30 | 719,57 | 0,26 |
| 02:24:00 | 730,43 | 0,26 |
| 02:24:30 | 741,30 | 0,26 |
| 02:25:00 | 752,17 | 0,26 |
| 02:25:30 | 763,04 | 0,26 |
| 02:26:00 | 773,91 | 0,26 |
| 02:26:30 | 784,78 | 0,26 |
| 02:27:00 | 795,65 | 0,26 |
| 02:27:30 | 806,52 | 0,26 |
| 02:28:00 | 817,39 | 0,26 |
| 02:31:00 | 882,61 | 0,26 |
| 02:34:00 | 947,83 | 0,26 |
| 02:37:00 | 1013,04 | 0,26 |
| 02:40:00 | 1078,26 | 0,26 |
| 02:43:00 | 1143,48 | 0,26 |
| 02:46:00 | 1208,70 | 0,26 |
| 02:49:00 | 1273,91 | 0,26 |
| 02:52:00 | 1339,13 | 0,26 |
| 02:55:00 | 1404,35 | 0,26 |
| 02:58:00 | 1469,57 | 0,26 |
| 03:01:00 | 1534,78 | 0,26 |
| 03:04:00 | 1600,00 | 0,26 |

**Table F.24:** Oil saturation, time and pore volume for the second round of low rate injection of water.

| Time [hh:mm:ss] | PV injected | Oil saturation [fraction] |
|---|---|---|
| 00:00:10 | 0,72 | 0,27 |
| 00:00:20 | 1,45 | 0,27 |
| 00:00:30 | 2,17 | 0,27 |
| 00:00:40 | 2,90 | 0,27 |
| 00:00:50 | 3,62 | 0,27 |
| 00:01:00 | 4,35 | 0,27 |
| 00:01:10 | 5,07 | 0,27 |
| 00:01:30 | 6,52 | 0,27 |
| 00:01:40 | 7,25 | 0,27 |
| 00:01:50 | 7,97 | 0,27 |
| 00:02:00 | 8,70 | 0,27 |
| 00:02:30 | 10,87 | 0,27 |
| 00:03:00 | 13,04 | 0,27 |
| 00:03:30 | 15,22 | 0,27 |
| 00:04:00 | 17,39 | 0,27 |
| 00:04:30 | 19,57 | 0,27 |
| 00:05:00 | 21,74 | 0,27 |
| 00:05:30 | 23,91 | 0,27 |
| 00:06:00 | 26,09 | 0,27 |
| 00:06:30 | 28,26 | 0,27 |
| 00:07:00 | 30,43 | 0,27 |
| 00:07:30 | 32,61 | 0,27 |
| 00:08:00 | 34,78 | 0,27 |
| 00:08:30 | 36,96 | 0,27 |
| 00:09:00 | 39,13 | 0,27 |
| 00:09:30 | 41,30 | 0,27 |
| 00:10:00 | 43,48 | 0,27 |
| 00:15:00 | 65,22 | 0,27 |
| 00:20:00 | 86,96 | 0,27 |
| 00:25:00 | 108,70 | 0,27 |
| 00:30:00 | 130,43 | 0,27 |
| 00:45:00 | 195,65 | 0,27 |
| 01:00:00 | 260,87 | 0,27 |
| 01:15:00 | 326,09 | 0,27 |
| 01:30:00 | 391,30 | 0,27 |
| 01:45:00 | 456,52 | 0,27 |
| 02:00:00 | 521,74 | 0,26 |
| 02:15:00 | 586,96 | 0,26 |
| 02:18:00 | 600,00 | 0,26 |

**Table F.25:** Oil saturation, time and pore volume for the second round of high rate injection of water.

| Time [hh:mm:ss] | PV injected | Oil saturation [fraction] |
|---|---|---|
| 02:18:10 | 603,62 | 0,25 |
| 02:18:30 | 610,87 | 0,24 |
| 02:18:40 | 614,49 | 0,23 |
| 02:18:50 | 618,12 | 0,23 |
| 02:19:00 | 621,74 | 0,23 |
| 02:19:10 | 625,36 | 0,24 |
| 02:19:20 | 628,99 | 0,23 |
| 02:19:40 | 636,23 | 0,23 |
| 02:19:50 | 639,86 | 0,24 |
| 02:20:00 | 643,48 | 0,23 |
| 02:20:30 | 654,35 | 0,24 |
| 02:21:00 | 665,22 | 0,23 |
| 02:21:30 | 676,09 | 0,24 |
| 02:22:00 | 686,96 | 0,24 |
| 02:22:30 | 697,83 | 0,23 |
| 02:23:00 | 708,70 | 0,23 |
| 02:23:40 | 723,19 | 0,23 |
| 02:24:00 | 730,43 | 0,23 |
| 02:24:30 | 741,30 | 0,23 |
| 02:25:00 | 752,17 | 0,23 |
| 02:25:40 | 766,67 | 0,23 |
| 02:26:00 | 773,91 | 0,23 |
| 02:26:40 | 788,41 | 0,23 |
| 02:27:00 | 795,65 | 0,23 |
| 02:27:30 | 806,52 | 0,23 |
| 02:28:00 | 817,39 | 0,23 |
| 02:31:00 | 882,61 | 0,23 |
| 02:34:00 | 947,83 | 0,23 |
| 02:37:00 | 1013,04 | 0,23 |
| 02:40:00 | 1078,26 | 0,23 |
| 02:43:10 | 1147,10 | 0,23 |
| 02:46:00 | 1208,70 | 0,23 |
| 02:49:00 | 1273,91 | 0,23 |
| 02:52:00 | 1339,13 | 0,23 |
| 02:55:00 | 1404,35 | 0,23 |
| 02:58:00 | 1469,57 | 0,23 |
| 03:01:00 | 1534,78 | 0,23 |
| 03:04:00 | 1600,00 | 0,23 |

## F.6 1% CNC, low rate flooding

**Table F.26:** Oil saturation, time and pore volume for the low rate waterflooding.

| Time [hh:mm:ss] | PV injected | Oil saturation [fraction] |
|---|---|---|
| 00:00:20 | 1,45 | 0,61 |
| 00:00:30 | 2,17 | 0,65 |
| 00:00:40 | 2,90 | 0,50 |
| 00:01:00 | 4,35 | 0,52 |
| 00:01:10 | 5,07 | 0,51 |
| 00:01:20 | 5,80 | 0,49 |
| 00:01:30 | 6,52 | 0,49 |
| 00:01:50 | 7,97 | 0,47 |
| 00:02:00 | 8,70 | 0,47 |
| 00:02:30 | 10,87 | 0,46 |
| 00:03:00 | 13,04 | 0,46 |
| 00:03:30 | 15,22 | 0,46 |
| 00:04:00 | 17,39 | 0,45 |
| 00:04:30 | 19,57 | 0,44 |
| 00:05:00 | 21,74 | 0,43 |
| 00:05:30 | 23,91 | 0,41 |
| 00:06:00 | 26,09 | 0,40 |
| 00:06:30 | 28,26 | 0,39 |
| 00:07:00 | 30,43 | 0,39 |
| 00:07:30 | 32,61 | 0,38 |
| 00:08:00 | 34,78 | 0,38 |
| 00:08:30 | 36,96 | 0,38 |
| 00:09:00 | 39,13 | 0,37 |
| 00:09:30 | 41,30 | 0,37 |
| 00:10:00 | 43,48 | 0,37 |
| 00:15:00 | 65,22 | 0,37 |
| 00:20:00 | 86,96 | 0,37 |
| 00:25:00 | 108,70 | 0,38 |
| 00:30:00 | 130,43 | 0,37 |
| 00:54:00 | 234,78 | 0,37 |
| 01:00:00 | 260,87 | 0,36 |
| 01:18:00 | 339,13 | 0,35 |
| 01:30:00 | 391,30 | 0,35 |
| 01:45:00 | 456,52 | 0,34 |
| 02:00:00 | 521,74 | 0,34 |
| 02:15:00 | 586,96 | 0,34 |
| 02:18:00 | 600,00 | 0,34 |

**Table F.27:** Oil saturation, time and pore volume for the low rate nanoflooding.

| Time [hh:mm:ss] | PV injected | Oil saturation [fraction] |
|---|---|---|
| 02:18:10 | 600,72 | 0,33 |
| 02:18:30 | 602,17 | 0,33 |
| 02:18:40 | 602,90 | 0,33 |
| 02:18:50 | 603,62 | 0,32 |
| 02:19:00 | 604,35 | 0,33 |
| 02:19:20 | 605,80 | 0,32 |
| 02:19:30 | 606,52 | 0,32 |
| 02:19:40 | 607,25 | 0,32 |
| 02:19:50 | 607,97 | 0,32 |
| 02:20:00 | 608,70 | 0,32 |
| 02:20:30 | 610,87 | 0,32 |
| 02:21:00 | 613,04 | 0,32 |
| 02:21:30 | 615,22 | 0,33 |
| 02:22:00 | 617,39 | 0,32 |
| 02:22:30 | 619,57 | 0,32 |
| 02:23:10 | 622,46 | 0,32 |
| 02:23:30 | 623,91 | 0,32 |
| 02:24:00 | 626,09 | 0,32 |
| 02:24:30 | 628,26 | 0,33 |
| 02:25:00 | 630,43 | 0,33 |
| 02:25:30 | 632,61 | 0,33 |
| 02:26:00 | 634,78 | 0,34 |
| 02:26:30 | 636,96 | 0,34 |
| 02:27:00 | 639,13 | 0,34 |
| 02:27:30 | 641,30 | 0,34 |
| 02:28:00 | 643,48 | 0,34 |
| 02:34:00 | 669,57 | 0,34 |
| 02:38:00 | 686,96 | 0,34 |
| 02:43:00 | 708,70 | 0,34 |
| 02:48:43 | 733,55 | 0,34 |
| 03:12:00 | 834,78 | 0,34 |
| 03:18:00 | 860,87 | 0,34 |
| 03:33:00 | 926,09 | 0,34 |
| 03:48:00 | 991,30 | 0,34 |
| 04:03:00 | 1056,52 | 0,34 |
| 04:18:00 | 1121,74 | 0,34 |
| 04:33:00 | 1186,96 | 0,34 |
| 04:36:00 | 1200,00 | 0,34 |

# Appendix G

# Risk assessment

| | | | |
|---|---|---|---|
| **ID** | 29280 | **Status** | **Dato** |
| **Risikoområde** | Risikovurdering: Helse, miljø og sikkerhet (HMS) | Opprettet | 25.04.2018 |
| **Opprettet av** | Siri Hjelt Salvesen | Vurdering startet | 25.04.2018 |
| **Ansvarlig** | Siri Hjelt Salvesen | Tiltak besluttet | |
| | | Avsluttet | 25.04.2018 |

**Risikovurdering:**

## Master thesis spring 2018

**Gyldig i perioden:**
1/15/2018 - 6/11/2018

**Sted:**
Reservoir Laboratory -IGP-NTNU, PTS 3. floor

**Mål / hensikt**
Avoid injuries and damage on equipment during laboratory work.

**Bakgrunn**
A Risk Assessment is required for laboratory work during the Master Thesis.

**Beskrivelse og avgrensninger**
Subjects that might be affected by the risks evaluated in this risk assessment are me and my co-workers in the lab. The risk assessment is applicable for work in the PTS-lab only.

**Forutsetninger, antakelser og forenklinger**
Some similar experiments has been done previously, during the project.

**Vedlegg**
[Ingen registreringer]

**Referanser**
[Ingen registreringer]

## Oppsummering, resultat og endelig vurdering

I oppsummeringen presenteres en oversikt over farer og uønskede hendelser, samt resultat for det enkelte konsekvensområdet.

| | | | |
|---|---|---|---|
| **Farekilde:** | **Toxic chemicals** | | |
| **Uønsket hendelse:** | **Inhalation of toxic chemicals** | | |
| **Konsekvensområde:** | Helse | Risiko før tiltak: | Risiko etter tiltak: |
| **Uønsket hendelse:** | **Spilling of toxic chemicals** | | |
| **Konsekvensområde:** | Helse | Risiko før tiltak: | Risiko etter tiltak: |
| **Farekilde:** | **Flammable waste** | | |
| **Uønsket hendelse:** | **Fire** | | |
| **Konsekvensområde:** | Helse | Risiko før tiltak: | Risiko etter tiltak: |
| | Materielle verdier | Risiko før tiltak: | Risiko etter tiltak: |
| **Farekilde:** | **Needles** | | |
| **Uønsket hendelse:** | **Wound on skin** | | |
| **Konsekvensområde:** | Helse | Risiko før tiltak: | Risiko etter tiltak: |

**Endelig vurdering**

The uncertainties associated with this risk assessment are based on how dangerous inhaling/spilling of the toxic chemicals are. As long as the safety equipment is used at all times and the waste is handlet properly and kept out of flammable areas, the general risk is considered small.

## Involverte enheter og personer

En risikovurdering kan gjelde for en, eller flere enheter i organisasjonen. Denne oversikten presenterer involverte enheter og personell for gjeldende risikovurdering.

**Enhet /-er risikovurderingen omfatter**

- NTNU

**Deltakere**

Reidun Cecilie Grønfur Aadland

**Lesere**

[Ingen registreringer]

**Andre involverte/interessenter**

[Ingen registreringer]

## Følgende akseptkriterier er besluttet for risikoområdet Risikovurdering: Helse, miljø og sikkerhet (HMS):

| Helse | Materielle verdier | Omdømme | Ytre miljø |
|---|---|---|---|
|  |  |  |  |

## Oversikt over eksisterende, relevante tiltak som er hensyntatt i risikovurderingen

I tabellen under presenteres eksisterende tiltak som er hensyntatt ved vurdering av sannsynlighet og konsekvens for aktuelle uønskede hendelser.

| Farekilde | Uønsket hendelse | Tiltak hensyntatt ved vurdering |
|---|---|---|
| Toxic chemicals | Inhalation of toxic chemicals | Fume hood and waste bucket |
| | Inhalation of toxic chemicals | HSE Introductory Course |
| | Spilling of toxic chemicals | Safety equipment |
| | Spilling of toxic chemicals | HSE Introductory Course |
| Flammable waste | Fire | Fume hood and waste bucket |
| | Fire | HSE Introductory Course |
| | Fire | Lab tour |
| Needles | Wound on skin | Safety equipment |
| | Wound on skin | HSE Introductory Course |

**Eksisterende og relevante tiltak med beskrivelse:**

**Safety equipment**

Safety goggles, lab coat and shoes.

**Fume hood and waste bucket**

A fume hood is present where dangerous liquids are in contact with air, and used when cleaning the equipment. There are waste buckets for both flammable/toxic liquid and solid waste.

**HSE Introductory Course**

An online HSE Introductory Course were taken prior to entering the lab.

**Lab tour**

A guided tour through the lab were given prior to the lab work, to get to know the equipment and dangers in the laboratory.

## Risikoanalyse med vurdering av sannsynlighet og konsekvens

I denne delen av rapporten presenteres detaljer dokumentasjon av de farer, uønskede hendelser og årsaker som er vurdert. Innledningsvis oppsummeres farer med tilhørende uønskede hendelser som er tatt med i vurderingen.

**Følgende farer og uønskede hendelser er vurdert i denne risikovurderingen:**

- **Toxic chemicals**
  - Inhalation of toxic chemicals
  - Spilling of toxic chemicals
- **Flammable waste**
  - Fire
- **Needles**
  - Wound on skin

**Detaljert oversikt over farekilder og uønskede hendelser:**

**Farekilde: Toxic chemicals**

Several toxic liquids are used when cleaning the equipment, as toluene, methanol and aceton.

**Uønsket hendelse: Inhalation of toxic chemicals**

*Årsak:* Handling of toxic chemicals without using the fume hood

*Sannsynlighet for hendelsen (felles for alle konsekvensområder):* **Lite sannsynlig (2)**

*Kommentar:*

As long as the safety equipment is used properly, there should be a small risk of inhaling the chemicals.

**Konsekvensområde: Helse**

***Risiko:***

*Vurdert konsekvens:* **Stor (3)**

*Kommentar:* Some of the chemicals are very toxic

**Uønsket hendelse: Spilling of toxic chemicals**

*Årsak:* Handling chemicals without using the proper safety equipment

*Sannsynlighet for hendelsen (felles for alle konsekvensområder):* **Lite sannsynlig (2)**

*Kommentar:*

As long as the safety equipment is used properly, there should be a small risk of spilling chemicals on your skin.

**Konsekvensområde: Helse**

***Risiko:***

*Vurdert konsekvens:* **Stor (3)**

*Kommentar:* Some of the chemicals are very toxic.

**Farekilde: Flammable waste**

**Uønsket hendelse: Fire**

*Årsak:* Poor waste handling

*Årsak:* Equipment malifunction

*Sannsynlighet for hendelsen (felles for alle konsekvensområder):* **Lite sannsynlig (2)**

*Kommentar:*
[Ingen registreringer]

**Konsekvensområde: Helse**

*Vurdert konsekvens:* **Stor (3)**

*Kommentar:* [Ingen registreringer]

***Risiko:***

**Konsekvensområde: Materielle verdier**

*Vurdert konsekvens:* **Stor (3)**

*Kommentar:* [Ingen registreringer]

***Risiko:***

**Farekilde: Needles**

**Uønsket hendelse: Wound on skin**

*Årsak:* Poor handling of equipment

*Sannsynlighet for hendelsen (felles for alle konsekvensområder):* **Lite sannsynlig (2)**

*Kommentar:*
[Ingen registreringer]

**Konsekvensområde: Helse**

*Vurdert konsekvens:* **Middels (2)**

*Kommentar:* [Ingen registreringer]

***Risiko:***

## Oversikt over besluttede risikoreduserende tiltak:

Under presenteres en oversikt over risikoreduserende tiltak som skal bidra til å reduseres sannsynlighet og/eller konsekvens for uønskede hendelser.

**Detaljert oversikt over besluttede risikoreduserende tiltak med beskrivelse:**

**Detaljert oversikt over vurdert risiko for hver farekilde/uønsket hendelse før og etter besluttede tiltak**